SCRIPPS INSTITUTION OF OCEANOGRAPHY
UNIVERSITY OF CALIFORNIA, SAN DIEGO
Dr. William A. Nierenberg, Director
Principal Investigator

ADVANCED OCEAN ENGINEERING LABORATORY

Technical Progress Report

December 31, 1971

Sponsored by
ADVANCED RESEARCH PROJECTS AGENCY
ADVANCED ENGINEERING DIVISION
ARPA Order Numbers 1348, 1730 and 1607
Program Code NR 293-005

Administered by the OFFICE OF NAVAL RESEARCH
Contract N00014-69-A-0200-6012
Contract Effective Date: December 15, 1968
Contract Expiration Date: October 31, 1972
Total Contract Amount $3,960,675.00

SIO Reference Number 72-2
AOEL Report #26

DISCLAIMER NOTICE

THIS DOCUMENT IS THE BEST QUALITY AVAILABLE.

COPY FURNISHED CONTAINED A SIGNIFICANT NUMBER OF PAGES WHICH DO NOT REPRODUCE LEGIBLY.

Unclassified

Security Classification

DOCUMENT CONTROL DATA - R & D

(Security classification of title, body of abstract and indexing annotation must be entered when the overall report is classified)

1. ORIGINATING ACTIVITY *(Corporate author)*
The Regents of the University of California
University of California, San Diego
La Jolla, California 92037

2a. REPORT SECURITY CLASSIFICATION
Unclassified

2b. GROUP
Not Applicable

3. REPORT TITLE
Technical Progress Report
Advanced Ocean Engineering Laboratory

4. DESCRIPTIVE NOTES *(Type of report and inclusive dates)*
July 1, 1971 to December 31, 1971

5. AUTHOR(S) *(First name, middle initial, last name)*
Dr. William A. Nierenberg
Dr. Fred N. Spiess
Dr. Walter H. Munk
Dr. William A. Prothero
Dr. Douglas L. Inman
Dr. William G. Van Dorn

6. REPORT DATE
February 15, 1972

7a. TOTAL NO. OF PAGES
118

7b. NO. OF REFS
27

8a. CONTRACT OR GRANT NO.
N00014-69-A-0200-6012

b. PROJECT NO.

c.

d.

9a. ORIGINATOR'S REPORT NUMBER(S)
SIO Reference No. 72-2

9b. OTHER REPORT NO(S) *(Any other numbers that may be assigned this report)*
AOEL Report #26

10. DISTRIBUTION STATEMENT
Distribution of this document is unlimited

11. SUPPLEMENTARY NOTES

12. SPONSORING MILITARY ACTIVITY
Advanced Research Projects Agency
c/o Office of Naval Research
Arlington, Virginia 22217

13. ABSTRACT

This semi-annual report reflects the technical status of projects conducted within the Advanced Ocean Engineering Laboratory at the Scripps Institution of Oceanography. These projects are: (1) Stable Floating Platform - to conceive, design, build and demonstrate the feasibility of large stable floating platforms in the open sea. (2) Benthic Array - a program to develop and construct a quartz vertical accelerometer, appropriately packaged and adapted for long term ocean bottom or perhaps sub-bottom use. (3) Advanced Studies in Nearshore Engineering - field studies of the water-sediment interface under wave action in and near the breaker zone; and laboratory investigation of the velocity field of breaking waves. (4) Electromagnetic Roughness of the Ocean Surface - utilization of radio signals scattered from the sea surface to determine the directional spectrum of ocean waves.

DD FORM 1 NOV 65 1473 (PAGE 1)
0102-014-6600

Unclassified

Security Classification

14. KEY WORDS	LINK A		LINK B		LINK C	
	ROLE	WT	ROLE	WT	ROLE	WT
Advanced Ocean Engineering						
Stable Floating Platform						
FLIP						
Floating Islands						
Benthic Array						
Acoustic Command & Telemetry Logic						
Explosive cable cutter						
Quartz crystal oscillator						
Frequency-shift-keying mode						
Bi-phase decoder						
Pulse code modulation decommutator						
Nearshore Engineering						
Breaking waves						
Water-sediment interface						
Vortex sublayer						
Digital wave staff						
Hot-film velocity probes						
Electromagnetic Roughness of the Ocean Surface						
Ocean-wave directional spectrum						
Bistatic LORAN equipment						
Doppler frequency						

Disclaimer

The views and conclusions contained in this document are those of the authors and should not be interpreted as necessarily representing the official policies, either expressed or implied, of the Advanced Research Projects Agency or the U. S. Government.

Advanced Ocean Engineering Laboratory

TECHNICAL PROGRESS REPORT

Table of Contents

Part I

STABLE FLOATING PLATFORM

Principal Investigator
Dr. Fred N. Spiess
Phone (714) 453-2000, Extension 2476

ADVANCED OCEAN ENGINEERING LABORATORY

Sponsored by

ADVANCED RESEARCH PROJECTS AGENCY
ADVANCED ENGINEERING DIVISION

ONR Contract N00014-69-A-0200-6012

Part I

Stable Floating Platform

Table of Contents

List of Figures

I. INTRODUCTION

At the start of this semi-annual reporting period, the Floating Platform program was moving forward with design of a two-module, four leg platform (Fig. 1) whose mission would be the support of ocean research. This was the result of previous agreement with personnel of the Advanced Technology section of the sponsoring agency (ARPA) over the previous two year period (reported, for example, in Ref. 1). The configuration of the structure of the individual modules was well-defined with the major area of investigation focussed on the manner in which they would be joined together. Work was starting on detailed design looking toward preparation of construction specifications. In parallel with the design effort, further work was laid out in the model study regime.

In early November, a project review was conducted by the sponsor, at which the principal finding was that ARPA's objectives (in spite of the agreement referred to above) were tied solely to technology relevant to very large platforms ("floating islands"). This led the review panel (Ref. 2) to suggest a number of lines of investigation other than those in progress and has resulted in some re-orientation of the program. Most particularly, work on preparation of plans for platform construction was terminated pending the outcome of studies to be conducted in calendar 1972.

Activities which were carried on during this six month period were focussed primarily on two areas: Design of the concrete leg structure and investigation of various modes of coupling the two modules together. Other work included a first cut at detailing the laboratory and living space portion of the platform.

II. CONCRETE LEG DESIGN

This portion of the design is close to completion except for detailed calculation of stresses at key points (e.g., intersections between cylindrical shell and transverse bulkheads). A number of iterations have been made as a result of the problems of reconciling weight and buoyancy distribution, moment distributions due to both vertical and horizontal bending of the legs while in the horizontal (towing) mode, compartmentation as it relates to ballast changes during the flipping transition, moments produced during the transition, access (particularly for installation and repair of air storage tanks) and a number of other lesser points. The result, in addition to controlling the nature of the concrete structure itself, has influenced other aspects of the design. Four items in this regard are worthy of mention.

1. The lateral bending moments produced by the wave forces when the catamaran is in the towing configuration (legs horizontal) were calculated to be quite severe when the two hulls were joined together only at their ends as earlier planned (Ref. 3). Since additional structure would have carried further weight penalties, and since each of the existing cross connecting members already served some additional function (the forward one as the cross shaft of the trunnion mount of the laboratory and living space, the after one as a key off-axis ballast tank in the flipping operation) it was clear that some modification would have to be made. The most effective and least costly (in dollars) was the solution adopted which moved the after (bottom) cross tube forward (up) about 50 feet, thus providing

more effective lateral support, but with a slight (about 10%) degradation of heave response in the vertical.

2. Consideration of the vertical forces on the legs (while under tow in the horizontal mode) has led to limits on freedom to dispose ballast in such a manner as to give adequate stability when the platform is in the vertical position with clearance (separation between sea level and bottom of work platform) adequate for operation in severe weather. The solution to this problem has been to take advantage of the fact that this "severe weather" condition will only rarely be used and to define two vertical operating conditions -- normal (20 ft. clearance) and emergency (40 ft. clearance). Movable ballast (gravel) is then provided which in the normal condition is amidships but which can be released to fall through a chute to the bottom of the leg (in the vertical) to provide the needed stability in the emergency vertical configuration. At the conclusion of the operation, this ballast can then be dropped into the sea before towing back to port, thus avoiding the existence of this weight at an unfavorable location relative to operation in the horizontal.

3. The legs constitute a long, slender structure. As detailed analyses of the strength and weight of the concrete structure were developed, it became clear that it would not be possible to develop adequate resistance to bending (and at the same time stay within weight and displacement limits) while using a simple cylindrical structure. Additional material was needed as far off axis in the vertical plane as possible. It was thus decided that

both a dorsal and a ventral ridge would be added (Fig. 2). While this would contribute to somewhat increased draft in the towing configuration, this would not be an important disadvantage. Moreover, it now appears that these ridges can have a useful function as an anchoring structure for the circumferential post-tensioning tendons in the concrete shell.

4. The initial configuration chosen for each leg was taken (for reasons relating to heave response and convenience) to be a pair of cylinders joined by a cone with all three elements coaxial. This configuration, together with the nature of the work platform, made it necessary to place the forward (upper) cross tube (trunnion shaft) fairly low in the work platform structure. This, in turn, made it impossible to distribute the weight of the work platform in such manner as to make it pendulously stable in its rotation about the trunnion axis during change of attitude from horizontal to vertical. This had not appeared to be a serious problem since we had anticipated flipping the legs with the house in the water, then locking the house to the legs and de-ballasting to lift the house to the desired clearance. Model studies, however, (1/100 and 1/8 scale), showed that a dangerous condition existed in the intermediate position (legs down, house in water). Furthermore, tests at 1/8 scale showed that, if the work platform were ballasted to be pendulously stable, the flipping operation proceeded in a single, well-behaved sweep (Fig. 3) from horizontal to vertical (with house at proper clearance) and vice-versa. With these facts in mind, a re-design was initiated to make it possible to

raise the trunnions and re-ballast the house to be pendulously stable. This could only be accomplished by re-arranging the cylinders and cone to have a common topmost element (viewed with legs horizontal, Fig. 2), thus not only solving the problem of an adverse longitudinal buoyancy distribution but also assuring that the legs would stand truly vertical when ballast tanks were filled.

The concrete structure itself (Fig. 4) is now visualized as using light weight (expanded shale) aggregate, cast in sections short enough to be handled by a large crane and then assembled end to end. Holes would be included to allow passage of post tensioning tendons both circumferentially and longitudinally. The circumferential reinforcing would be anchored to the top and bottom longitudinal ridges while the longitudinal ones, which essentially hold the structural segments together, would terminate at steel plates at each end of the leg. The shell thickness is about 9 inches throughout. Considerable supervisory care will be required during construction to assure that the structure will, in fact, develop its full strength and that it will have the necessary low water absorption properties and will resist de-lamination. Further work is yet to be done in detailing such elements as joints between outer shell and bulkheads and in calculating the stresses at those locations.

III. MODULE COUPLING AND RELATED INVESTIGATIONS

The problem of developing an adequate coupling, viewed both as a structural matter and an operational one (how to make the hookup), is the most serious one remaining. In fact, one member of the November

review panel is on record as being quite dubious as to whether hookup can ever be achieved in anything but flat, calm seas. With the idea that demonstration of feasibility in the two-module case would in itself represent an advance of technology, the work on this topic prior to the November meeting was pointed toward the specific problem of joining these two modules. The emphasis which the review meeting gave to very large platforms led the reviewers to urge a broader consideration of this problem in the context of directly obvious extrapolation to multiple-module connection in both horizontal dimensions.

Of all the relevant numbers which one can compute concerning platform motions and forces (in vertical position), the three driving ones turn out to be:

(1) Torque about the axis normal to the plane of the leg pairs and through the two work platforms. (Tx)

(2) Torque about the axis through the joining edge of the platforms (or alternatively torque about the trunnion axis). (Ty)

(3) Relative surging motion of the two units when uncoupled.

The calculated torques turn out to be quite large. For a completely rigid four legged platform of the dimensions proposed, the maximum values occur for wave periods of 10 seconds. Tx is maximum for a quartering sea and Ty for an ahead sea. For an 80 foot, regular wave at that period, the values are Tx = 112 x 10^6 ft. lb. and Ty = 424 x 10^6 ft. lb. The relative surging motion for closely spaced but unconnected modules is a maximum for a 9 second wave and is $\pm$ 7.5 ft. for a 20 foot wave of that period. This was taken as the design maximum condition for attempting module hookup.

Structures to constrain these turn out to be quite massive and difficult to visualize as being demountable or make-break connections. For this reason, our investigations centered on connecting structures which would leave one or both of these rotational degrees of freedom unconstrained. This does not seem particularly objectionable since the magnitudes of the corresponding angular displacements are small (3^{o} & 7^{o} for 80 foot wave and less than 1/4 of that for normal operating circumstances).

On this basis, several alternate configurations were tested in a number of ways. Operational feasibility of a simple trailer-hitch type of connection was investigated in San Diego Bay, using the recently completed pair of 1/8 scale modules (Fig. 5). While the sea conditions were quite favorable, the operation indicated that an approach using a pair of breast lines and with both units in tandem tow (actually one unit anchored in the tidal current in the bay) was not unrealistic.

The most extensive testing was done at 1/100 scale (Ref. 4) in the Scripps Hydraulic Facility. Here work was done with the module platforms rigidly connected but the trunnions unlocked, with a double hinge at the platform connection and the trunnions locked, and with a single hinge plus vertical slider connection (again trunnions locked). These tests did not demonstrate any inherent structural problems. Instead, however, they opened up an entirely new area of investigation. The relative motions in the unconstrained rotations (and relative heave, also) for the platforms with these couplings were observed to be very much larger than predicted for a few drive frequencies and in every such case the observed large motion was at a substantially lower frequency (longer period) than the

exciting waves. The periods of the motion were in general close to the heave resonance or some similar frequency which would be expected not to be present in a realistic ocean wave spectrum, although the wave periods which excited these motions in fact, did scale into ones which would be of importance in the real world (e.g. 13½ sec.).

After a careful investigation to determine whether the driving waves might inadvertently contain energy at these lower frequencies, and some careful repetition of measurements, it became clear that this was a phenomenon not observed previously (Ref. 5) in the full scale, single leg case (FLIP). Moreover, the effect appeared to have a threshold (small waves would not excite these motions). Consideration of the equations of motion led to the conclusion that the effect could be seen in the mathematics for a simple case (single spar and exciting frequency about double the heave resonance frequency) by proper choice of wave amplitude and drag coefficient.

Further model study seemed called for, and to provide for better insight it was decided to do this at a substantially different scale. 1/30 was chosen and runs were made late in December at the Offshore Technology facility in nearby Escondido. Similar effects were observed and documented. Data reduction on these latter model studies is in progress. This same test sequence was used to investigate operational aspects of coupling and it was found that, with one model under tow and the second hooked to it, the relative positions could be reasonably well controlled using the connecting lines in fairly heavy seas.

Theoretical studies of these large motions have continued and are yielding the understanding that their source is in the finite

(though small) amplitude of the platform motion at the driven frequency. Quantitative correspondence between the 1/30 scale results and the theory, in some aspects, has been shown but further development is required before full understanding of this important phenomenon exists.

As a result of the observations of performance of various coupling arrangements, particularly relative to the excitation of the large amplitude motions, it appeared that the best approach would be to use the single hinge plus free rotation about the fore and aft axis. A trial, full scale design for such a linkage was made in early November, resulting in a very massive structure. This, with the renewed emphasis on the very large "island" having, presumably many modules, led to a decision in December to shift to a connection philosophy which had originally been considered as part of the long range engineering program to follow the construction and availability of the full scale platforms -- namely to connect the two modules rigidly both above and well below the sea surface. Such a connection scheme copes much more easily with the large moments, permits no relative motions of modules and can more easily be generalized into a multi-module situation. It also provides some side benefits--for example, the deep cross-connection could support a large "damping plate" which would contribute substantially to the effective mass of the platform. Operationally, it opens the possibility of coupling the bottoms together as a first step since at that level the relative surging motions should be very much less than at the platform level. Thus, the first step could constrain the gross relative alignment in azimuth and transverse displacement and make for the beginning of restriction of relative surge before it would have to be met at the platform level. Beyond this,

the rigid coupling would make possible some de-ballasting to allow greater clearance or deck load, shifting reliance for stability against overturning on the existence of the resulting available metacentric height.

IV. PLATFORM ARRANGEMENTS

As was noted above, work has been done on internal arrangements for the platform modules. Fig. 6 shows these, indicating the availability of ample space for crew and scientists, meeting the requirements for ordinary ship habitability and leaving ample uncommitted space for research equipment to cope with the tasks indicated in our earlier utilization analysis report (Ref. 6).

Inasmuch as consideration has shifted, at least for the time being, away from this aspect of the program, no further refinement of these plans is anticipated. The configuration of whatever is eventually built may well be substantially different, reflecting altered philosophy of coupling and greater emphasis on these modules as giving direct guidance for design of modules for larger platforms.

V. ACKNOWLEDGMENT

During this period, a large number of people have contributed to this work, particularly Dr. P. Rudnick, Messrs. Oversmith, Bellows, Van Hoy, Mundy, and Bronson of the AOEL and MPL staffs, and outside contractors L. R. Glosten and Associates, Skilling, Helle, Christiansen, Robertson of Seattle, Offshore Technology, and Alaa Mansour of MIT. The most notable contribution has been from Dr. Robert Corell of the University of New Hampshire who has played a major role while in residence at SIO on sabbatical leave from his home university.

VI. References

1. Advanced Ocean Engineering Laboratory, Annual Report Scripps Institution of Oceanography, University of California, San Diego, SIO Ref. No. 71-4, AOEL Report #16, 31 December 1970.

2. Tachmindji, A. J. Report of the Advisory Committee on Floating Platforms, Institute for Defense Analyses, Systems Evaluation Division, Report #N-804, IDA Log No. HQ 71-13728, November, 1971.

3. Advanced Ocean Engineering Laboratory, Technical Progress Report, Scripps Institution of Oceanography, University of California, San Diego, SIO Ref No. 71-22, AOEL Report #23, 30 June 1971.

4. Advanced Ocean Engineering Laboratory, Technical Report "1/100 Scale Model Experiments, Stable Floating Platform A-59.", Scripps Institution of Oceanography, University of California, San Diego, SIO Ref No. 71-17, AOEL Report #22, August 1971.

5. Rudnick, P. Motion of a Large Spar Buoy in Sea Waves, Journal of Ship Research, Vol. II, No. 4, pp. 257-267, December, 1967.

6. Anderson, V. C. Reports on Applications of ARPA Platform Marine Physical Laboratory, Scripps Institution of Oceanography, SIO Ref. No. 71-20, 15 July 1971.

Figure 1: Scale Models of Two-module, four leg Stable Floating Platform in Vertical Position

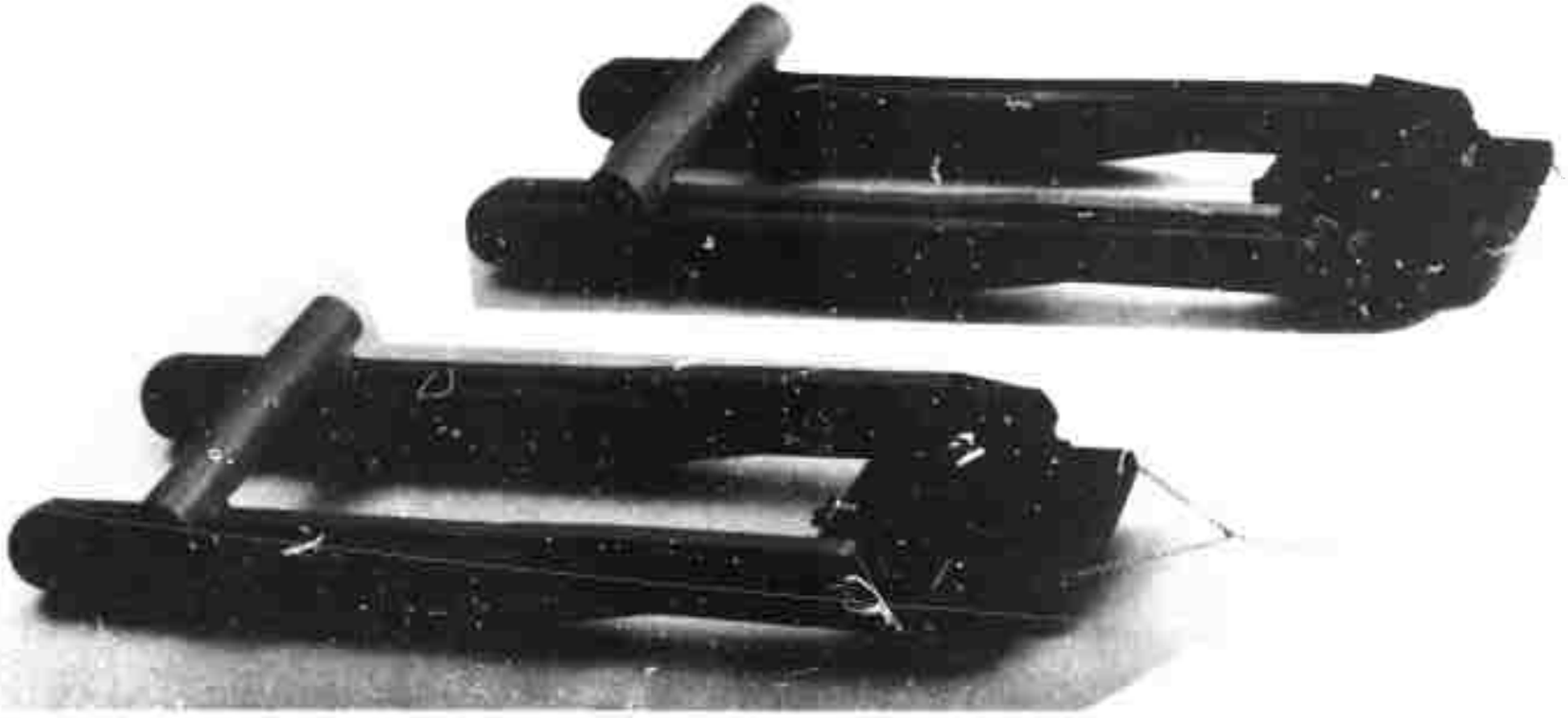

Figure 2: Scale Models of Two Stable Floating Platform Modules in Towing Position

Figure 3: One-eighth Scale Model of a Stable Floating Platform Module during Flipping Sequence, with Pendulous Superstructure

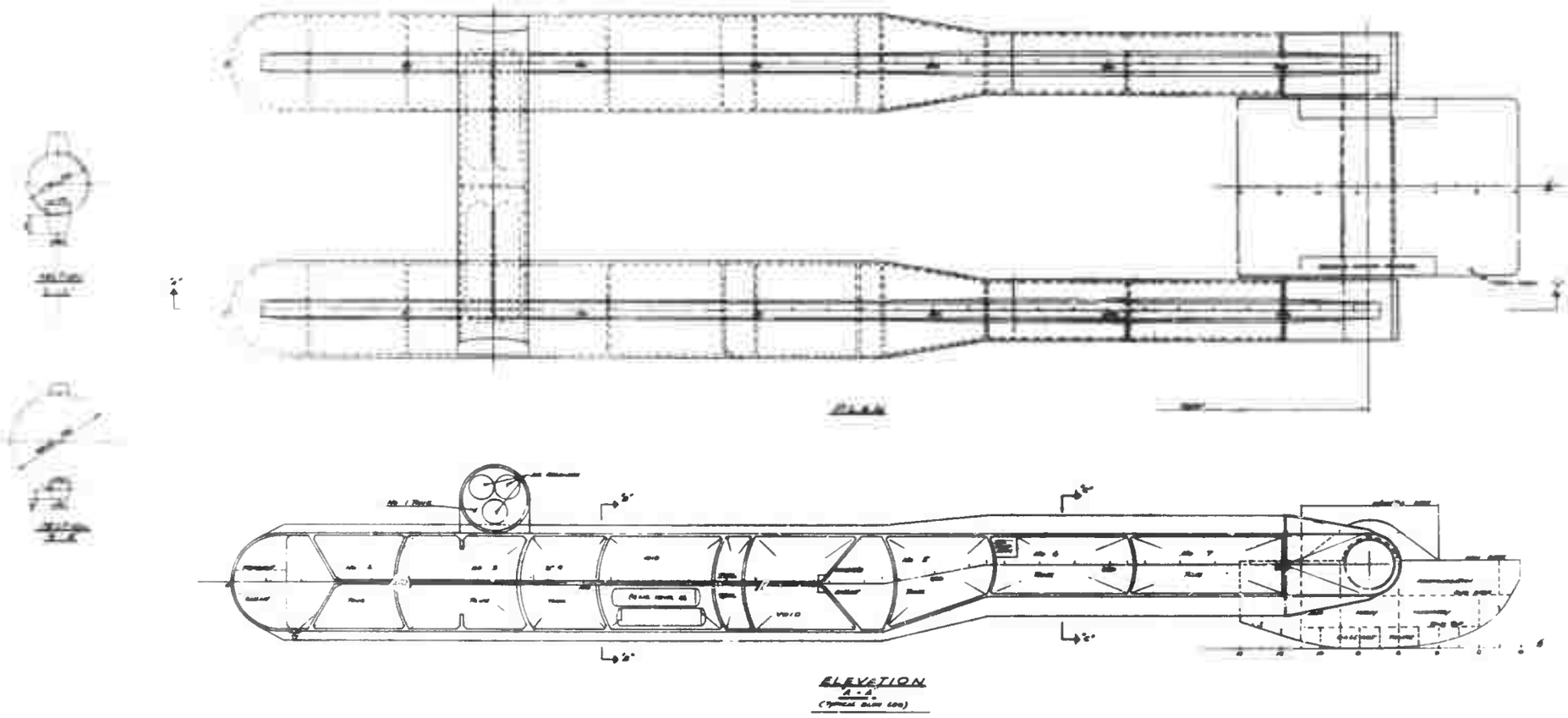

Figure 4: Engineering Drawing of Single Stable Floating Platform Module Showing Major Component and Bulkhead Arrangements

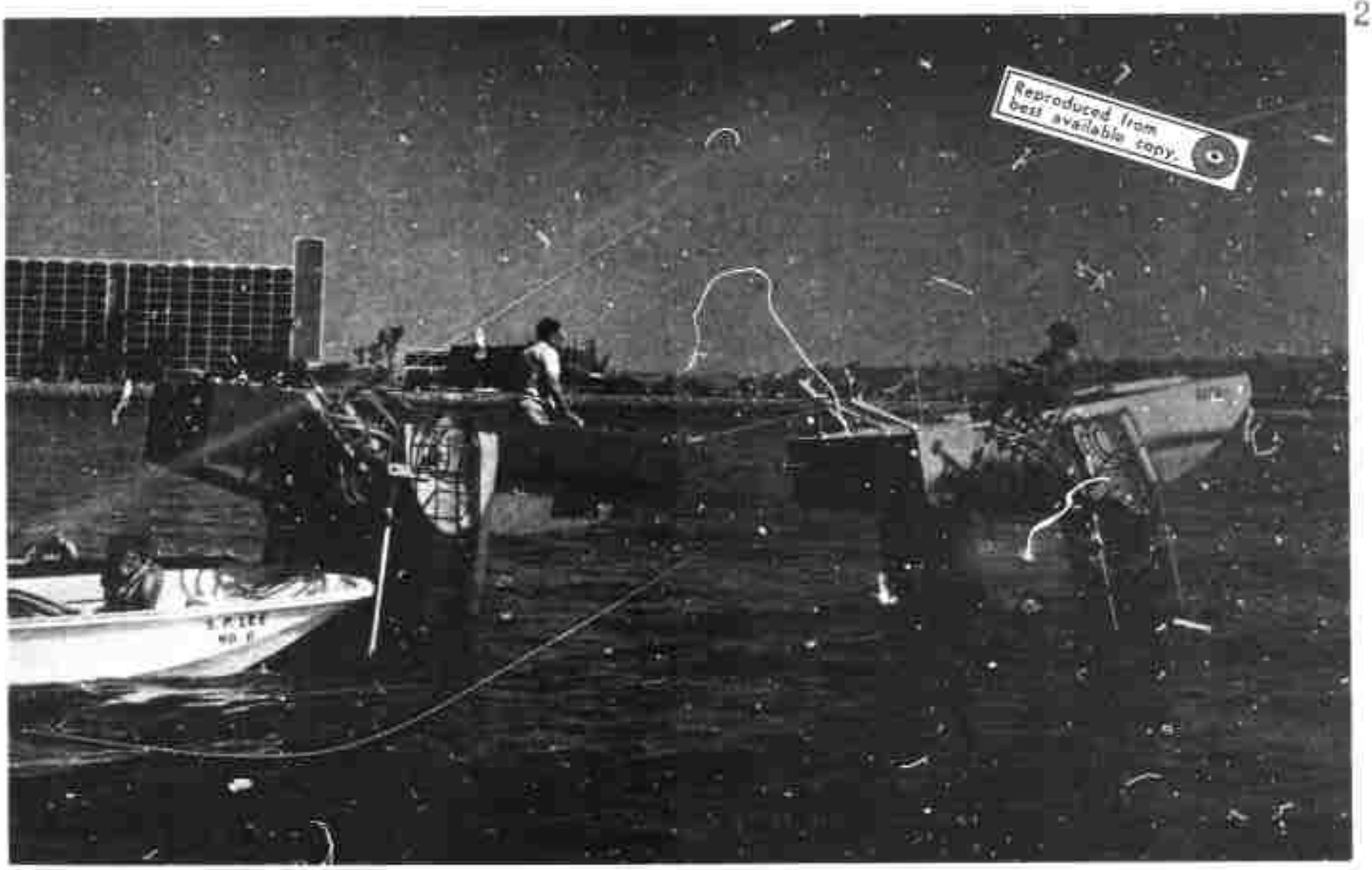

Figure 5: Coupling Experiments with One-eighth Scale Models of Two Stable Floating Platform Modules Just Prior to Coupling the Superstructures

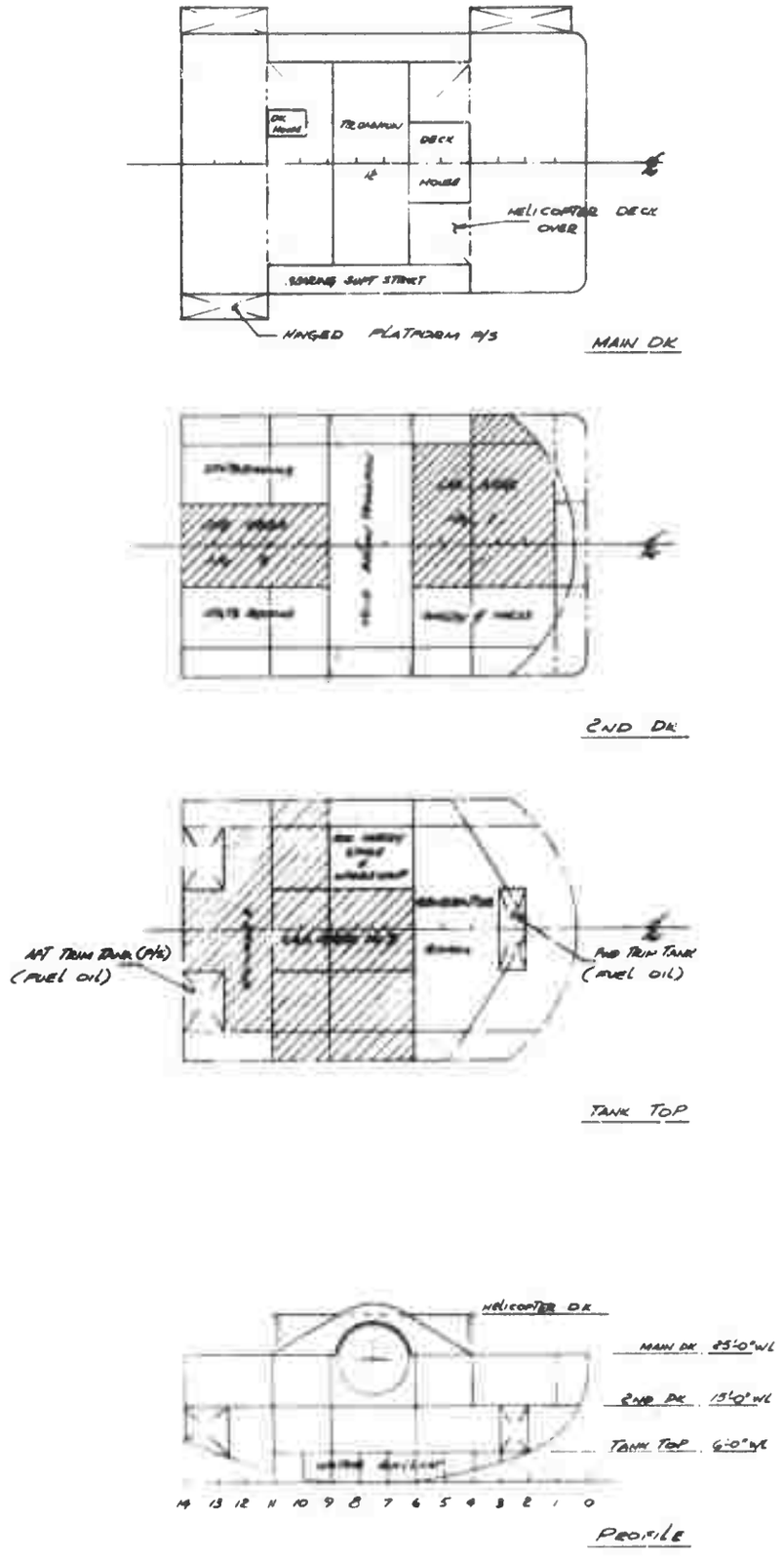

Figure 6: Arrangement Drawings of the Various Deck Levels of the Stable Floating Platform Superstructure

Part II

BENTHIC ARRAY

Co-Principal Investigators

Dr. Walter H. Munk
Phone (714) 453-2000, Extension 1741

Dr. William A. Prothero, Jr.
Phone (714) 453-2000, Extension 1688

ADVANCED OCEAN ENGINEERING LABORATORY

Sponsored by
ADVANCED RESEARCH PROJECTS AGENCY
ADVANCED ENGINEERING DIVISION

ONR Contract N00014-69-A-0200-6012

Part II

Benthic Array

Table of Contents

List of Figures

List of Appendices

I. SUMMARY

The work for the last six months has been to complete vault testing of the accelerometer and data logging electronics, refine and complete the acoustic control logic, and specify and complete the remaining mechanical components of the system so that it will be ready for the first ocean bottom test in mid-March, 1972.

II. TECHNICAL REPORT

A major task which has been accomplished is to finish the design of the physical package configuration. It was determined that an extra flotation sphere would have to be added for buoyancy. It adds very little bulk to the package and the extra space will be useful for the horizontal seismometers which we hope to add in the future. Figure 1 shows the important external parts of the package. The support tripod and lead-acid batteries are left on the ocean bottom when the package is released. Final assembly of the hydrophone and flotation sphere mounts is now in progress.

The backup release has been designed and constructed. It is contained in a separate pressure housing and is independent of all other systems. The body of the explosive cable cutter screws into the end of the pressure housing so that no wires are exposed to the ocean environment. Timing is provided by a quartz crystal oscillator that is divided in frequency by COS/MOS binary counters. The design is similar to that used by Meredith Sessions of S.I.O. A deep water test of the backup release alone is scheduled to begin January 21, 1972.

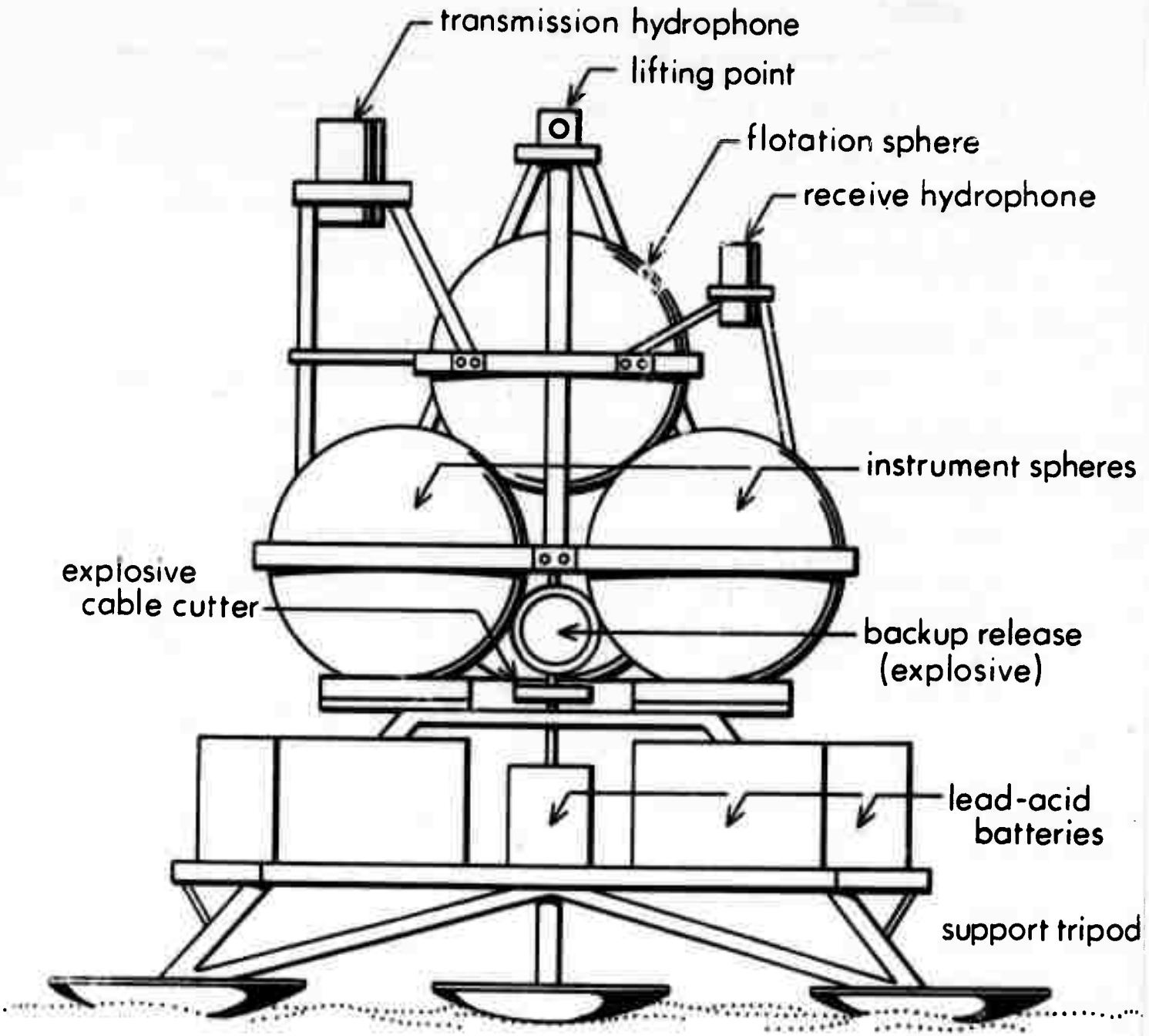

INSTRUMENT PACKAGE CONFIGURATION

FIGURE 1

Preliminary testing of the accelerometer, tiltmeter, data logging and command and control electronics has been completed in the IGPP vault. This site is on the ocean front and a high noise level is present due to breaking waves, but a rough correlation with signal outputs from other instruments indicates we are measuring ground noise. A few minor electronics problems showed up and the complete system is being readied for another vault test near zero °C. This will occur very early in January 1972.

Figure 2 shows the output from the tide filter. The upward trend indicates increasing gravity and may be due to drift in the temperature control circuit, or the steady cooling of the vault during the run. Figure 3 is the band-pass filter output. It has a gain of unity for D.C. and a gain of 100 between 1 and 360 cph. Some of the lower frequency noise in the record appears to be instrumental in origin. There was some problem with interaction between the temperature monitoring circuits and the accelerometer electronics, as well as parasitic oscillations. The installation of the accelerometer in the gimballed support does not seem to be causing trouble and the electronics problems are fairly trivial, so major obstacles to completion and testing on schedule seem unlikely.

The acoustic control logic has been constructed and the circuit boards have tested. Final modifications are being made so that the entire system can be tested together. Appendix I is a detailed description of the command system.

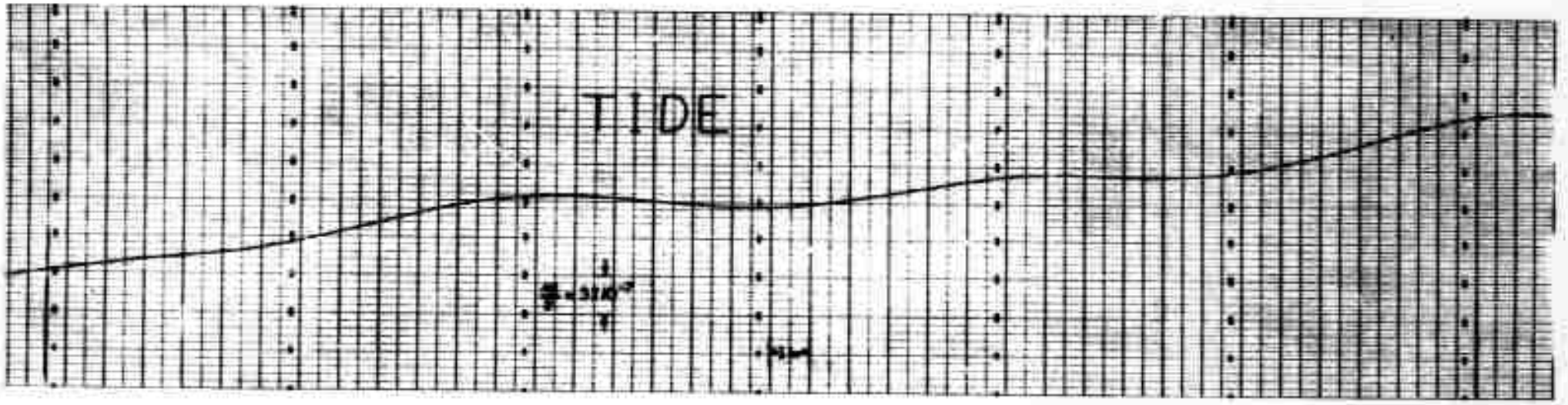

TIDE OUTPUT

FIGURE 2

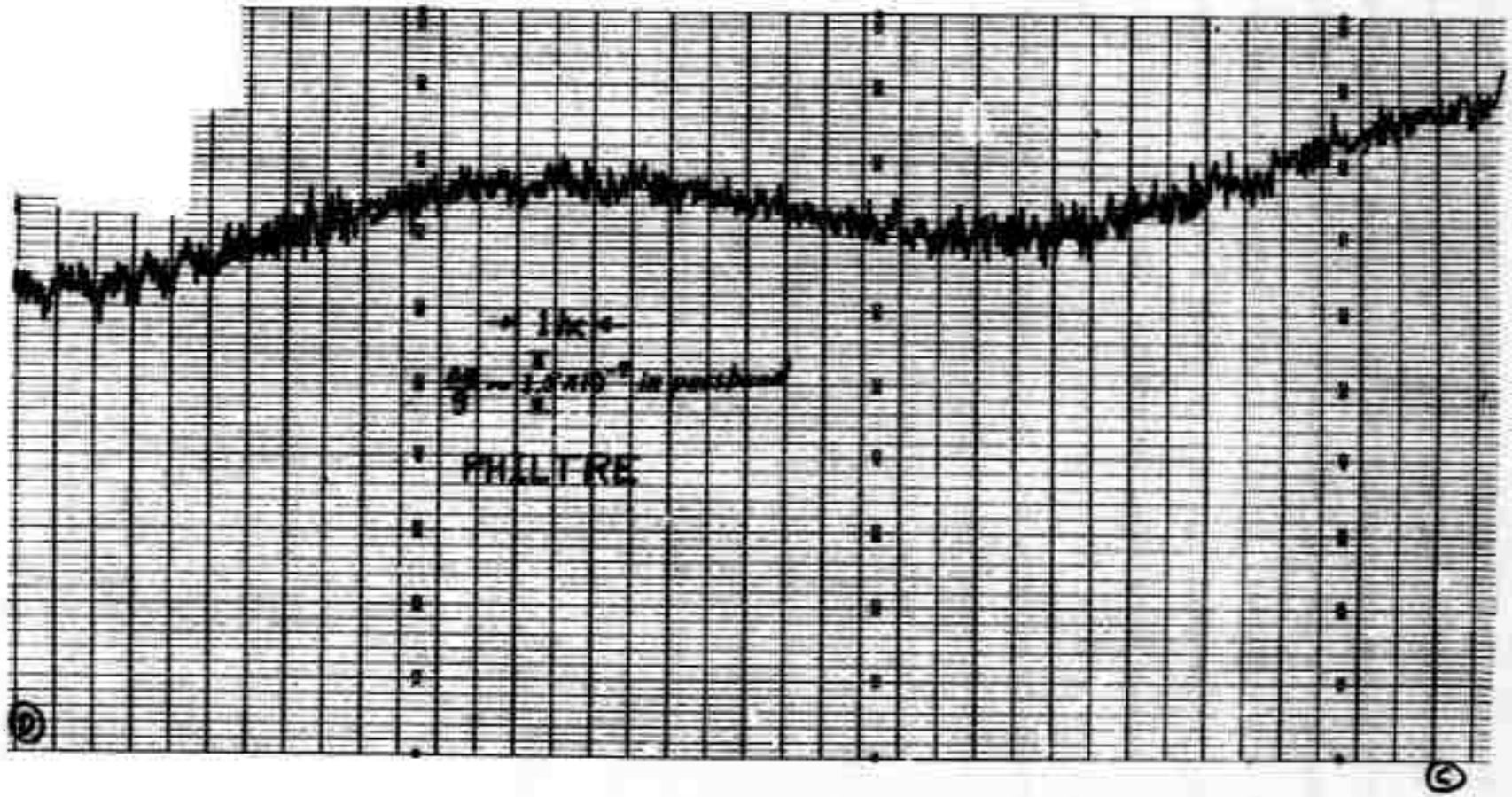

BAND PASS FILTER OUTPUT

FIGURE 3

A change in the diagnostic data transmission mode has been made. The EDO acoustic command system is capable of transmitting data digitally in a frequency-shift-keying mode (FSK). Figure 4 and 5 are block diagrams showing the diagnostics acquisition, encoding, and telemetering process. A bi-phase decoder has been purchased to decode, store and display the information transmitted. Digital acoustic telemetry has been used infrequently in the ocean, but will represent a significant advance in the art of complex self-contained instruments. The possibility of storing data in a memory which can be interrogated without recovering the capsule is an important one cost-wise. Dr. F. Snodgrass at IGPP is working on such a system for his deep-sea tide capsules and our mutual experiences in this regard should prove extremely interesting. We transmit data at 100 bits per second. As a backup system, we will transmit the bits very slowly as individual ping patterns which can be decoded by ear. Thus, if the normal digital system fails for any reason, the diagnostics will still be available.

Appendix II describes the mechanical and electrical specifications of the instrument package in detail.

III. PLANS

The capsule is now being readied for cold testing of the complete system. Two ocean bottom tests are scheduled in 5,000 ft of water near San Clemente Island, near San Diego during March and July. The instrument will be deployed for one month each time if diagnostic information indicates that the capsule is working properly. A proposal has been submitted to the National Science Foundation for funding for two deep ocean deployments in the North Pacific Basin during 1973-74. Horizontal accelerometers are to be added so that Love waves can be recorded as well as Rayleigh waves traveling across the deep ocean basin from earthquakes in the Aleutian Island chain.

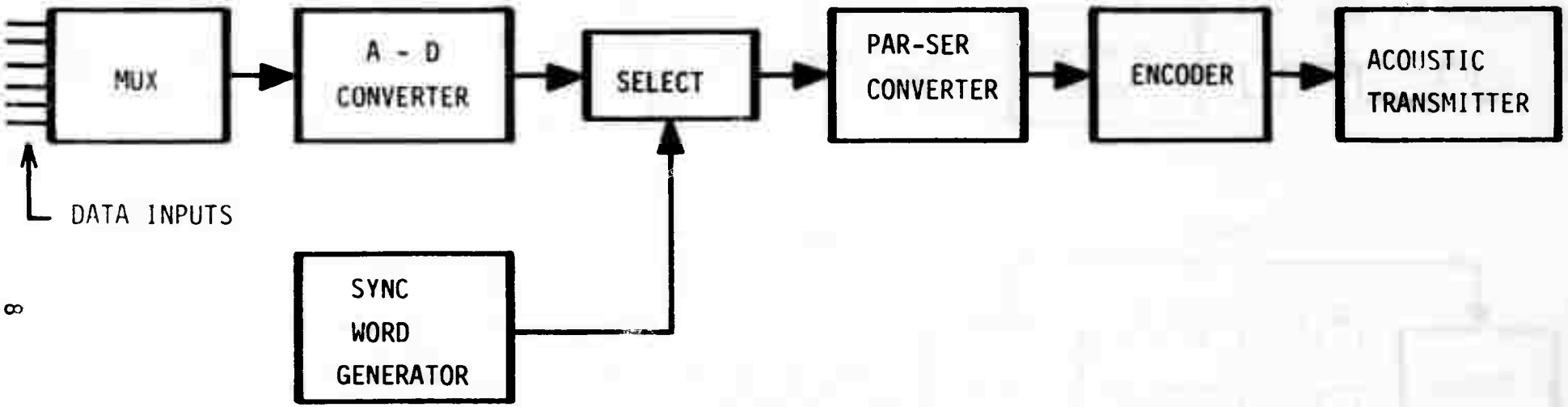

SUBSURFACE DIGITAL DIAGNOSTICS

FIGURE 4

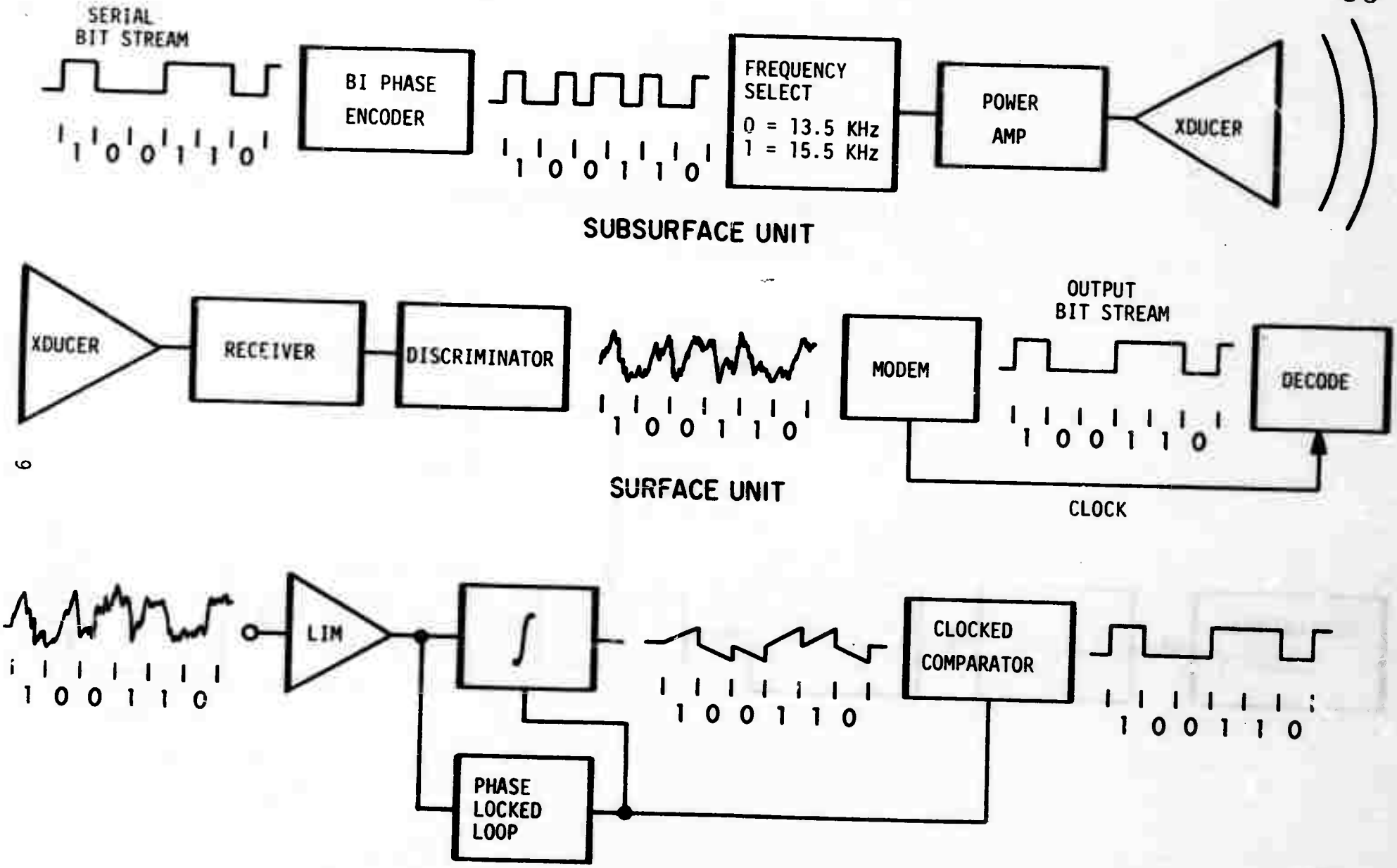
SERIAL
BIT STREAM
1 1 0 0 1 1 0
BI PHASE
ENCODER
1 1 0 0 1 1 0
FREQUENCY
SELECT
0 = 13.5 KHz
1 = 15.5 KHz
POWER
AMP
XDUCER
SUBSURFACE UNIT
XDUCER
RECEIVER
DISCRIMINATOR
1 0 0 1 1 0
MODEM
OUTPUT
BIT STREAM
1 0 0 1 1 0
DECODE
SURFACE UNIT
CLOCK
1 0 0 1 1 0
LIM
∫
1 0 0 1 1 0
CLOCKED
COMPARATOR
1 0 0 1 1 0
PHASE
LOCKED
LOOP
MODEM

FIGURE 5

APPENDIX I

ACOUSTIC COMMAND AND TELEMETRY LOGIC

General Description

This logic operates in conjunction with the EDO acoustic communications equipment to provide the means for diagnostic data telemetry and for remote commanding of operations within the instrument package.

The EDO system will transmit a maximum of 10 commands from ship to instrument, and can transmit either ping pulses or digital data from instrument to ship. Digital data is transmitted by selecting one of two possible transmission frequencies, each of which correspond to a logic level. The surface receiver then amplifies the signal and outputs logic levels corresponding to the frequency received.

The acoustic command and telemetry logic has three functions:

1) Interfaces the subsurface receiver and the instrument.
2) Keys the subsurface transmitter to send ping codes to verify correct reception and completion of commands.
3) Selects, digitizes, formats, and encodes data for transmission.

The logic is set up to command 16 different functions. Since the EDO system can transmit only 10 distinct commands, a double command arrangement must be used. This is done by dividing the commanded functions into two sets of eight. A set is selected by transmission of EDO command number 1 or 2. Once a set has been selected, a particular command function within this set is initiated by transmission of one of the EDO commands 3 through 10. Once the logic has been switched to a particular set, it will remain in it until the other set is commanded; i.e., a double command code transmission need be made only when changing sets.

Following is a list of the command functions and their purpose.

EDO Command No.	Name and Purpose
1 - 3	RELEASE - Fires an explosive cable cutter which separates the instrument package from its ballast.
1 - 4	SPARE - Not used at present.
1 - 5	AUTO RECLAMP - Clamps the tiltmeter mass in preparation for instrument release.
1 - 6	SECONDARY DIAGNOSTIC - Transmits following data to the surface: 1) Ambient temperature 2) Gravimeter temperature 3) & 4) Tiltmeter outputs 5) Tide filter output 6) Philtre (seismic) filter output 7) Gravimeter output
1 - 7	ENGINEERING DIAGNOSTIC - Transmits following data to the surface: 1) Gravimeter output 2) Recorder operation verification 3) Capsule pressure 4 - 12) Battery voltages
1 - 8	GRAVIMETER DIAGNOSTIC - Transmits seven words of gravimeter output.

EDO Command No.	Name and Purpose
1 - 9	SEND ALERTS - Transmits any codes which are on in alert code generator.
1 - 10	MASTER RESET - Resets all command outputs from the logic. Used in case of a lockup in an operation.
2 - 3	UNSTOP GIMBALS - Unlocks backup clamp on gravimeter gimbals.
2 - 4	AUTO BEGIN - Performs following sequence: 1) Undamps gimbals (allowing gravimeter to level) 2) Clamp gimbals 3) Unclamp tiltmeter mass
2 - 5	LEVEL UP COARSE - Roughly zeroes gravimeter output by moving sensing plates in one direction. Moves a fixed amount, waits, then transmits gravimeter output.
2 - 6	LEVEL DOWN COARSE - Same as above, except that plates move in opposite direction.
2 - 7	LEVEL UP FINE - Accurate zeroing of gravimeter by tilting slightly in one direction. Moves a fixed amount, waits, then transmits gravimeter output.
2 - 8	LEVEL DOWN FINE - Same as 2 - 7 above, except motion in opposite direction.
2 - 9	RECORD AZUMITH - Triggers a unit which photographically records instrument azimuth and tilt.
2 - 10	START TAPE - Resets and starts data logger.

In all but two cases a complete command cycle consists of:

1) Transmission of a "command received" alert code, which is unique to the particular command, to indicate proper reception.
2) Performance of the commanded operation. In the cases where data transmission or a short operation are involved, this does not begin until the "command received" alert code has been sent.
3) Transmission of an "operation complete" alert code. This is the same as the "command received" alert code, but is transmitted twice as fast.

The two exceptions are MASTER RESET and SEND ALERTS, both of which transmit just one alert code, and perform their operation simultaneously with the alert code.

All data transmission is done on command. Data for a particular transmission sequence is selected by a programmable multiplexer. This multiplexer has a 24 channel capability and may be hardwire programmed to scan up to four different sequential sets of any length from the 24 inputs.

The analog output of the multiplexer is converted to 12 bit digital words. Each data channel is assembled in parallel with a sync word, a channel I.D. number and a parity bit. This is then unloaded through a biphase encoder and transmitted to the surface at a 102 B.P.S. rate. At the surface a Coded Communications Corp. pulse code modulation decommutator converts the encoded data back to a simple digital format, separates out the channels along with their respective I.D. numbers, and stores them in a memory. The data may then be read out from the memory at leisure.

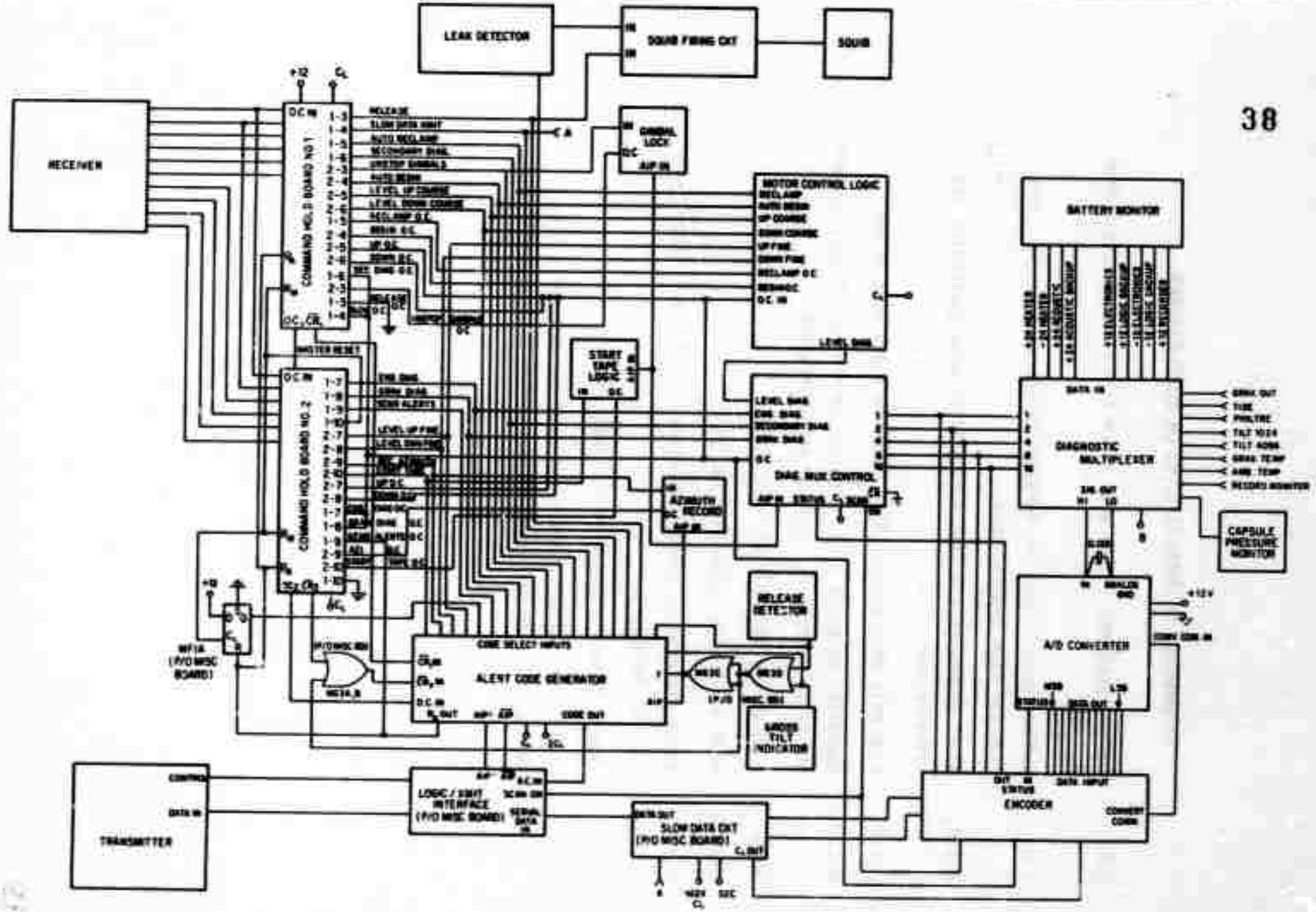

ACOUSTIC COMMAND and TELEMETRY LOGIC

EXPLANATION OF ABBREVIATIONS ON BLOCK DIAGRAM

C.R.	Command Received - High when there is a command output from receiver.
C.H.	Command Hold - High for duration of operation cycle. One line for each command code.
A.I.P.	Alert In Progress - High during alert code generation and transmission.
A.I.P.'	High only when an operation complete alert code is on.
O.C.	Operation Complete - Short pulse (generally 1/2 sec) to mark end of an operation. One for each operation.
SCAN	High during multiplexer scan cycle.
STATUS	High during A/D conversion (80 μs).
R_A	Reset produced by alert code generator at end of code cycle. 1/2 sec duration.
R_M	Master Reset, produced on external command.
C_L	1 Hz clock. Other clocks indicated by frequency, e.g. - 1024 C_L is 1024 Hz clock.

APPENDIX II

BENTHIC ARRAY INSTRUMENT PACKAGE SPECIFICATIONS

Depth Limit:	16,400 feet
Materials:	7178 Alcoa aluminum hemispheres hard anodized and epoxy painted
	7178 aluminum center ring - hard anodized
Bottom Time Limit:	3 months maximum
Stored Capacity	1,000 amp-hours at 12 volts
Release:	Explosive cable cutter activated by a surface command
Weight:	Approximately 1600 lbs. including stand, batteries and internal instrumentation

RECORDING SYSTEM

Word Length:	12 bits
Dynamic Range:	1:4096
Input Voltage:	$\pm$ 10 v.
Least Count:	5 mv.
Input Channels:	8
Storage Capacity:	2.5×10^6 samples on 2400 ft. reel 29 days at 1 sample/second
Maximum sample rate:	50/second by internal modification
Nominal sample rate:	1/second
Power Requirements:	12 v., 12.8 amp-hr. per reel of tape, independent of stepping rate.

ACCELEROMETER AND TILTMETER

Accelerometer Instrumental Noise:

Less than 5×10^{-23} $(\Delta g/g)^2$/cph (1 cph to 1 Hz) for UCSD Camp Elliott, the land based unit at the seismic station. At 25 sec. period thru .02 Hz bandwidth digital filter, the noise is less than 15 millimicrons. (M_s = 2.4 at Δ = 30°).

Accelerometer Response: Flat to acceleration (DC to .2 Hz)

Power Requirements: 25 ma at 12 v.
25 ma at -12 v.
50 ma at 48 v. for temperature control

Analog Outputs

Tide Filter:

Response, D.C. to 1 cpm (3 db pt.)

Full Scale, 2×10^{-6} $\Delta g/g$

Least count, 5×10^{-10} $\Delta g/g$

Seismic Filter:

Response, 1 cph to .1 Hz (3 db pts)

Full Scale, 2×10^{-8} $\Delta g/g$ (in pass band)

Least Count, 4×10^{-12} $\Delta g/g$ (in pass band)

Tiltmeter:

Full Scale, 1 degree on 2 axes

Least Count, 2.5×10^{-4} degrees

ACOUSTIC COMMAND SYSTEM

Range: 7 - 10 miles

Number of Commands: 10 commands (expandable)

Digital Diagnostic Telemetry

- Transmission Rate: 100 bits/second, 4 readings/second
- Voltage Resolution: 5 mv
- Error Rate: To be determined from ocean testing
- Range During Transmission: Must be nearly over the capsule

Backup VCO Diagnostic Telemetry

- Transmission Rate: .5 bits/second, each bit transmitted as an alert code recognizable by ear.
- Voltage Resolution: 5 mv.
- Error Rate: To be determined from ocean testing.

Release: On command from surface

Backup Release: At a preset time from 0 to 9999 hours (Completely self-contained)

Power Requirements: 2 ma at 48 v. quiescent
2 amps at 48 v. when transmitting

Part III

ADVANCED STUDIES IN NEARSHORE ENGINEERING

Co-Principal Investigators

Dr. Douglas L. Inman
Phone (714) 453-2000, Extension 1175

Dr. William G. Van Dorn
Phone (714) 453-2000, Extension 1179

ADVANCED OCEAN ENGINEERING LABORATORY
Sponsored by
ADVANCED RESEARCH PROJECTS AGENCY
ADVANCED ENGINEERING DIVISION

ONR Contract N00014-69-A-0200-6012

ADVANCED STUDIES IN NEARSHORE ENGINEERING

TABLE OF CONTENTS

VI LIST OF FIGURES

I PROJECT SUMMARY

The studies in Advanced Nearshore Engineering which proceeded during the reporting period have been directed towards understanding the basic factors governing the behavior of sediment transport phenomena. Insight gained through these studies has enabled us to suggest a variety of new techniques for the beneficial control of sand transport phenomena in harbors and nearshore waters. These techniques include: phase-dependent roughness elements for sediment transport control; structures which could effectively control nearshore circulation; and, new technology such as the crater-sink sand transfer system.

The vigorous interplay of waves, currents, and erosion products from the land involve complex processes which result in intense interactions. However, it has been shown that their driving forces are principally systematic and of low frequency. These low frequency forces are masked by a high level of background noise which is associated with the process of energy dissipation. The reduction of these driving forces and their interactions into first principles that can be applied to practical problems has been the guiding principle of these studies.

The Velocity Field in Breaking Waves

This portion of the nearshore engineering program was originally proposed as a comprehensive laboratory and field investigation of the velocity field and momentum flux within the breaker zone formed by a succession of waves approaching a sloping beach. We have been concerned not only with the motions occurring within individual waves, but also with the transient surging motions and mean vertical circulation that results from mass transport over the sloping bottom. Because there is no adequate theory that describes motions in this regime, nor any previous

experiments of significance, our objectives have been to conduct careful measurements of enough variables to reasonably define these fields, and to present the results in parametric form as a basis for further analysis and for direct engineering use.

Within the past six months we have completed the laboratory phase of this investigation, comprising over 7000 individual observations of wave height, bottom pressure, orbital velocity, and particle displacement at nine stations for four wave periods and three beach slopes. All data have been reduced to digital format and the pertinent flow parameters evaluated. While some of our early results are presented below, the volume of useful data is so large and its potential uses so diverse, it will be published as a special report under this contract.

In order to continue with similar measurements under natural surf conditions (field phase), we have also designed and constructed a "portable" instrument platform that can be carried piecewise to any point and rapidly assembled without tools by two men. The platform is 15 feet high, and contains all sensing and calibration equipment to simultaneously measure surface elevation and the horizontal and vertical components of wave orbital velocities at any depth as functions of time. The platform, and its accessory recording instrumentation and cabling, has been fully tested and calibrated. However, owing to the loss of our entire technical staff (through injury or termination), we have so far been unable to undertake actual field measurements. It is hoped to continue this work next year, if our somewhat-revised program priorities permit.

Field and Laboratory Study of the Water-Sediment Interface Under Wave Action

This portion of the nearshore engineering program has resulted in a concentrated study of the mechanics at the water-sediment interface,

and the development of new techniques for the control of transport phenomena at the interface. The studies have included: (a) analysis and comparison of wave-induced boundary layer theories with field and laboratory investigation over smooth beds and beds of differing roughness; (b) photo interpretation and analysis of particle movement in the vicinity of the vortex sublayer at the water-sediment interface; (c) measurement and analysis of natural sand ripples at various localities, including nearshore waters of the Gulf of California; and, (d) construction and preliminary testing of techniques of constructing phase-dependent roughness elements for use in the hydraulic laboratory wave tanks and in the field.

Having demonstrated feasibility of controlling the transport of sediment by means of phase dependent roughness elements, we now wish to develop this theme and proceed with the attractive prospects in their practical application. Therefore concentrated efforts to optimize the design of phase-dependent roughness elements and develop suitable prototype elements is the subject of the coming year's program.

II. Velocity Field in Breaking Waves

A. Objectives

a) Laboratory Phase

1. Under controlled and reproducible conditions, representative of the normal range of prototype waves and beach slopes, to make measurements of important flow parameters within periodic waves breaking on uniform slopes, so as to reasonable define their mass, velocity, and momentum fields -- both before and after breaking.

2. To present the results of these measurements in general parametric form for engineering uses; such as, the design of structures and/or vehicles intended for operation in a breaking wave environment, the design of devices for controlling sediment erosion or deposition, and as a basis for improving theoretical understanding of breaking wave behavior.

b) Field Phase

To perform similar measurements under a range of natural wave conditions, so as to evaluate scale effects, perturbations introduced by normal wave variations, and three-dimensional aspects of mean flow not amenable to laboratory study.

B. Present Status

Experiments under the laboratory phase were completed in September, 1971. The last three months of this contract year have been devoted to processing the

considerable bulk of numerical data in digital format suitable for rapid analysis, and writing FORTRAN programs for presentation of these data in parametric form. This work is now completed, and we are presently generating curves of wave properties and comparing them with existing theoretical models. Because of the volume of data and because the results represent a considerable breakthrough in wave dynamics, a supplementary report will be published within the next three months.

During the past six months, the field phase of our study has proceeded with the design and construction of a portable wave-measurement platform that can be transported and assembled in the surf zone by two men. The platform, together with accessory instrumentation was completed, tested, and calibrated by the end of October. However, the above-cited loss of personnel, and the impossibility of replacing them near the termination date of a contract not officially renewed, has delayed our intended field measurements. It is hoped that this program can be continued next year, under Dr. Inman's supervision.

C. Measurements

Instrumentation and procedures for the laboratory measurements are fully described in our report of June 30, 1971. Outlined below are the measurements undertaken with reference to Figure 1 for orientation.

1. Surface elevations were obtained by three independent systems:

   a) Digital wave staffs
   b) Bottom pressure
   c) Strobe photography referenced to ε 10-cm orthogonal grid.

2. Horizontal flow velocities in both forward and backward directions were recorded by constant-temperature hot-film probes, and also by strobe photography of neutral-density particles.

3. Vertical flow velocities were obtained from strobe photography of suspended particles and free surface changes between flashes.

4. Slow circulation velocities were inferred from progressive deformation of vertical dye streaks photographed at integer multiples of incident wave period.

5. Wave runup was recorded on a digital slope staff.

6. Turbulent velocities within breakers were also recorded by the hot-film probes, although only the extreme ranges were reported in our data.

7. Flow trajectories were obtained by streak photographs of small particles.

8. Accelerations, in some cases, could be determined from incremental particle displacements, or from the rates of

change of pressure and surface elevation.

9. Phase velocities were observed by timing the passage of individual phase maxima between two wave staffs set 15 cm apart.

Our measurement system was designed to be heavily redundant, and often the best estimates of a particular parameter could be obtained only by careful comparison of independent measurements. As a result, our raw data file alone, comprising transient (five waves) and steady state histories of four wave periods incident upon each of three beach slopes, runs to 176 pages of computer printout.

D. Preliminary Results

Being now only midway of our parametric analysis of the data, it is difficult to generalize results, except to say that most of these are new and unprecedented. At a recent Advanced Seminar on Waves and Beaches, eminent authorities were gratified to find that someone had made a significant breakthrough in this very difficult field, and strongly commended our methods and progress. Perhaps the best approach is to first give a qualitative description of the breaking process, as observed in our experiments, and then to point out the effects of changing wave amplitude, period, and beach slope. Lastly, we shall give some specific examples of these changes and the range of magnitudes of important flow parameters.

As qualitatively well established, periodic waves advancing into shoaling water undergo progressive transitions of waveform. In the linear, small-amplitude approximation, the wave period remains constant and both wavelength and phase speed decrease monotonically with water depth. Wave height first decreases

slightly as the group velocity undergoes a transient maximum, and then increases continuously until each wave surges up the shore slope without breaking, and is optically reflected.

Waves of finite height behave somewhat differently in that wave crests are accelerated--and troughs decelerated--relative to small-amplitude waves, such that the crests become narrow and peaked while the troughs are broadened and flattened, and the mean surface elevation is depressed slightly. As in all of our experiments, if the deep-water wave steepness exceeds a limiting value given roughly by $(2\pi H/gT^2)^{\frac{1}{2}} > 0.23S$, where S is the beach slope, the waves will break, and thereafter decrease monotonically to zero height at the shoreline. Because breaking involves a significant net shoreward mass transport, the average surface elevation within the surf zone will similarly increase shoreward to a maximum at the shoreline (wave setup). Shoreward transport is strongest at the surface, and mass continuity is maintained by subsurface return flow, which rises at the breaker point to complete the circulation cell. Under some period and slope combinations, there may be several such cells within the breaker zone (Fig. 2).

In concert with the establishment of the breaker zone cell(s), a much weaker counter-rotating circulation appears seaward of the breaker point; comprising a relatively strong shoreward flow at the bottom, rising at the breaker point with a sluggish offshore surface transport that is strongest at mid-depth.

In addition to these quasi-steady state phenomena, other periodic flow perturbations often appear--even after a long continued succession of identical waves. Most of these

perturbations can be associated with normal mode oscillations (standing waves) of the wedge of water inshore of the break point; of the wedge inshore of the slope toe; and of the entire volume of water within the wave channel. Other perturbations appear to be associated with interactions between these modes, but are not so easily identified. All act to produce local variations in the heights and orbital velocities of individual waves that--in turn--are reflected by continued excitation of the normal modes. Except over a slope of 0.02, where most of the incoming wave energy is dissipated by gradual, spilling breakers, we have found it difficult or impossible to maintain a steady-state equilibrium free of secular perturbations.

While the flow regime is most easily observed under steady conditions, natural breakers continually vary in height, frequency, and to a lesser extent, direction. Therefore, we have paid particular attention to the transient motions within the breaker zone associated with the arrival of the first 3-5 waves of a uniform series. Because the first waves propagate in relatively undisturbed water, and because it takes 40-50 waves to establish equilibrium conditions, the cumulative mass transport of the early waves results in a vigorous initial surge. Succeeding breakers, traveling in relatively deeper water, often overtake their predecessors, such that the initial surge rises to a shoreline elevation two or three times as high as the equilibrium wave setup, and is reflected as a broad intumescence that propagates back and forth along the channel, taking 4-5 minutes to die away. The duration of this surge is roughly equal to the time required for breakers to travel from the initial break point to the shore

and back again, both duration and uprush are related to beach slope, wave height, and wave period.

The reflected surge--and its following trough--strongly perturb succeeding waves and the points at which they break. We have observed local variations as high as 30 percent in wave height and orbital velocity during its passage. Since natural surf zones comprise a continuous succession of such surges--roughly one for each wave group--it is evident that any description of individual wave properties must necessarily be statistical, as these effects are not distinguishable from surge motions. However, in the laboratory channel, the surge preserves its identity and, to the extent that its interaction with individual waves can be considered linear, its history provides some clue to the transient momentum flux. Similarly, the equilibrium wave setup is a measure of steady-state momentum flux. Taken together, we hope to form some opinion about the energy balance within the breaker zone.

The general trend of transient wave behavior is illustrated in Figs. 3-5 for waves of four different periods incident upon uniform slopes of 0.02, 0.04, and 0.083, respectively. Each experiment consists of a train of five waves of constant initial amplitude in uniform water depth of 36 cm. The solid curves are envelopes of maximum (crest) and minimum (trough) elevation as functions of distance from a standard reference station (A) 10 m. from the wave generator. The dashed lines similarly indicate maximum horizontal particle (orbital) velocities at the crests and troughs. The shaded zones give the range of turbulent velocities after breaking. In all cases, points A - F are observation stations, adjusted so that station D is located at

the point of first breaking inception, and E (by trial-and-error) at the point of maximum crest particle velocity.

In almost all cases, surface elevation and wave height increase relatively smoothly past the breaking point to station E (fully-developed breaking), and then diminish smoothly--but more rapidly--to the shoreline. Because these are early waves, uprush is small, and is not shown in these figures.

In contrast, horizontal particle velocity first increases in proportion to wave height until the wave has advanced over the slope from 70-80 percent of the distance from the slope toe to the breaking point--beyond which it increases very rapidly. Subsurface velocities (not shown) increase similarly, and the vertical velocity profile beneath the crest is roughly parabolic. At point D, particle velocities approach the phase speed, and at E often substantially exceed it. Strobe photos at this point show that a jet of water develops on the upper lip of the crest and plunges forward and downward, producing a pair of counter-rotating vortices that quickly degenerate into random turbulence. This vortex motion is manifested by the double humps in the shaded turbulent zones for periods of 3.4 and 4.8 seconds in Fig. 4.

Because all waves were generated at the same paddle stroke setting, the shortest-period waves are initially highest, and break earliest on each slope. However, this tendency is reversed for the 4.8 sec. waves, despite the fact that their heights and particle velocities are lower than those for the 3.6 sec. waves. However, the differences are small and may not be significant.

To a rough approximation, the breaking heights and maximum particle velocities are the same for each wave period, independent

of initial height or beach slope. Both values were largest for the 1.6 sec. waves and decreased fairly regularly by about 35 percent for 4.8 sec. waves. On a model:prototype scale of 1:16, the corresponding maximum stagnation impact pressures were about 550 and 330 lbs/ft^2.

E. Field Measurement Program

Figure 6 shows a perspective view of the portable platform constructed for measuring wave heights at orbital velocities in the surf zone. A 15 ft. triangular tower is bolted to a trapezoidal, angle-iron base with ball-lock pins for rapid assembly. Various instrumental components include:

1. Two digital wave staffs capable of recording waves up to 10-ft. high.
2. A pair of oppositely-directed hot-film velocity probes mounted on a sliding head that can be raised and lowered to any point within a wave, and raised clear for calibration. The probe assembly can be rotated to record either vertical or horizontal velocities up to 6 m/sec.
3. An operator's seat and watertight enclosure for accessory electronics, and a six-conductor signal cable connected to a shore recorder.
4. A pressurizing cylinder, flow reservoir, and calibrating flow nozzle for performing rapid calibrations of the film probes. Flow pressure and probe output are simultaneously recorded ashore.

This assembly has been fully calibrated and field tested, but owing to late-stage personnel problems, has not been employed in actual field measurements.

F. FUTURE WORK

Upon completion of our special report covering our laboratory investigation of breaking waves, it is hoped that Mr. Tsang will be able to continue with field measurements under Dr. Inman's supervision. Dr. Van Dorn is now commencing laboratory and field investigation of deep-water wave breaking under a separate proposal to this contract. This study will be conducted jointly with Prof. R. E. Davis as co-principal investigator, and is concerned with the mechanism whereby wave breaking occurs by virtue of wave-wave interactions in a random sea.

III. FIELD AND LABORATORY STUDY OF THE WATER-SEDIMENT INTERFACE UNDER WAVE ACTION

In order to understand the deformation and sand transport processes which occur on a sand bottom influenced by surface gravity waves, it is necessary to know the boundary layer properties - thickness, velocity profile, flow regime - which have a bearing on these processes. A mathematical solution is difficult because of the non-linear interactions which occur under oceanic conditions: other investigators have attempted to describe the boundary layer by starting with the theory for laminar oscillatory motion over a smooth plate, and then modifying it to include both turbulent flow and rough bottoms. Although the basic smooth plate theory is well developed, the further modifications are empirical.

This report considers the details of proposed theoretical models and previous laboratory work and then observes the occurrences under both laboratory and real oceanic conditions in order to determine to what extent theory, laboratory, and real world might differ.

A. Boundary Layer Over a Smooth Bottom

Airy wave theory states that the fluid motion in the water column when a wave passes is governed by the following relations,

$$u = a\sigma \frac{\cosh k(z + h)}{\sinh kh} \cos(kx - \sigma t) \qquad (1)$$

$$v = a\sigma \frac{\sinh k(z + h)}{\sinh kh} \sin(kx - \sigma t) \qquad (2)$$

where u is the horizontal orbital velocity; a is the wave amplitude (at the surface); $\sigma = 2\pi/T$ is the radian frequency; $k = 2\pi/L$ is the wave number; T is the wave period; L is the wavelength; x is the horizontal coordinate; z is the vertical coordinate, positive upward

from the water surface; t is time; h is the water depth; and v is the vertical orbital velocity.

Examination of these two relations show that as the bottom interface ($z = -h$) is approached, the vertical velocity diminishes (which it must do to satisfy the condition that no flow can go across the solid boundary) such that the flow becomes purely horizontal. The horizontal bottom velocity is given by

$$u_o = \frac{a\sigma}{\sinh kh} \cos(kx - \sigma t) \tag{3}$$

The maximum velocity u_m attained during any given wave passage is thus given by

$$u_m = \frac{a\sigma}{\sinh kh} \tag{4}$$

The maximum horizontal displacement d_o of a particle during a wave period is given by

$$d_o = \frac{H}{\sinh kh} = \frac{2a}{\sinh kh} \tag{5}$$

This reasoning establishes a simple sinusoidal velocity field at the sediment interface with maximum velocity u_m and back-and-forth displacement d_o. Work by Wiegel (1964) and also Le Mehaute (1968) have shown that these equations are accurate to within 10 to 15% of actual experimental values, making Airy theory a quite good representation of the bottom velocity for short period waves, and a reasonable approximation for longer period waves.

Descriptions of the vertical velocity profile caused by oscillatory flow over flat bottoms date back to Stokes (1851). Stokes solved the problem of an oscillating plate with a stationary fluid above it. Lamb (1932) showed that with a suitable change of the coordinate system the same solution applied to a sinusoidally oscillating fluid above a flat plate. His solution has been used and modified by several authors to apply to wave generated water motion over a solid surface. Longuet-Higgins (1953) solved the Navier-Stokes Equations for two-dimensional wave motion in a constant depth of real fluid over a smooth bottom in order to get the mass transport and boundary layer velocity. His solution assumes that the convective acceleration term is negligible, but that the viscosity term is retained. This "conduction solution" is theoretically restricted to laminar flows in which $H/\delta << 1$ where H is the wave height and δ is the boundary layer thickness. Russell and Osorio (1961) demonstrated that the mass transport velocity from their flume experiments fit the conduction solution even though the flow was not laminar and $H/\delta \geq 1$. Longuet-Higgins (1961) showed how the conduction solution might also apply to a turbulent boundary layer and, in fact, is valid independent of the functional form of the viscous coefficient.

Considering initially the laminar case, the horizontal orbital velocity component in the boundary layer u is related to the component just outside the boundary layer u_∞ by

$$\frac{\partial u}{\partial t} = \frac{\partial u_\infty}{\partial t} + \frac{\partial}{\partial z}\left(\nu \frac{\partial u}{\partial z}\right)$$

where ν is the kinematic viscosity and z is measured vertically upwards from the bottom. For constant viscosity the solution to

equation (6) is

$$u = u_\infty - u_m \exp(-z/\delta) \cos(\sigma t - kx - z/\delta) \qquad (7)$$

where $\delta = \left(\frac{2\nu}{\sigma}\right)^{\frac{1}{2}}$ is the boundary layer thickness. Thus, for a 10 second wave traveling over a smooth bottom in 20°C sea water δ would be about 2 mm. Figure 7 shows u for different phases during a single wave period. One important aspect of equation (7) is that there is a phase lead of the boundary layer velocity over the potential layer velocity which varies as a function of the height above the bottom. Figure 8a shows this phase change.

B. Boundary Layer Over a Rough Bottom

Sleath (1969) constructed an instrument which measured fluid velocity through the deflection produced in a thin glass wire under axial tension by a current flowing normal to its longitudinal axis. The small size of the instrument permitted direct measurements of the velocity profile in the boundary layer. Using this instrument Sleath (1970) studied the laminar boundary layer formed by progressive waves over a flat bottom. In addition to a smooth solid bottom he used a flat bed of medium sand (M_d = 389μ), a flat bed of coarse sand (M_d = 1030μ) and a flat sheet with a layer of coarse sand (M_d = 1030μ) glued to it. One of the objectives of the last two was to see if permeability influenced the velocity profile: in his experiments no effect was observed. He found that the boundary layer velocity profile fitted a modified form of equation (7) above,

$$u = u_\infty - A \exp(-z/c\delta) \cos(\sigma t - kx - z/c\delta) \qquad (8)$$

where $1.0 < c < 1.8$. Values of 1.0 for c were obtained with the smooth bottom and medium sand bed, and values of 1.8 were obtained from the two coarse sand beds. He also observed that for the coarse sand beds the phase-height relationship did not follow the curve in Figure 2a, but reached a maximum value at $z = c\delta$ and decreased again toward zero for $z < c\delta$ (Figures 8b, 8c). The phase-height relation for the medium sand bed more-or-less followed the smooth bottom relation (Figure 2d).

Sleath also noted that there was a periodic formation of eddies behind bottom roughness elements (sand grains) and that these eddies were thrown up into the water column as the flow decelerated. He felt that these vortices were responsible for the modification of the z/δ term. It should be noted that inclusion of the c term is the same as using an amended kinematic viscosity ν' such that

$$\nu' = c\nu$$

Further, he felt that the onset of turbulence in the boundary, which was described by Manohar (1955), could be due to the formation of eddies rather than a random process (Mahohar conducted his studies by dropping potassium permanganate into the water and observing the conditions under which the dye streak lost its integrity).

Other investigators have tried to solve the wave induced boundary layer problem for turbulent flows over both smooth and rough solid bottoms. Jonsson (1963) derived equations for the bottom friction factor and for a boundary layer thickness in the rough turbulent case by assuming that the velocity profile was logarithmic. He verified his equations using a propeller flowmeter (5 mm diameter). Johns (1970) proposed that

the velocity in the boundary layer could be given by

$$u = u_\infty(X)\left(1 - F(z')\right)e^{i\sigma t} \tag{10}$$

where $F(z')$ satisfies

$$\frac{d}{dz'}\left(\epsilon \frac{dF}{dz'}\right) - 2iF = 0 \tag{11}$$

and $z' = z/\delta$ is the non-dimensional distance from the boundary, and the other terms are as described before.

Johns solves equation (11) numerically and gives plots of real and imaginary parts of $F(z')$. Values from this plot have been used to compute the velocity as described by equation (10). Figure 9 compares the velocity profile obtained by this method with a profile obtained by Jonsson (1963). If the modified theory of Johns can be fitted to the Jonsson data, a possibility exists to predict the flow field over natural and artificially controlled rough bottoms.

Kajiura (1968) proposed a three layer boundary layer in which the form of the eddy viscosity ϵ_z changed between the three layers. The form of ϵ_z also depended on whether the bottom was hydraulically rough or smooth. The appropriate form of ϵ_z is substituted into equation (12) and velocity profile, phase difference, and shear stress criteria are generated.

$$\frac{\partial u}{\partial t} = \frac{\partial u_\infty}{\partial t} + \frac{\partial}{\partial z}\left(\epsilon_z \frac{\partial u}{\partial z}\right) \tag{12}$$

The solutions of Kajiura seem to work fairly well, within 5 to 10% over flat bottoms, but have the limitation of a rather unrealistic eddy

viscosity "layering" and a failure to describe the velocity profile above surfaces with any appreciable amount of bottom roughness, i.e., ripples.

Kajiura's theoretical results were tested by Horikawa and Watanabe (1968) using a hydrogen bubble technique to obtain the velocity profile in the boundary layer. They felt that the Kajiura solution fit their data fairly well (1 - 5% difference between experiment and theory), but they questioned the arbitrary nature of some of the parameters Kajiura used to define his three sublayers. They also pointed out that Kajiura's solution did not provide for a method of determining a z = 0 line for rough bottoms. This problem became apparent when they used solid ripple forms on the bottom.

C. Vortex Sublayer

Inman and Bowen (1963) studied sediment transport on a fine sand, wave-generated ripple bed. As part of their study they traced the paths of neutrally buoyant particles over many wave oscillations and in different parts of the water column (Figure 10). Particles behaved according to potential wave theory when their elevation z was greater than about a ripple wavelength above the bed. Particles closer to the bed followed a more complex path. During passage of the wave crest (Figure 11A) and of the wave trough (Figure 11C), the particles moved horizontally over the ripple crests and were caught in a vortex in the lee of the ripple crest. When the flow decelerated, the vortex, which had been suppressed by the strong horizontal flow was released and rose above the bed to a height of the order of a ripple wavelength (Figure 10D). This rising vortex carried sediment with it and the sediment is then transported horizontally by the accelerating flow until it settles out by gravity.

D. Previous Field Work

A forerunner of the system used in the present study was developed some years ago at the Scripps institution of Oceanography. Underwater motion pictures of particle motion against a grid gave measures of the velocities of wave suspended sand grains in the bottom 5 cm over a rippled sand bed. The method consisted of taking 16 mm motion pictures of motion relative to a fixed grid. Occasionally the vortex release during velocity reversal was observed. Since the camera housing had to be buried into the bottom, the resulting scour limited the value of the procedure. The procedure was improved by synchronizing the motion picture frames with measurements of wave pressure and water level (Koontz and Inman, 1967, Figure 17). The improved technique showed that two mechanisms operated to produce the suspension of sand. During the parts of wave period when the velocity reversals occur, the vortex is released and carries sand above the ripple crests where it is available for transport. During times of high horizontal velocity there is general sand movement called "sheet flow". In this situation some minimum velocity is necessary to start the sand grains moving. Koontz and Inman (1967, p 33) on the basis of four photographic sequences, suggested a velocity on the order of 50 cm/sec was necessary before this "sheet flow" mechanism became important.

E. Laboratory Study

Observations in the nearshore off Scripps Pier support the eddy theory: dye streaks maintained their integrity as they moved up the upstream side of a ripple, but were dissipated upon reaching the crest and lee side, where an eddy is observed to form. The next step in the study of the fluid motion caused by wave action is to delineate the development and movement of eddies and their influence on the formation of sediment ripples and sediment transport.

From the nature of oscillatory flow, the ripples generated under the action of surface gravity waves usually tend to be symmetrical in shape. The onshore and offshore faces of the ripple have similar slopes. In unidirectional flow, such as in rivers, the ripples generated are asymmetrical with the upstream side of the ripple crest having gentle slopes, and the downstream or lee side having steep slopes. Inman and Bowen (1963) observed that for certain conditions of wave and superimposed unidirectional currents, the sediment could be made to move in an upwave and upstream direction. They interpreted the phenomenon as follows. When asymmetrical bottom forms are subjected to oscillatory wave motion, a net transport of sand occurs in the direction that is out-of-phase with the velocity which produces the largest vortex. The velocity caused by the passage of the wave produces an intense vortex over the steep lee face which traps and suspends sediment. After which the reversal in direction of orbital motion causes the suspended sediment to rise and then to be carried in the direction opposite to that causing the vortex. During this reversed phase of the fluid motion, another but smaller vortex is produced over the gentle face which also traps and suspends a smaller amount of sediment. On a succeeding reversal, this smaller amount of sediment is carried in the direction faced by the steep face. In this manner the asymmetrical sloping sides of the ripple cause different, but characteristic eddy formations, and a prevailing direction for the net transport of sediment which is dependent upon the relation between the phase relation between the on-and-offshore velocities of the formation of the most intense vortex.

Experiments were conducted in the wind-wave tank of the Scripps Hydraulics Laboratory to extend the findings of Inman and Bowen. The

tank is 8 feet by 8 feet by approximately 150 feet long. Asymmetrical bottom forms were cast with plaster of paris and placed on the bottom of the wave tank. The motion of particles placed on the forms was then observed. The first studies were conducted in the small (50 cm wide x 100 cm deep) wave tank. It was observed that regardless of which way the forms were placed into the tank, sediment was transported in an upwave direction. This can be attributed to the fact that in the wave tank, along the bottom, the general direction of drift is in the downwave direction, compensation for the drift is provided by a return flow in the upwave direction above the bottom. The waves which were being generated were of sufficient intensity to throw the sediment up into this return flow layer, and hence it was carried upwave. It was also noted that in the small tank, the entire water column above the ripple forms was turbulent. This was observed by introducing potassium permanganate crystals into the tank above the forms. The experiment was relocated into a larger tank in order to overcome the return flow and turbulence problems.

Four sets of ripple forms were cast. Their dimensions are summarized in Table 1. During the tests the varied parameter was the orbital diameter, d_o, which was varied by changing wave height. d_o/λ vs. steepness was then plotted. For the forms A and D with steepness 0.15, the direction of sediment transport was always out-of-phase with the most intense vortex. This was also the case for the 0.3 steepness form, B, for low values of d_o/λ. However, for the rest of the test cases the direction of sediment transport was in-phase with the most intense vortex. The reason for these reversals is unknown. Even though the direction of sediment transport was reversed, the sediment could still be directed either up or downstream by reversing the roughness elements. By placing

asymmetrical ripple forms into the nearshore environment, the direction of sediment transport apparently may now be altered or controlled.

F. Field Work

Noteworthy results were obtained by the following demonstration. The ripple form used was form "D". The form was in two segments with three identical asymmetrical ripple wavelengths in each segment. The segments were arranged as shown in Table 2. For the first arrangement, particles were placed on the downwave end of the test section. The direction of particle transport was out-of-phase with the intense vortex and the particles moved upwave and off of the forms. In the second arrangement, the forms were turned around, and the particles were placed on the upwave end of the test section and the particles moved downwave and off of the forms. In the third arrangement, only the upwave form was turned around and a group of particles was placed in the center of the forms. Approximately one-half of the particles moved upwave and the other half of the particles moved downwave, both groups moving completely beyond the forms. For the fourth arrangement, both forms were turned around and groups of particles were placed on either end of the test section. In this case, both groups of particles moved toward the center of the section and remained in the center. This series of demonstrations show that: (1) the direction of transport is not determined by currents in the wave tank; and, (2) end effects are not important in the direction of motion of the sediment. From these results, it may be stated that the direction of motion of the sediment is determined by the asymmetrical ripple forms.

In an attempt to extend the data for asymmetrical ripple forms, the A forms were placed in the nearshore environment offshore of Scripps Pier in approximately 10 meters of water with their crests roughly parallel to shore. The forms were first positioned so that the steep side

faced offshore, and the forms were covered with about 3 cm of sand. The maximum d_o observed was about 120 cm for a d_o/λ ratio of 6.0. The average d_o observed was about 45 cm. The sediment on the ripple forms appeared to move only when the larger waves (with an implied larger d_o) were advancing. After an interval of 5 minutes it was observed that the sand seemed to be being removed at the seaward end. The sand appeared to be being transported in the onshore or out-of-phase direction. The forms were then reversed, and the same observations repeated. In this case, the forms appeared to be clearing at the onshore end. Again the sand was transported in the out-of-phase direction. It appears that these asymmetrical ripple forms may be used to manage the direction of sediment transport in the nearshore environment. The employment of such capability would be to prevent the erosion of beaches, and prevent transported sand from obstructing harbor channels.

G. Future Laboratory Work

The next step in the study will be to generate ripples in a bed of sand which is placed in the bottom of the tank. Using sand from Scripps Beach, and 3 second waves 20 cm in height, it has been determined that an interval of 3 hours is required for an equilibrium ripple pattern to be formed in the sand bed. After this length of time, ripples of constant wavelength, (about 7 cm) and constant height (about 2 cm) were developed. The sand had a median diameter of 0.18 to 0.2 mm. After the ripples have been generated, they will be solidified by a liquid chemical grout, American Cyanamid AM-9 or equal, which when prepared has the consistency and viscosity of water and later reacts to form a long chain polymer gel. The individual grains of sand are bound together within this matrix. Alternative methods of making a solid form of generated "equilibrium

ripples" include plaster of paris molding techniques, and a "frozen" flat bed that is porous.

The flow will be visualized by means of dye injection. Dye will be injected into the upper sediment layer through hypodermic size stainless steel needles inserted in the gelled ripple forms. A non-dispersive dye such as methyl-blue will be used. Sequence photography will be used to capture the relative motion of the water and to outline the generation, growth and subsequent relative motion of eddies developed in the lee of the equilibrium ripple crests. It is desired to be able to relate the size of the eddies to the revelant flow and sediment parameters such as maximum velocity, orbital diameter, sediment size and sediment density. These parameters are all related to the ripple height and wavelength.

In order to correlate the sequence photographs with the wave height, a time readout will be positioned in the field of view of the camera with a binary readout of the time code displayed alongside the output of a digital wave staff on a recorder. The wave staff provides a picture of the wave height as a function of time. Using the known properties of the wave, and the Airy theory developed earlier, it is possible to predict the pertinent fluid parameters just outside the boundary layer.

It is of interest to investigate the possibility of three dimensional effects in the experiment. Three dimensionality expresses itself by the formation of cross flow patterns in the generated ripple field. Earlier studies in the wave tank have shown that for a ripple wavelength of 20 cm and a ripple wave height of 3 cm, a significant amount of cross flow existed. Cross flow is also predicted by the data of Maull and East (1963) in their work with depressions inset into the

walls of wind tunnels. It was shown by Maull and East that certain ratios of the parameters of ripple height, ripple wavelength and ripple crest length provide for essentially two dimensional flow patterns. It was found that for the 7 x 2 cm ripples, in situ, generated in Scripps Beach sand no appreciable cross flow was observable, since the ripple crests extended the full width of the sand bed.

After the flow has been studied above the "equilibrium" ripples, the flow field will be altered by changing the wave period or height. In this manner, it is hoped to be able to understand what is special about the flow above the equilibrium ripples. Study of this equilibrium flow above several types of sand is indicated in order to gain an insight into the effects of grain size.

Previous wave tank and oceanic studies have suggested two phase dependent ways that shallow water surface waves could suspend granular sediments - "sheet flow" suspension at high horizontal velocity and the release and rise of the vortices during the maximum deceleration-acceleration portion of the orbit. The purpose of this study was to obtain more information on wave-sediment interactions in the oceanic environment with emphasis on the phase dependence of the suspended sediment and on potential layer-boundary layer relationships.

All measurements were taken at a station located 5 meters south of the most southwesterly piling of the Scripps Institution of Oceanography Pier (Figure 12). A bottom pressure sensor and surface digital wave staff were used to obtain the water surface trace (Figure 13) and a power spectrum of the wave motion (Figure 14). Simultaneously, short sections of 16 mm motion picture film were taken of suspended particle orbital motion in front of a wire grid located on the bottom (Figure 15). Disks of paper and cloth (d = 8 mm) were used as tracer particles. Correlation

between the film frame and the wave record was made possible by flashing the time onto the film every quarter of a second. A stop-action projector was used to analyze the photographic sequences frame-by-frame. Particle motion in the potential flow region was transferred from the film to paper thus permitting the direct measurement of the horizontal orbital displacement d_o. Then the sequence was rerun and particle motion at the bottom was observed in terms of the relative time of reversal and the maximum particle height. Any observable sand motion was also recorded. The instantaneous horizontal velocity for each data point was plotted (Figure 16). From this plot the maximum horizontal velocity u_m could be read directly for each half period.

The data reported on here are from DAS runs 226, 250, 251, 305 and 307. Thus, 226-2 refers to the second photographic sequence taken during DAS run 226. It should be noted that d_o, u_m, the wave period T, and the wave amplitude above (or below) mean water $H/2$ were taken for each crest and trough. The water depth h was measured with a leadline once during each run.

Theoretical analysis of the velocity profile in a wave induced boundary layer over a solid bottom indicates that the velocity has a phase lead over the potential layer velocity which depends on the relative height z/δ. In all the photographic sequences, particles less than one cm above the bottom showed this phase lead by reversing direction before particles higher in the water column (Table 3). The phase lead ranged from zero to 42 degrees which compares reasonably with theory and with the smooth bed observations of Sleath (1970). It should be noted that each phase lead is the maximum observed for the given reversal; the large size of the particles (diameter = 8 mm) compared with the height over which

the phase lead was observed (1 cm) prevented more refined measurements of the phase lead as a function of height. Also it is possible that these phase lead estimates are conservative because of the sheltering effect of the ripple crests on the particles and because of inertial effects caused by size. This latter effect is especially important during the smallest waves when no particles were moving.

The importance of the "sheet flow" mechanism in placing sand in suspension was gaged by recording the occurrence of any observable sand motion during each half wave period (Table 4). The sand motion was broken into four categories:

a) no sand motion

b) no sand in suspension but sand on ripple crests shifted with crest or trough passage

c) sand in suspension up to 3 cm. Ripples visible to partly obscured

d) sand in suspension above 3 cm and ripple crests obscured during crest or trough passage (highest observed sand height was 6 cm)

Figure 17 illustrates the relationship between u_m and bottom condition: it indicates that there is a relationship between the two such that as u_m increases, the amount of bed disturbance increases until at a u_m greater than 35 cm/sec the bed is completely obscured by the "sheet flow" of sand.

An attempt was made to evaluate the release and rise of the vortices by observing the height to which particles rose during the velocity reversal phase of the wave period. This data is listed in Table 3. The range of elevation is from zero to five cm, with the larger waves lifting the material higher, which is to be expected, since the

intensity of the horizontal flow during the previous half wave period determines the vigor of the vortex.

Comparisons were made between observed and calculated values of the horizontal orbital displacement and velocity maximum d_o and u_m. The calculated values were based on equations derived from Airy wave theory

$$d_o = 2(H/2)/\sinh\left(\frac{2\pi}{L}\right)h$$

$$u_m = \pi\frac{d_o}{T}$$

where d_o is the value observed in the film. The comparison of d_{oc} (calculated) and d_{oo} (observed) is shown in Figure 18 and the comparison of u_{mc} and u_{mo} is shown in Figure 19. The good approximation of each to a straight line indicates Airy wave theory can be applied.

H. Conclusions

The data from this work led to the following conclusions:

1. There is a phase lead of the boundary layer velocity over the potential layer velocity when shallow water gravity waves traverse a rippled, sandy bottom. The size of the phase lead is of the same order of magnitude as that observed in a flat bottom laboratory study.

2. At a u_m of about 25 cm/sec the sand on the ripple crests moved and by a u_m of 35-40 cm/sec the suspended sand concentration was large enough so the ripples were obscured.

3. Vortices arose above the bed to an observed height of 6 cm (maximum) under the wave conditions studied.

4. At the locations studied here, predictions of near-bottom orbital velocities by Airy theory were in fair agreement with measured velocities.

The dramatic effect of phase dependence, originally indicated in Inman and Bowen (1963) has been studied and verified by repeatable laboratory experiment. The implications of these demonstrations are far reaching and promise new methods and technologies for the management, and even control of sand transport. The only limitations at this writing, are those posed by lack of imagination or inability to pursue further investigation.

IV REFERENCES

Gibbs, R. and A. Soutar, 1961, "The motion of sediment due to the passage of a wave", SIO, unpublished class report.

Horikawa, K. and A. Watanabe, 1968, "Laboratory study of oscillatory boundary layer flow", Coast. Eng. in Japan, vol 11, p 13-28.

Inman, D. L. and A. J. Bowen, 1963, "Flume experiments on sand transport by waves and currents", Eighth Conf. on Coastal Eng., Amer. Soc. Civil Eng., p 137-50.

Johns, B., 1970, "On the mass transport induced by oscillatory flow in a turbulent boundary layer", Jour. Fluid Mech., vol 43, p 177-85.

Jonsson, I. G., 1963, "Measurements in the turbulent boundary layer", Int. Assoc. Hyd. Res. Congress, London, p 85-92.

Kajiura, K., 1968, "A model of the bottom boundary layer in water waves", Bull Earthquake Res. Inst., vol 46, p 75-123.

Koontz, W. A. and D. L. Inman, 1967, "A multi-purpose data acquisition system for field and laboratory instrumentation of the nearshore environment", Coastal Engr. Res. Center, Tech Memo 21, 38 pp.

Lamb, H., 1932, Hydrodynamics, 6th Edition, New York, Dover Publ.

Le Mehaute, B., D. Divoky and A. Lin, 1968, "Shallow water waves: a comparison of theories and experiments", Eleventh Conf. Coastal Eng., Amer. Soc. Civil Eng., vol 1, p 86-96.

Longuet-Higgins, M. S., 1953, "Mass transport in water waves", Phil. Trans. Roy. Soc. London, Series A, 245(903) p 535-81.

Longuet-Higgins, M. S., 1961, "The mechanics of the boundary layer near the bottom in a progressive wave", Sixth Conf. Coastal Eng., Amer. Soc. Civil Engineers, p 184-93.

77

Manohar, M., 1955, "Mechanics of bottom sediment movement due to wave action", U. S. Army Corps of Engineers, Beach Erosion Board, Tech Memo 75

Mauil, D. J. and L. F. East, 1963, "Three dimensional flow in cavities", Jour. Fluid Mech., vol 16, no 4, p 620-632.

Russell, R. C. H. and J. D. C. Osorio, 1961, "An experimental investigation in drift profiles in a closed channel", Sixth Conf. Coastal Eng., Amer. Soc. Civil Eng., p 171-83.

Simmons, J. I., 1965, "Orbital motion of ocean waves and its effect upon shelf sediments", SIO, unpublished report.

Sleath, J. F. A., 1969, "A device for velocity measurement in oscillatory boundary layers in water", Jour. Sci Insts., Series 2, vol 2, p 446-8.

Sleath, J. F. A., 1970, "Velocity measurements close to the bed in a wave tank", Jour. Fluid Mech., vol 42, p 111-123.

Stokes, G. G., 1851, "On the effect of the internal friction of fluids on the motion of pendulums", Camb. Trans. vol 9, no 8,(papers III.1)

Wiegel, R. L., 1964, Oceanographical Engineering, Prentice-Hall Inc., Englewood Cliffs, New Jersey, p 18.

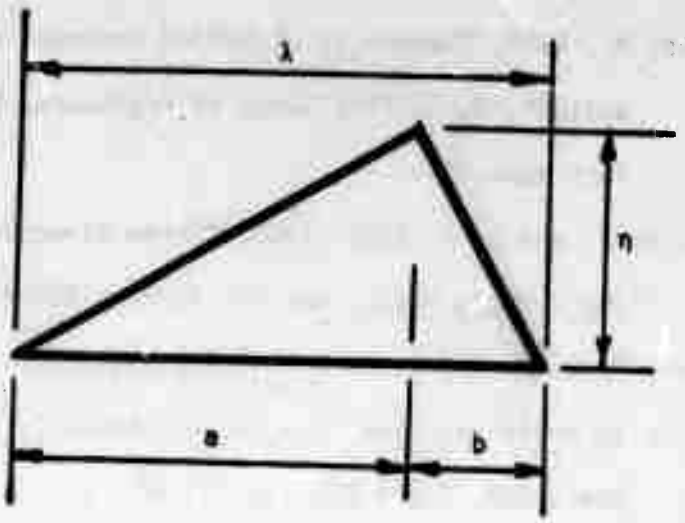

FORM	WAVELENGTH λ	HEIGHT η	STEEPNESS RATIO η/λ
A	20 cm	3 cm	0.15
B	10 cm	3 cm	0.3
C	5 cm	3 cm	0.6
D	10 cm	1.5 cm	0.15

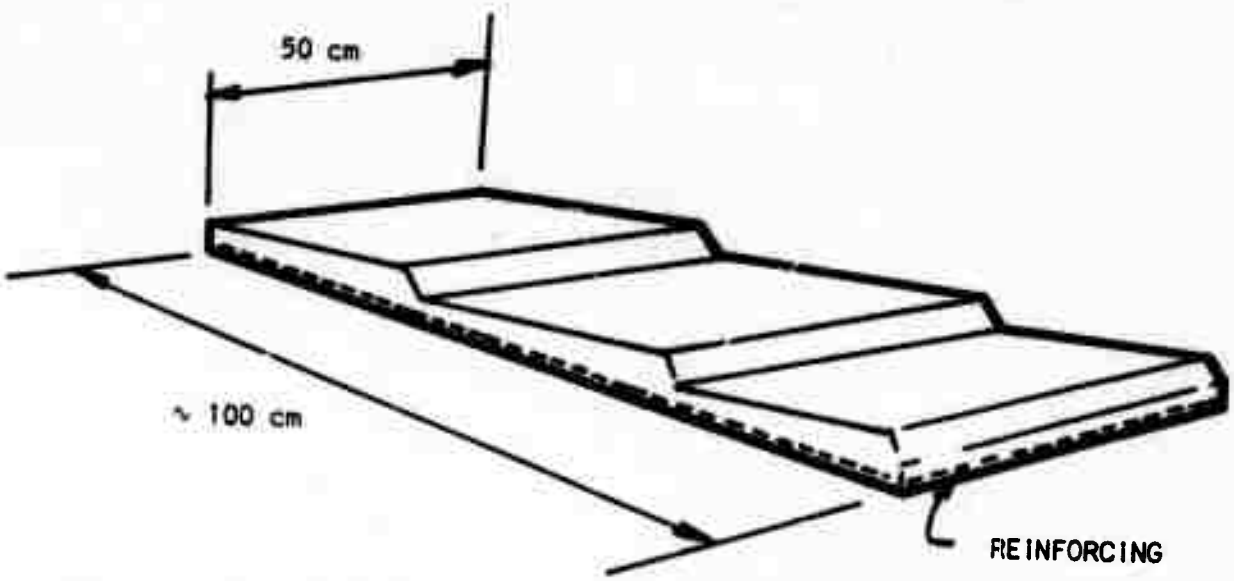

Table 1. Four sets of ripple forms were cast using wire reinforced plaster of paris. This table summarizes their dimensions. During the tests, the parameter varied was d_o.

Table 2. Movable cast segments were arranged as shown in the demonstrations. These demonstrations are repeatable at will, in the hydraulic laboratory wave tank.

Location:	8 x 8 ft wind wave channel	
Experimental Condition:	water depth	$h = 160$ cm
	wave period	$T = 3.4$ sec
	wave height	$H = 21$ cm
	orbital displacement	$d_o = 24$ cm
Tracer:	pvc (grey)	$\rho = 1.5$ gm/cm^3
	acrylic (red)	$\rho = 1.1$ gm/cm^3

Roughness Dimensions

λ	η	a	b
10 cm	1.5 cm	7.5 cm	2.5 cm

Waves Propagate from Left to Right, Direction of Particle Transport is Shown by the Arrows

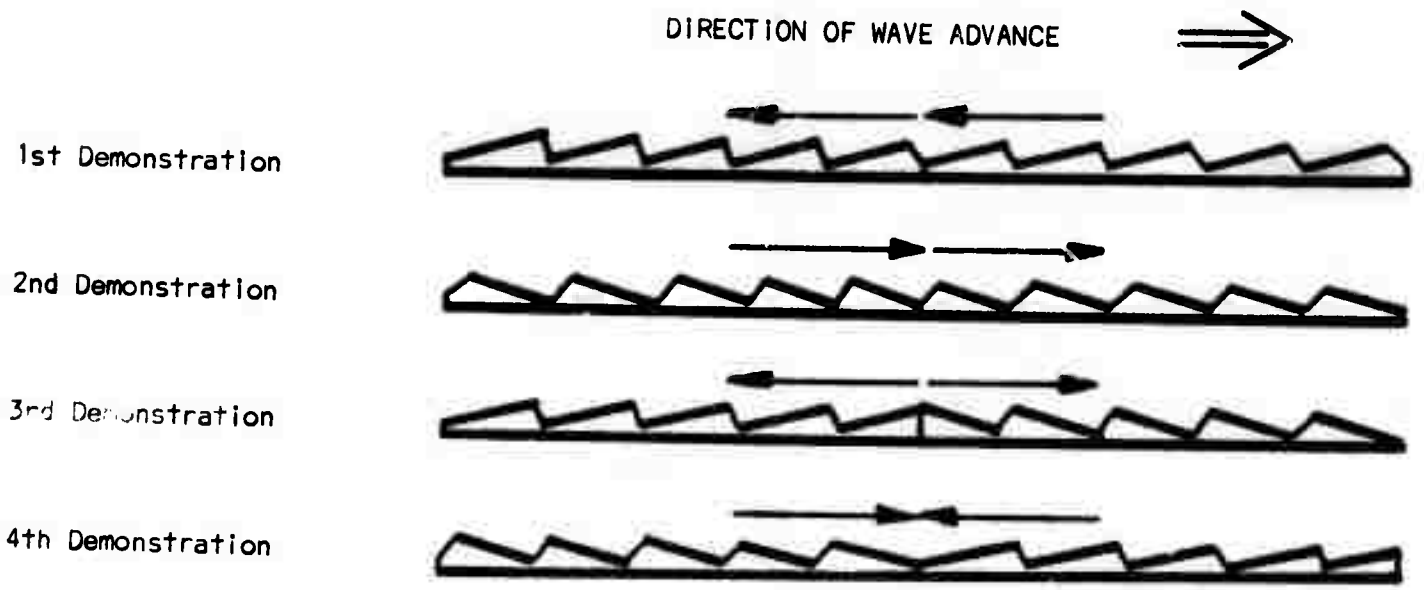

Table 3. Bottom condition during u_m and height to which particles rose during velocity reversal

DAS RUN	T sec	u_m*	Bottom Condition**	Height Reversal cm
226-1	2.5	- 3	a	0
	5.0	7	a	0
	10.0	-15	a	2
	5.5	13	a	0
	4.0	- 9	a	2
	5.0	15	a	2
	9.5	-35	b	3
226-2	5.5	-27	b	3
	7.5	22	a	-
226-3	10.0	-35	b	3
	10.5	43	c	4
	6.0	-32	b	4
250-1	12.5	-32	b	2
	13.0	53	d	5
	12.0	-31	b	3
	11.0	67	d	5
	15.5	-74	d	5
250-2	12.5	-29	c	3
	9.5	35	d	-
	11.0	-33	c	-
250-3	8.5	49	c	5
	15.0	-45	c	3
251-1	9.5	-23	b	3
	10.5	35	d	-
251-2	13.0	-27	c	3
	11.5	53	d	5
251-3	15.5	-61	d	5
	9.0	43	d	4
305-1	4.0	9	a	<1
	4.5	-10	a	"
	5.0	12	a	"
	5.5	-18	a	"
	8.0	10	a	"
	4.5	-10	a	"

Table 3. Continued

DAS RUN	T sec	u_m*	Bottom Condition**	Height Reversal cm
305-2	5.5	-28	b	5
	5.5	18	a	2
	4.0	- 3	a	0
	5.5	28	a	2
	3.5	-10	a	2
	4.5	13	a	2
305-3	2.0	- 7	a	0
	5.0	18	a	3
	9.0	-23	b	2
307-1	4.0	-24	b	3
	7.5	38	c	4
	6.0	-51	d	-
	4.5	28	c	-
	4.5	- 7	a	-
	5.5	28	b	2
	2.5	- 8	a	0
	4.5	28	b	2
	4.5	-22	b	2
	4.0	12	a	1
	4.0	-13	a	1

Note: * negative sign indicates offshore flow
** bottom condition at u_m (see text for a, b, c, d)

Table 4. Phase lead of the boundary layer velocity over the potential layer velocity.

DAS RUN	T sec	z cm	REVERSAL Offshore to Onshore	REVERSAL Onshore to Offshore	MAXIMUM PHASE LEAD sec	MAXIMUM PHASE LEAD Degrees
226-1	10.5	<1		↓	1/2	17
	2.5	"	↑		0	0
	5.0	"		↓	0	0
	10.0	"	↑		1/2	18
	10.5	"		↓	1/4	16
	4.0	"	↑		0	0
	5.0	"		↓	1/4	17
	9.5	"	↑		1/2	19
226-2	7.0	<1		↓	1/4	13
	5.5	"	↑		1/4	16
	7.5	"		↓	1/2	24
226-3	12.0	<1		↓	1/2	15
	10.0	"	↑		1/2	18
	10.5	"		↓	1/2	17
	6.0		↑		1/4	15
250-1	12.5	<1	↑		1/2	22
	13.0	"		↓	3/4	21
	12.0	"	↑		1/2	15
	11.0	"		↓	1/2	16
	15.5	"	↑		1/2	12
250-2	12.5	<1		↓	1/2	22
	12.5	"	↑		1/2	22
	9.5	"		↓	1/2	19
	11.0	"	↑		1/2	16
250-3	9.5	<1	↑		1/4	10
	8.5	"		↓	1/2	21
	15.0	"	↑		1	24
251-1	12.5	<1		↓	1/2	22
	9.5	"	↑		1/4	10
	10.5	"		↓	1/2	17
251-2	13.0	<1	↑		1/2	14
	11.5	"		↓	3/4	24

Table 4. Continued

DAS RUN	T sec	z cm	REVERSAL Offshore to Onshore	REVERSAL Onshore to Offshore	MAXIMUM PHASE LEAD sec	MAXIMUM PHASE LEAD Degrees
251-3	12.5	<1		↓	1/2	22
	15.5	"	↑		3/4	18
	10.5	"		↓	1-1/4	42
305-1	4.0	<1		↓	1/4	22
	4.5	"	↑		1/4	20
	5.0	"		↓	1/2	36
	5.5	"	↑		1/2	32
	8.0	"		↓	1/2	22
	4.5	"	↑		1/4	20
305-2	5.5	<1	↑		1/2	32
	5.5	"		↓	1/4	16
	4.0	"	↑		0	0
	5.5	"		↓	1/2	32
	3.5	"	↑		0	0
	4.5	"		↓	1/2	40
305-3	2.0	<1	↑		0	0
	5.0	"		↓	1/2	36
	9.0	"	↑		3/4	30
307-1	4.0	<1	↑		1/2	22
	7.5	"		↓	1/2	24
	6.0	"	↑		-	-
	4.5	"		↓	1/4	20
	4.5	"	↑		1/4	20
	5.5	"		↓	1/2	32
	2.5	"	↑		0	0
	4.5	"		↓	1/2	40
	4.5	"	↑		1/4	20
	4.0	"		↓	1/4	22
	4.0	"	↑		1/4	22

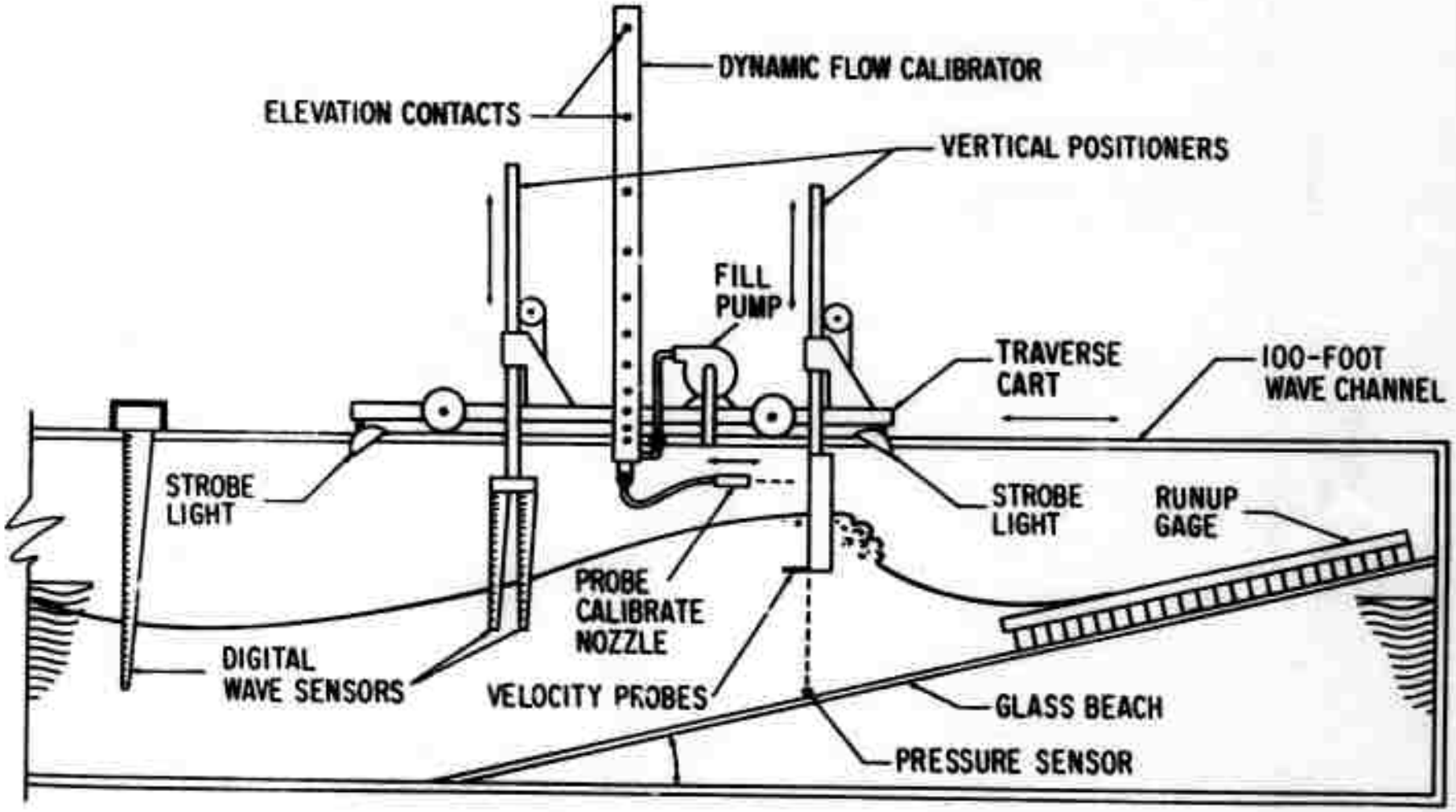

Figure 1. Diagram of revised laboratory instrumentation. With these instruments, data were assimilated for surface elevation, horizontal flow velocity, vertical flow velocity, wave run-up, acceleration, turbulence and individual phase maxima.

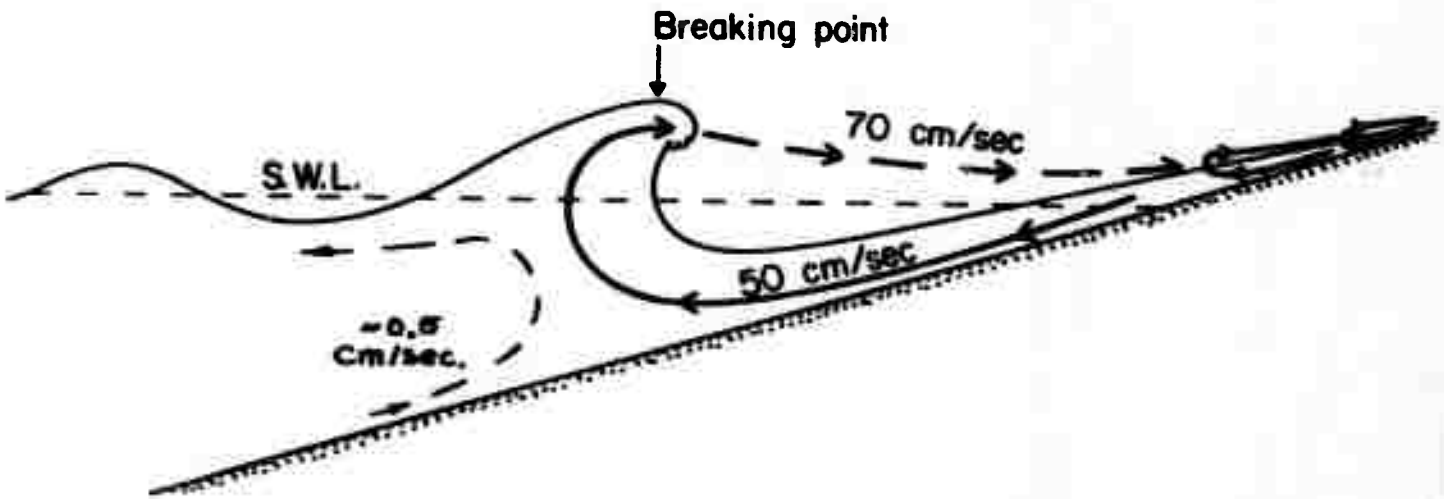

Figure 2. Wave breaking involves a significant shoreward mass transport. It is strongest at the surface, and mass continuity is maintained by subsurface return flow which rises at the break point to complete the circulation cell. There may be several such cells within the breaker zone.

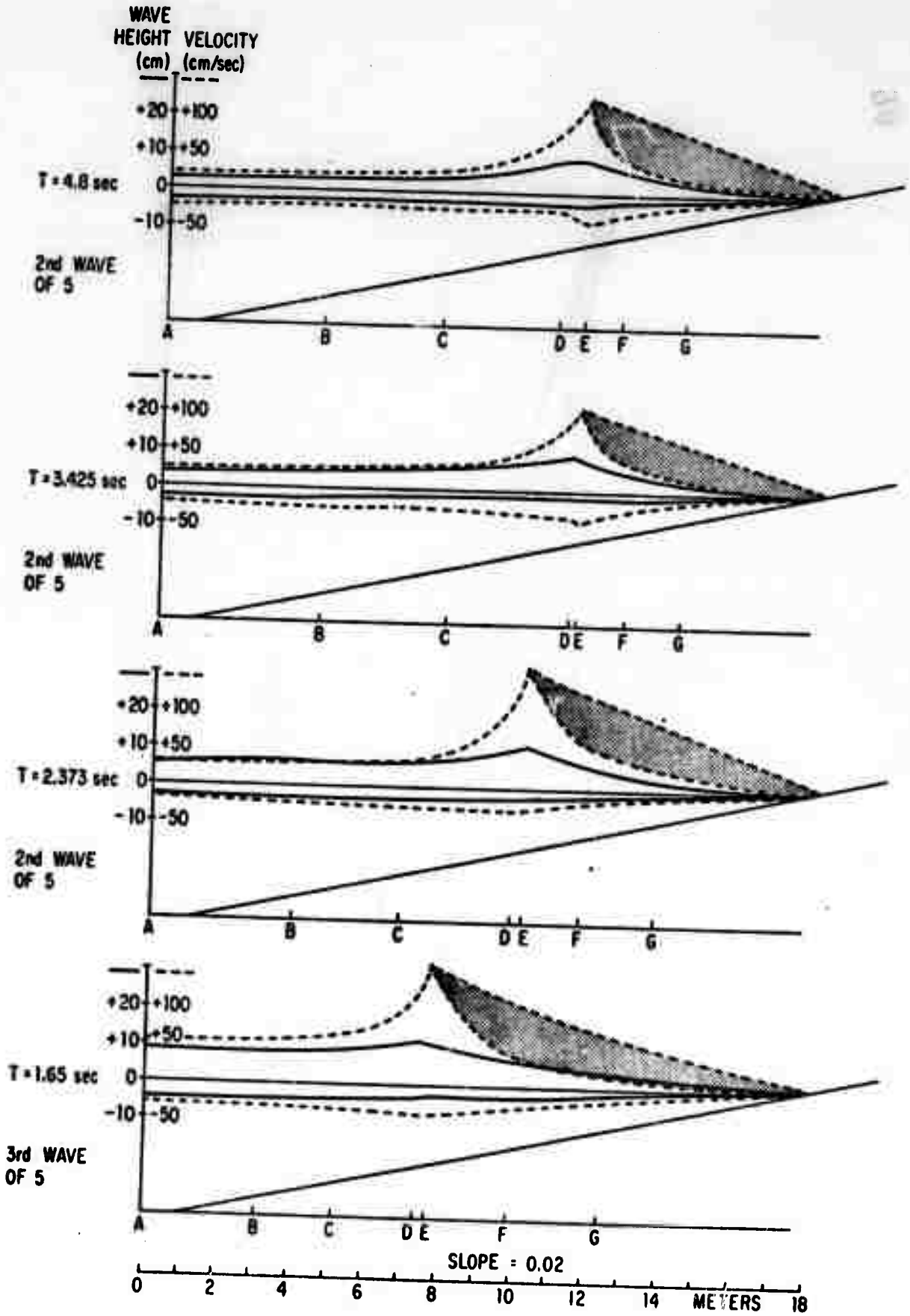

Figure 3. Envelopes of maximum and minimum surface elevation and horizontal velocity as functions of wave period for a beach slope of 0.02.

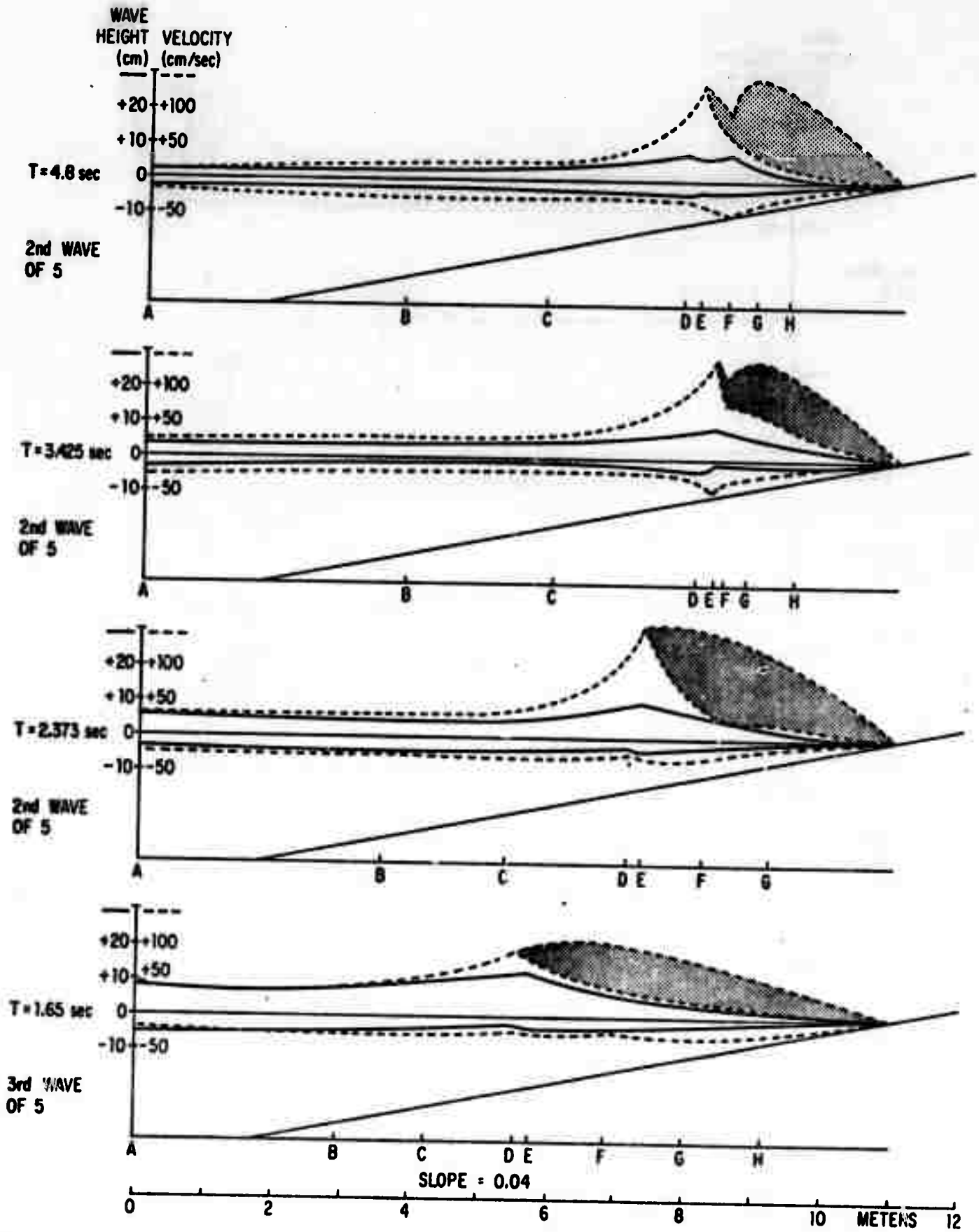

Figure 4. Envelopes of maximum and minimum surface elevation and horizontal velocity as functions of wave period for a beach slope of 0.04.

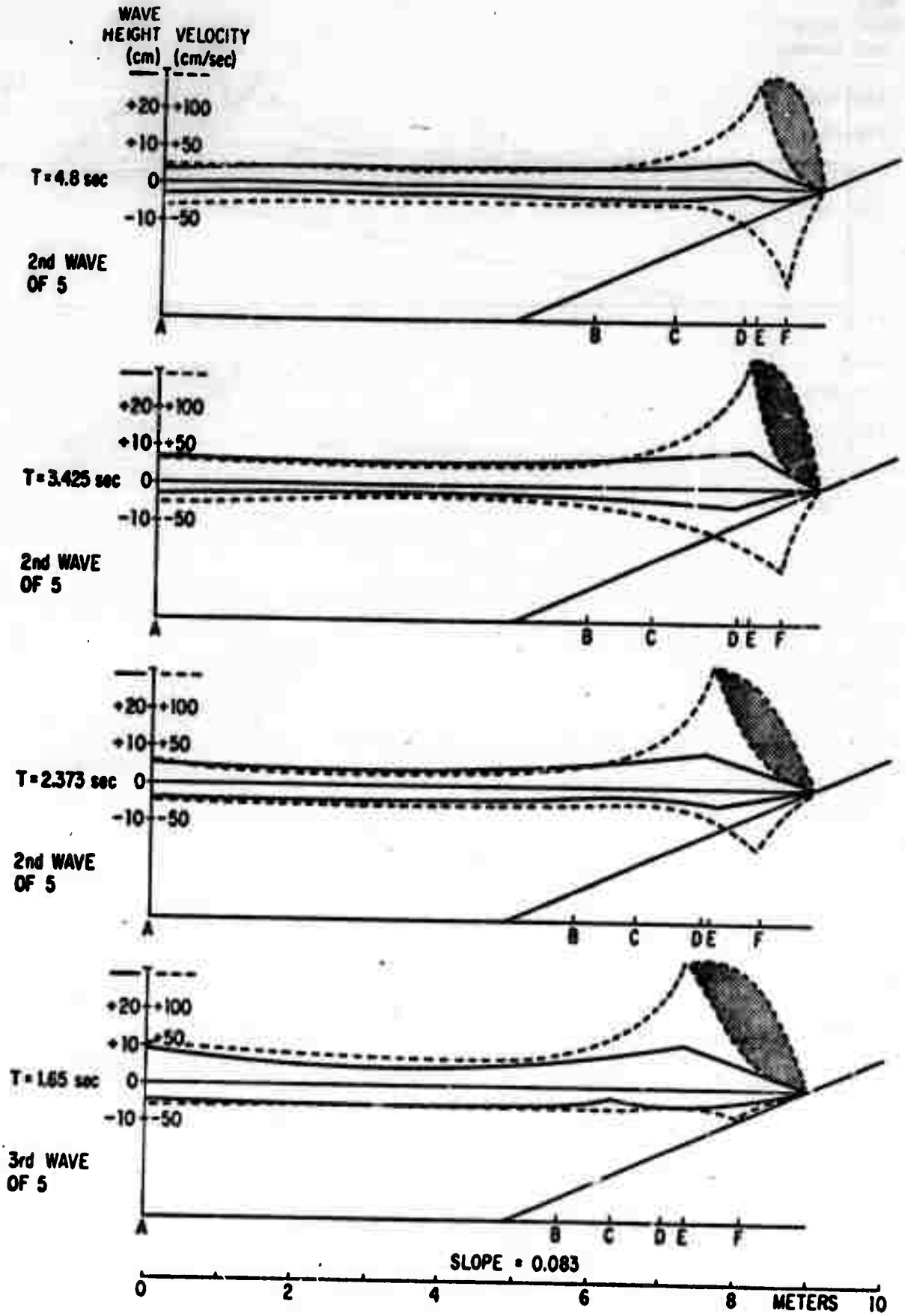

Figure 5. Envelopes of maximum and minimum surface elevation and horizontal velocity as functions of wave period for a beach slope of 0.083.

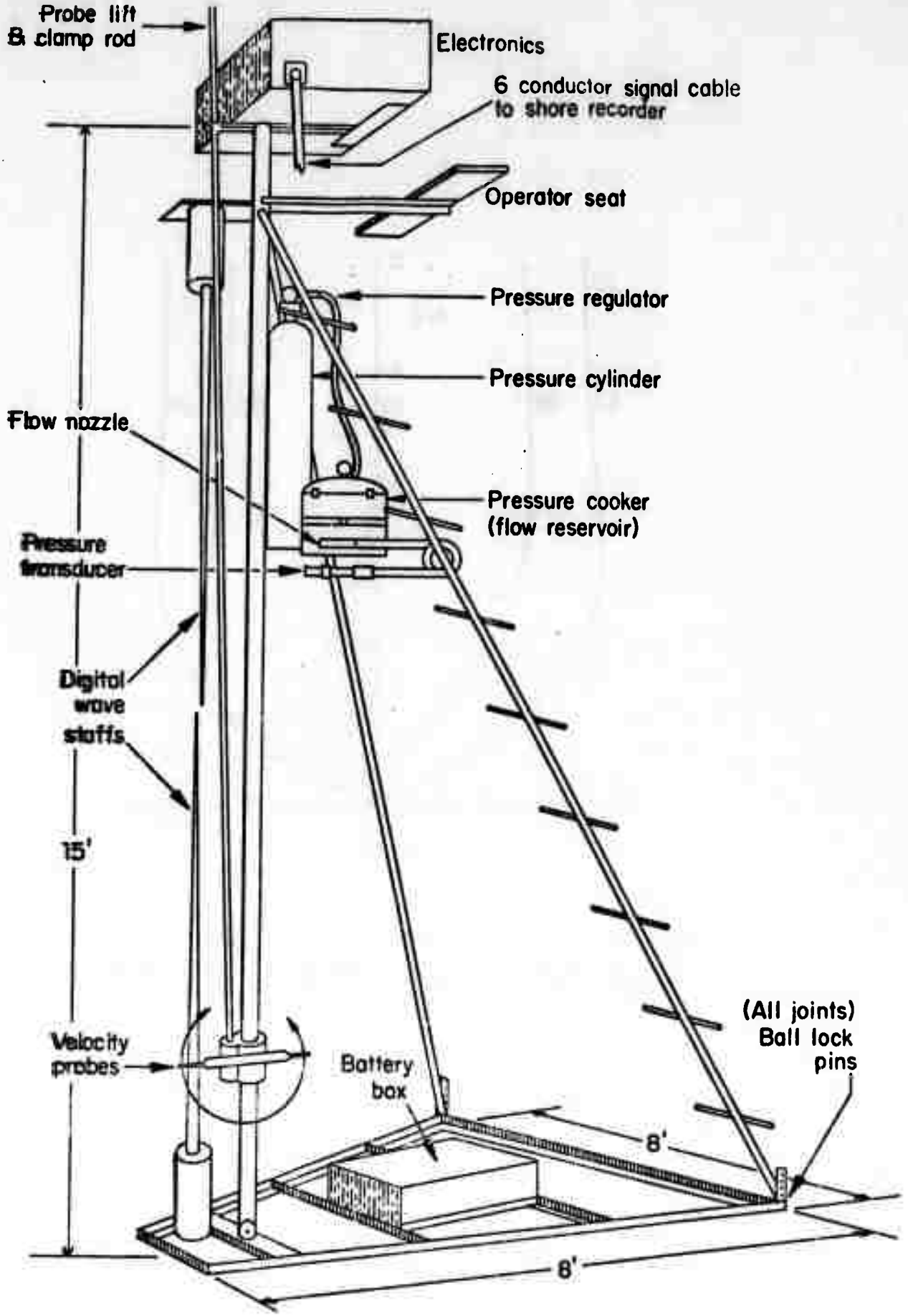

Figure 6. Instrumented platform for use in the surf zone, the construction is modular and may be erected in the field by two men. Ball lock pinned joints are for assembly without hand tools. The platform is intended to record wave heights up to ten feet.

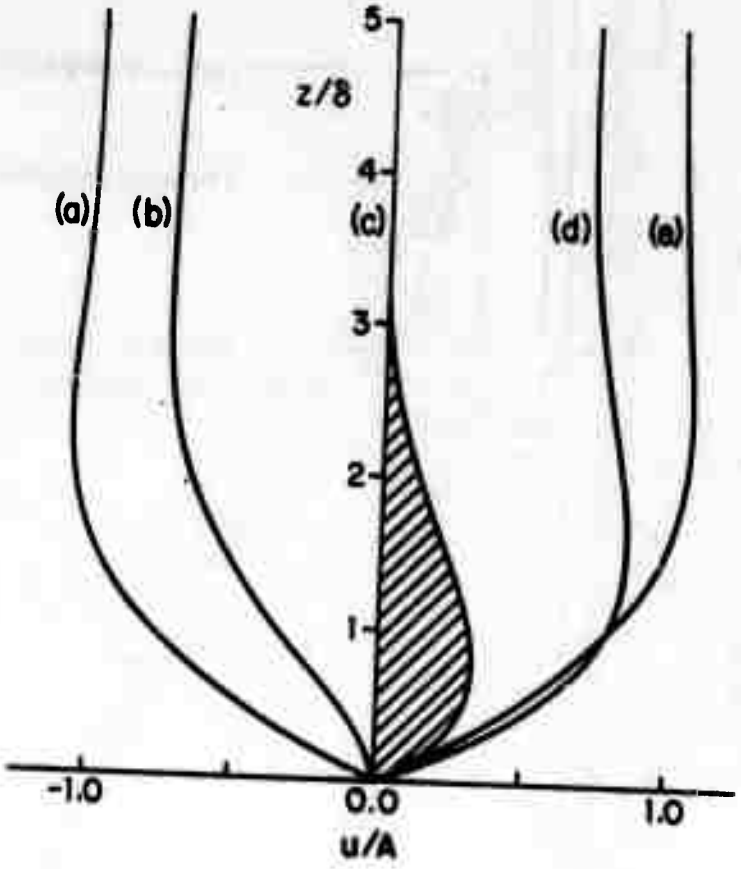

Figure 7. Horizontal velocity profile above a smooth, flat plate during different phases of a wave period. (adapted from Longuet-Higgins, 1961).

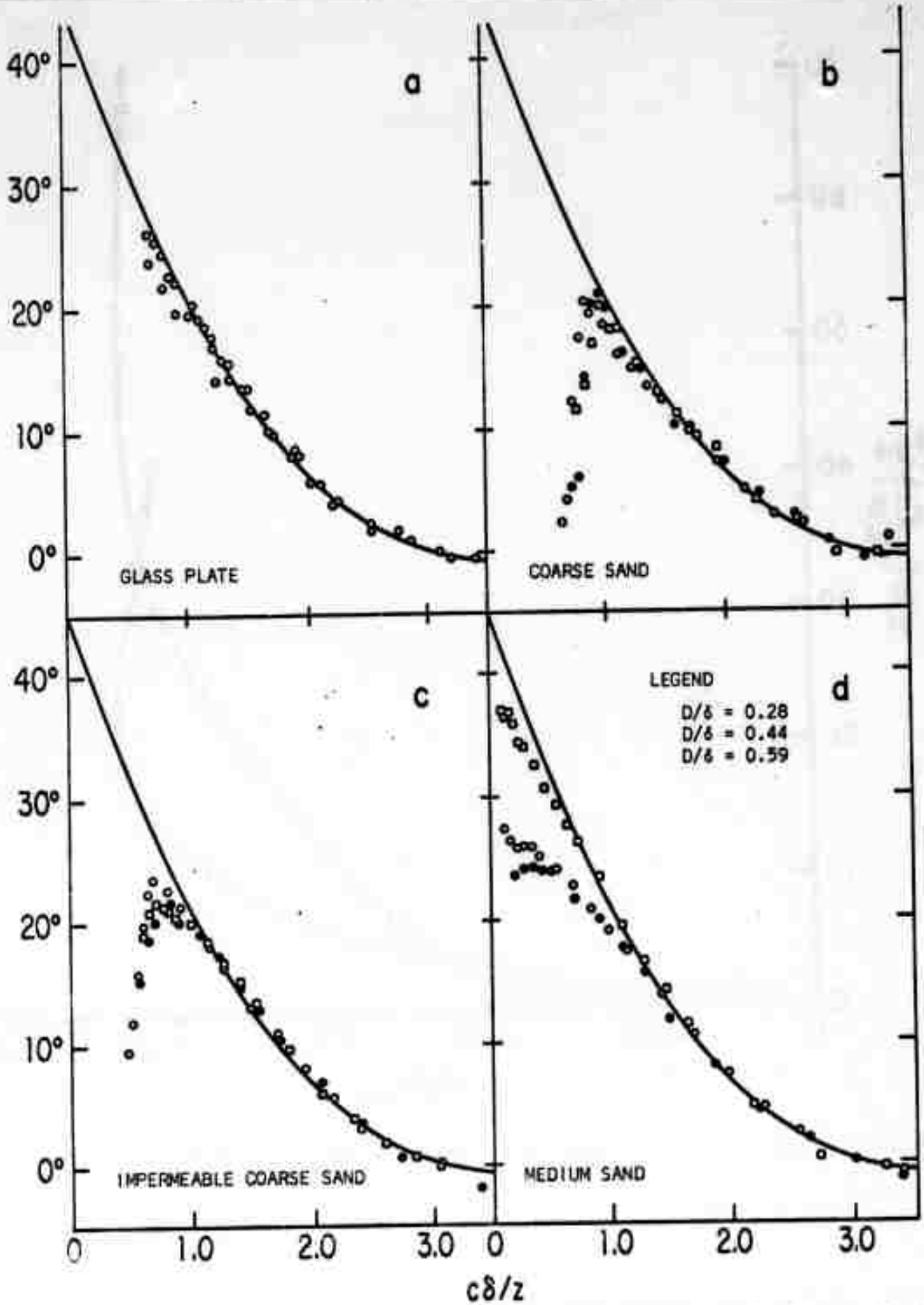

Figure 8. Phase lead of boundary layer velocity over potential layer velocity as a function of height above bottom. The different types of flat beds are: a - smooth plate; b - coarse sand; c - coarse sand cemented on flat plate; d - medium sand (Sleath, 1970).

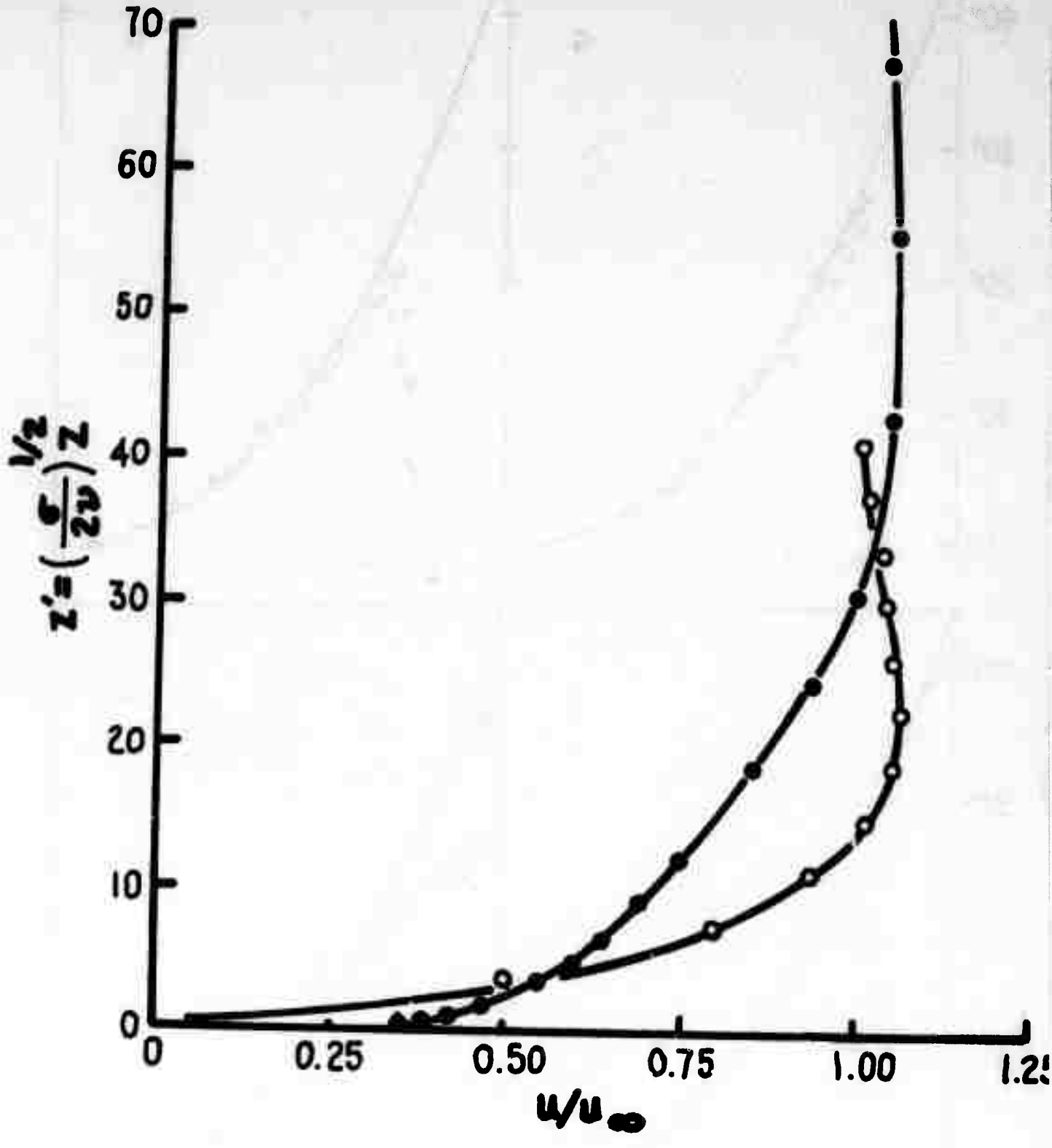

Figure 9. Comparison between Johns theory (O) and Jonssons data (●) for $z' = 6.18z$.

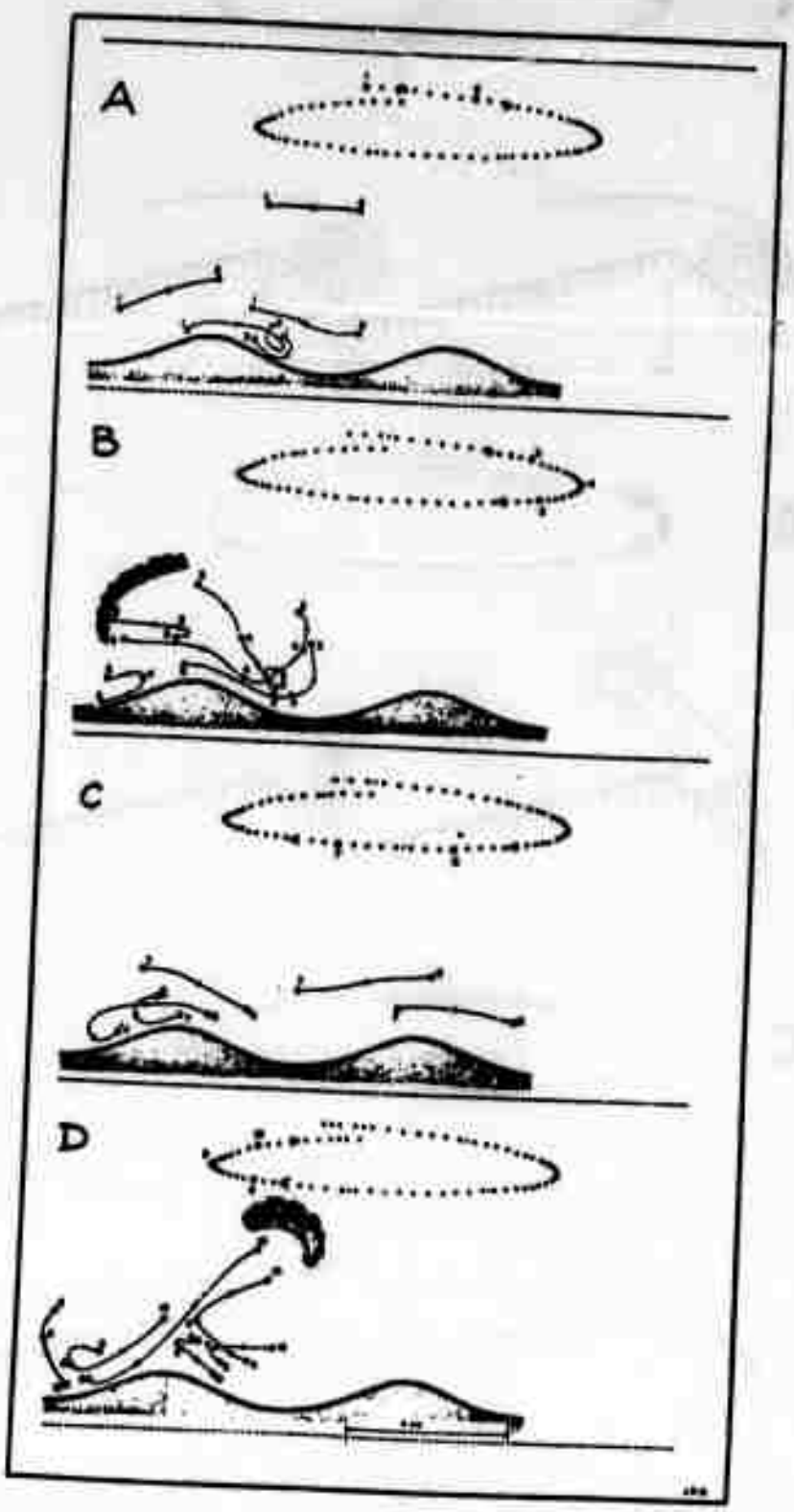

Figure 10. Particle trajectories over a rippled bed showing the height of the vortex-sublayer (Inman and Bowen, 1963). 880.6

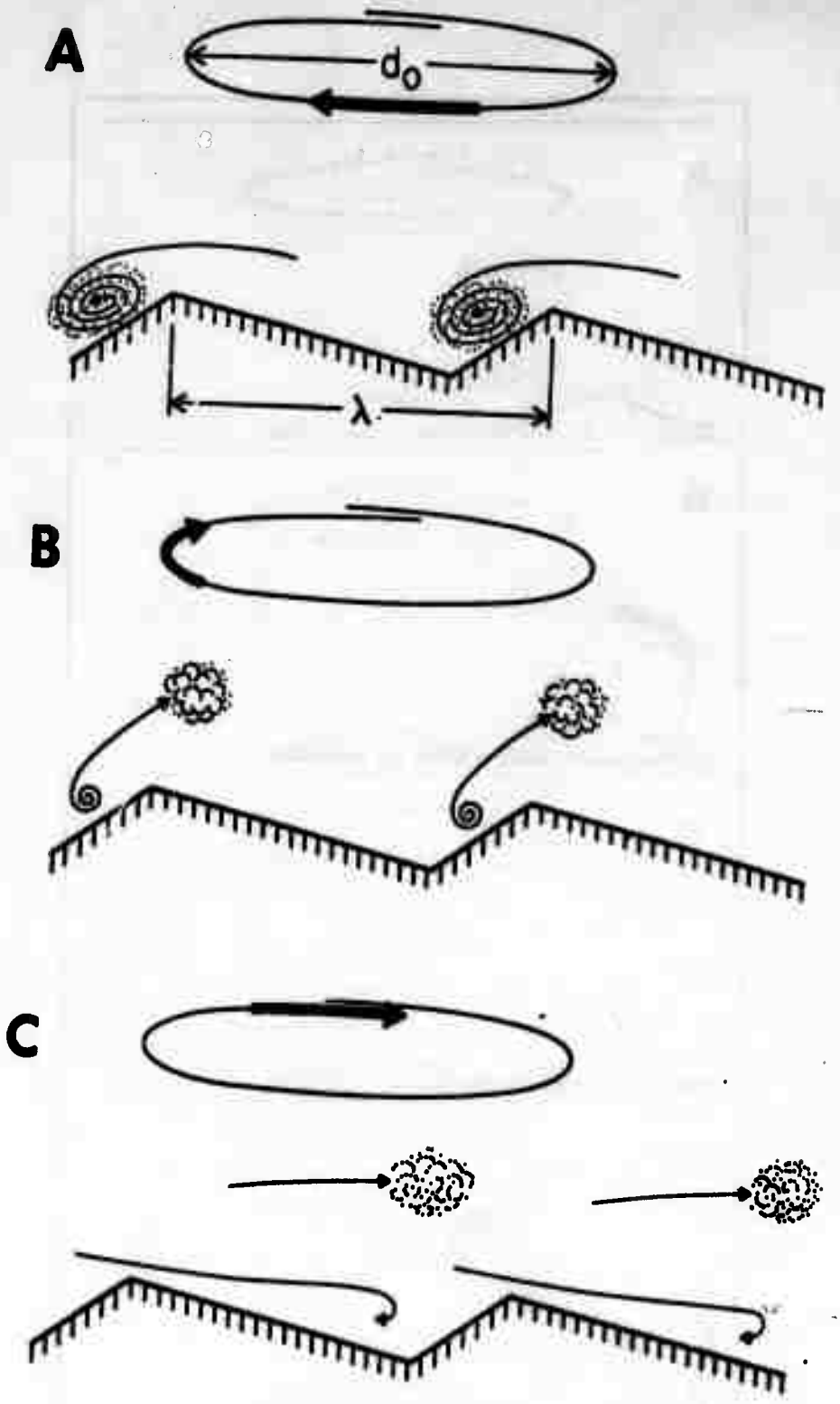

Figure 11. Asymmetrical bottom forms under oscillatory wave motion cause a net transport of sand in the direction that is out-of-phase with the velocity that produces the largest vortex. The orbital velocity of the wave forms an intense vortex over the steep lee face which traps and suspends sediment (A). The reversal in direction of the orbital motion causes the suspended sediment to rise (B), and to be carried in a direction that is opposite to that causing the vortex (C).

7/.7-1

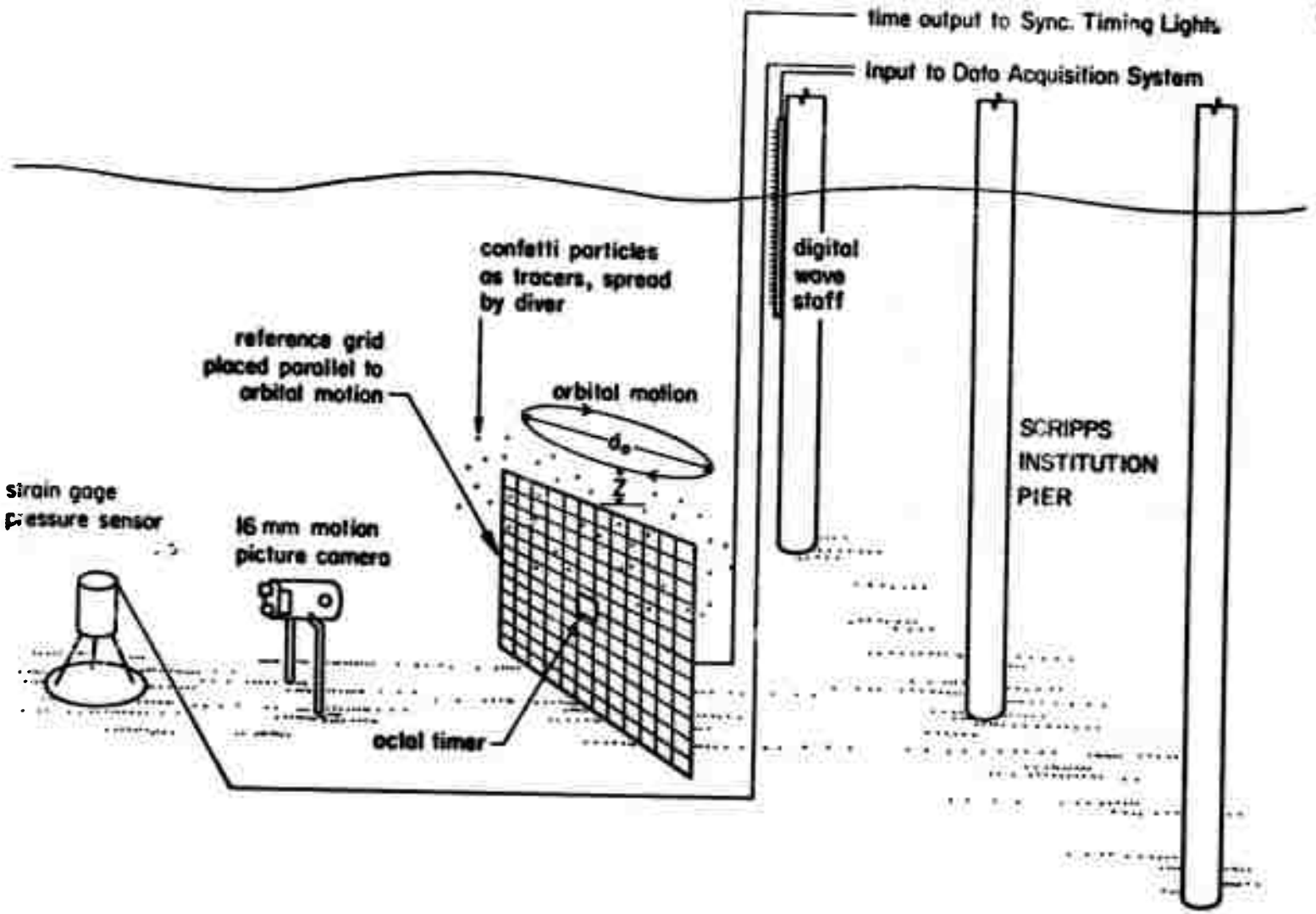

Figure 12. Position of pressure sensor, wave staff, motion picture camera, timing lights and grid with respect to the end of the Scripps Pier.

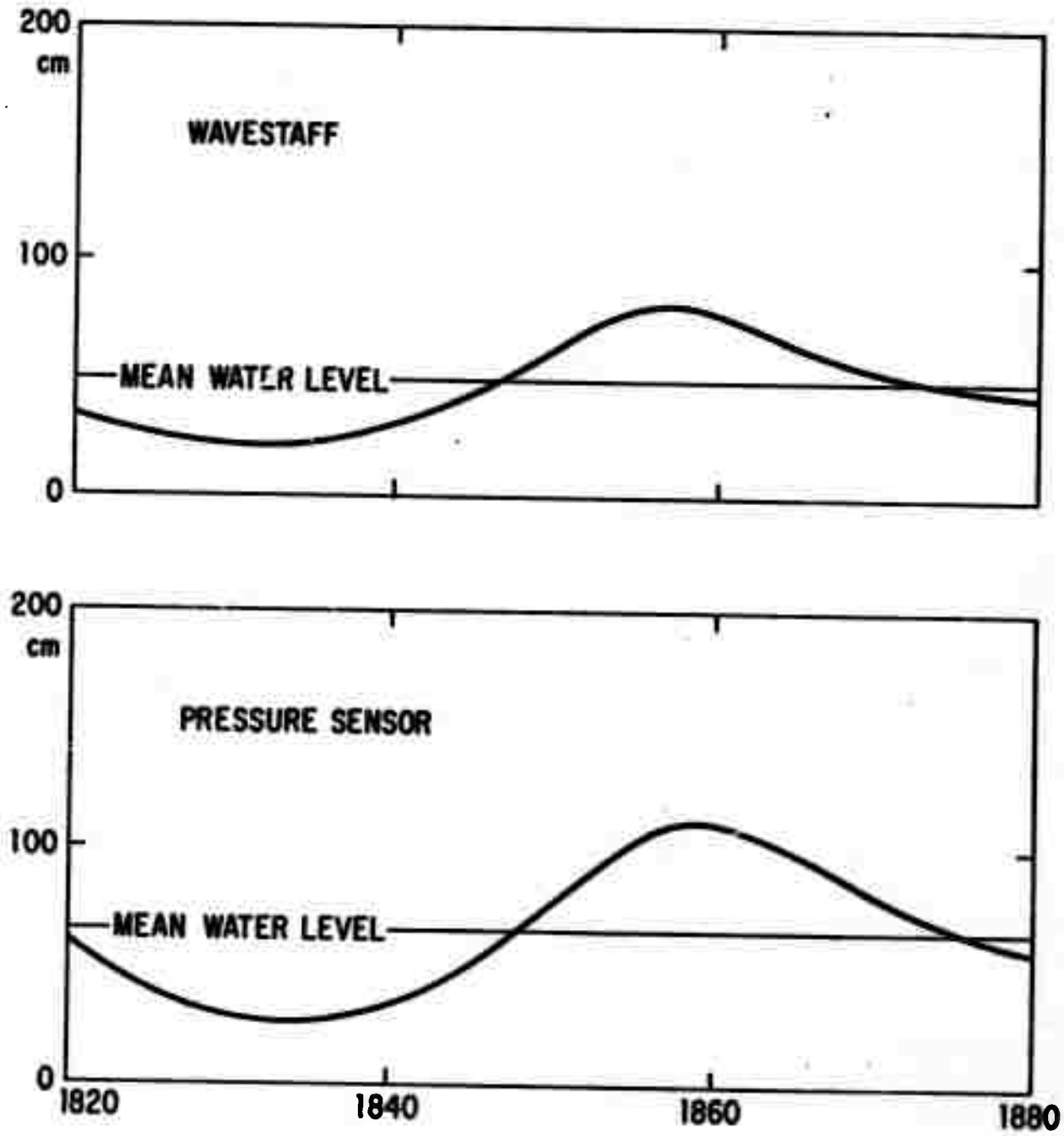

Figure 13. Analog record of water surface as measured by the digital wave staff and bottom pressure sensor for DAS 251, photographic sequence 2.

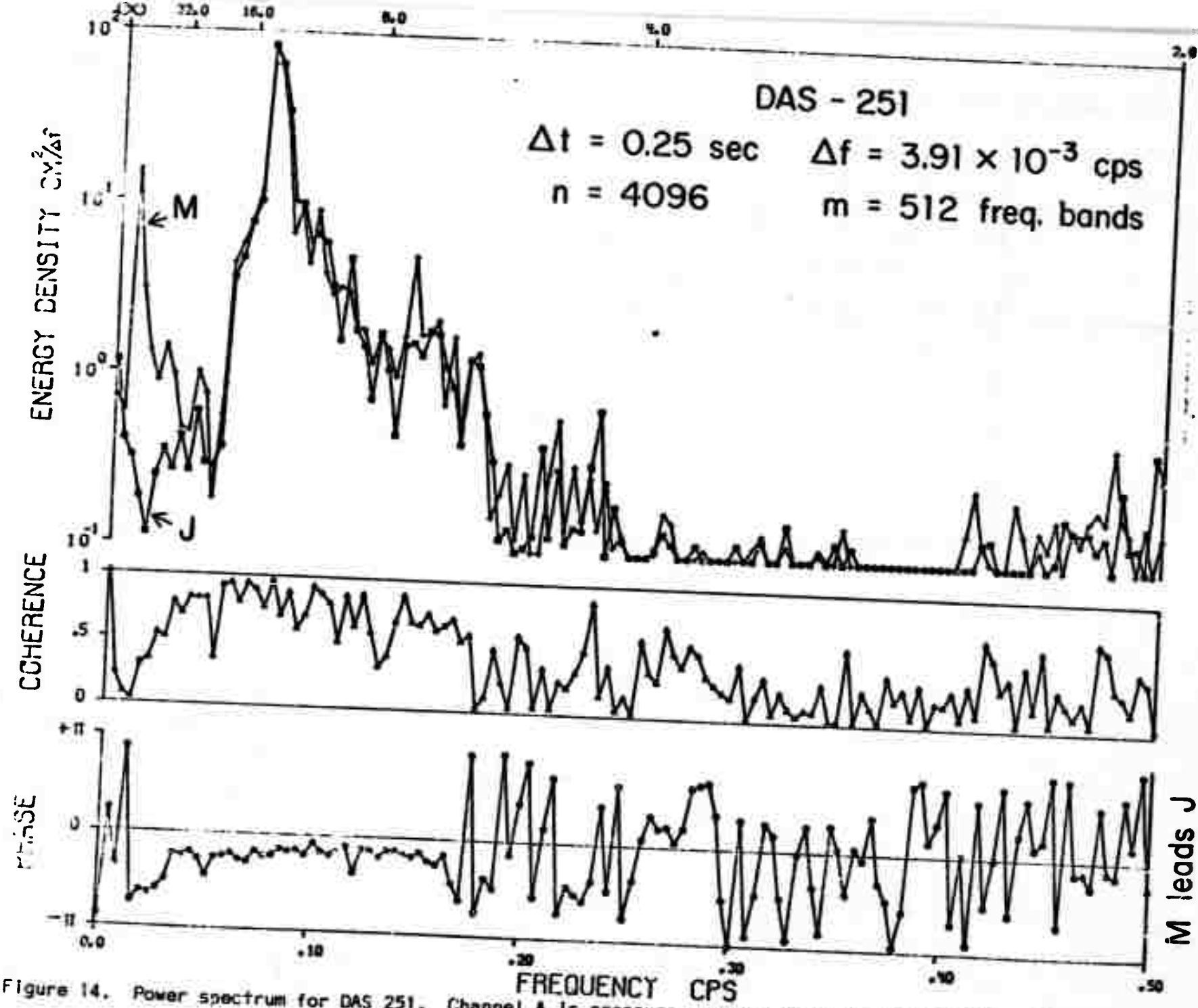

Figure 14. Power spectrum for DAS 251. Channel A is pressure sensor and channel M is wave staff.

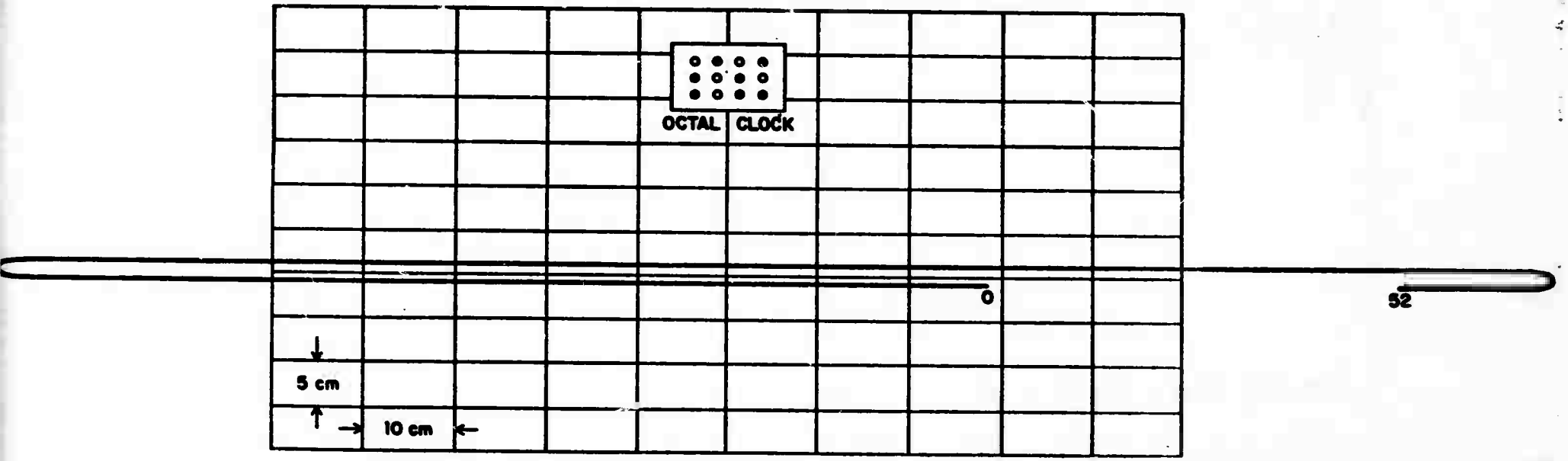

Figure 15. Composite diagram of particle traces during run 251-2. Reading on octal clock indicates time from start of DAS 251 to start of run 251-2 (1821 quarter seconds).

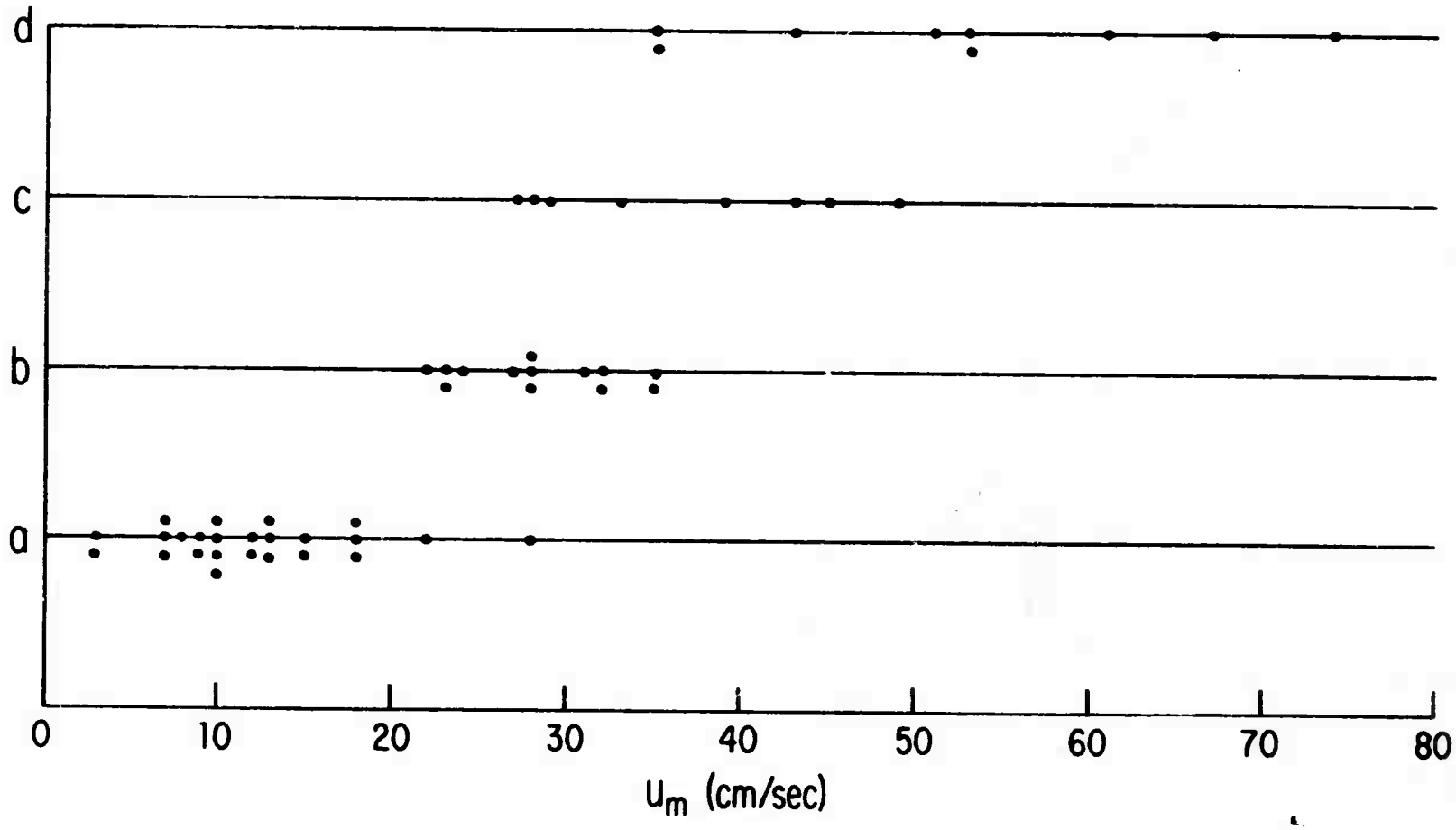

Figure 17. Range of observed velocities for each of the four categories of sand motion. a - no sand motion; b - no sand in suspension, but sand on ripple crests shifted with crest or trough passage; c - sand in suspension up to 3 cm with ripples visible to partly obscured; d - sand in suspension over 3 cm with ripples obscured during crest or trough passage.

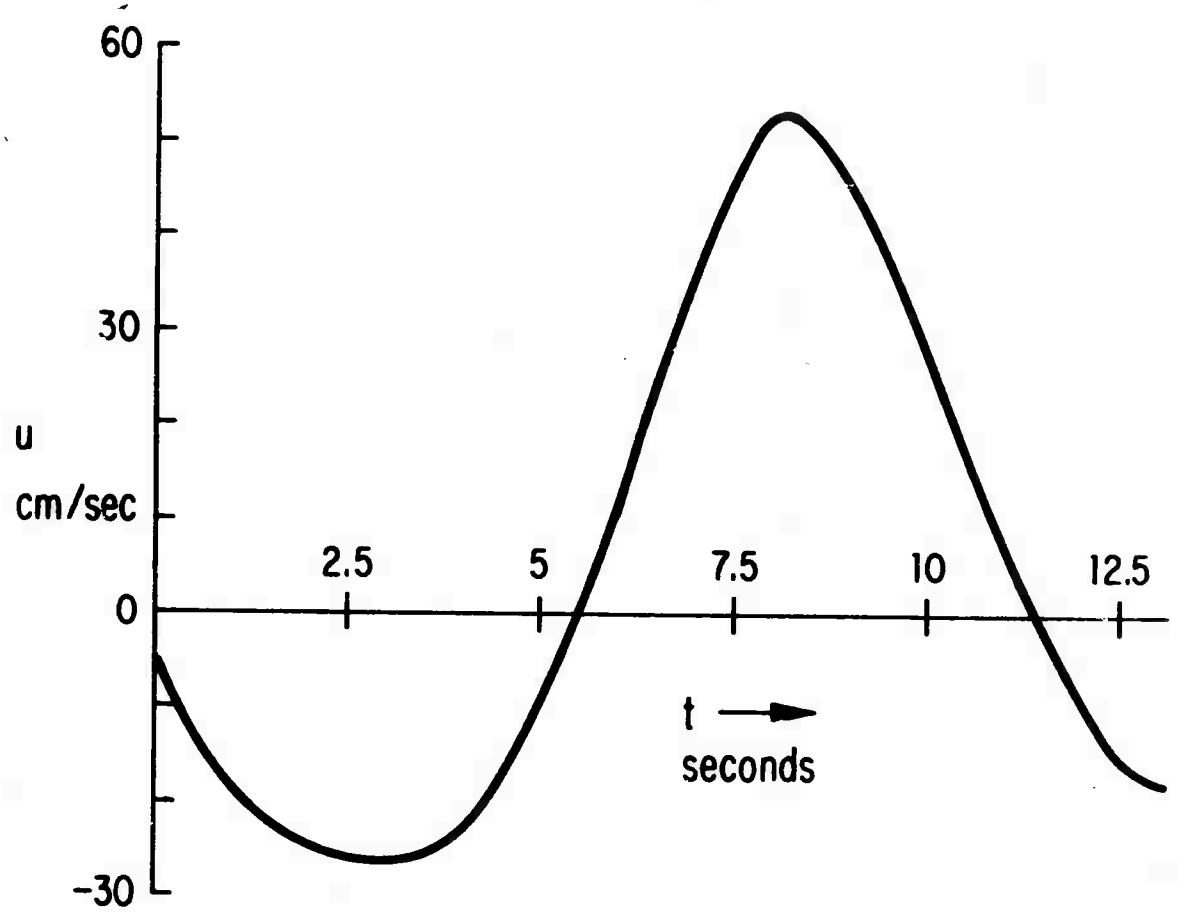

Figure 16. Instantaneous horizontal velocity sampled at quarter second intervals during photographic run 251-2.

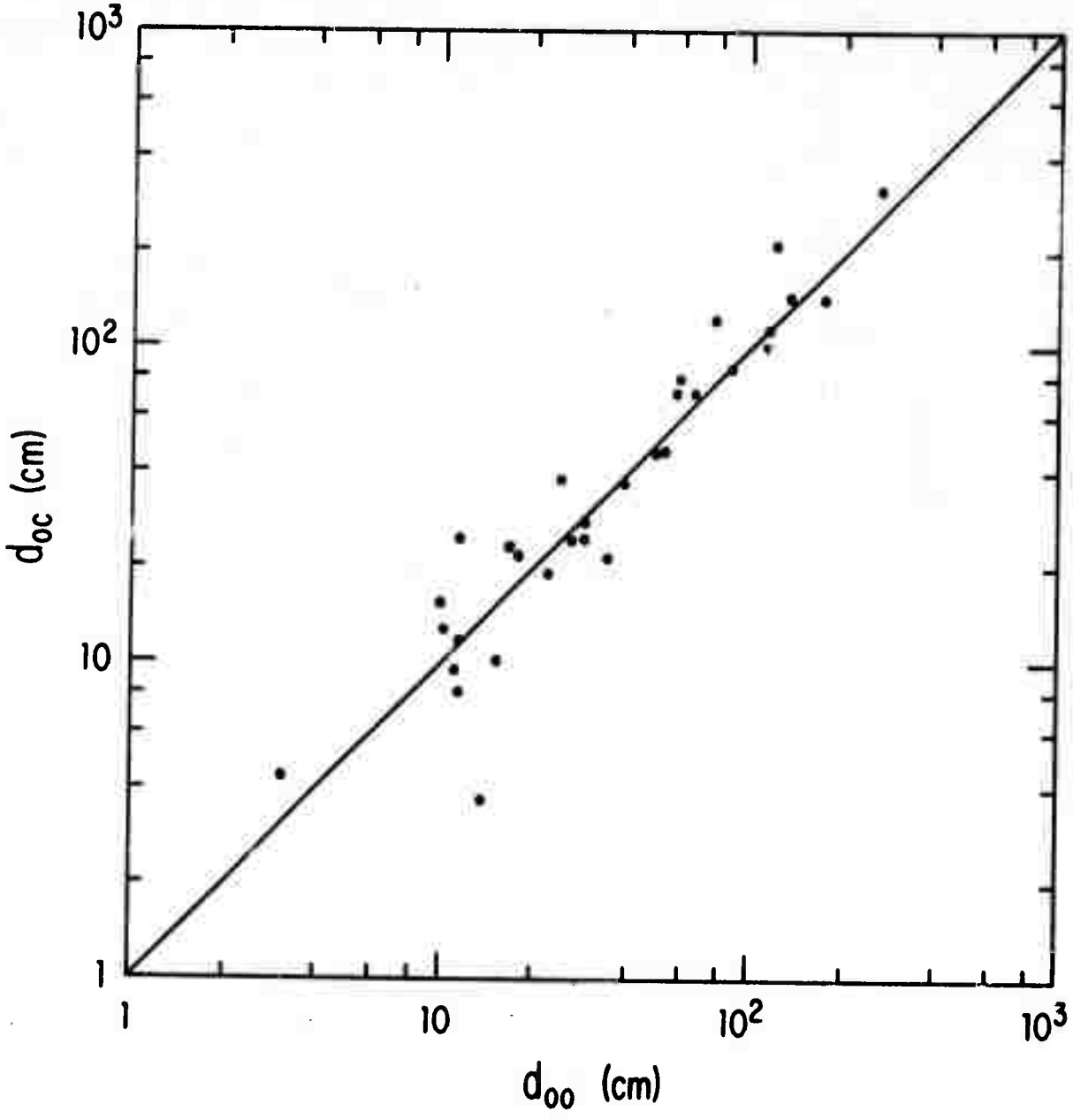

Figure 18. Comparison of bottom orbital displacements as calculated from Airy theory (d_{oc}) and observed in films (d_{oo}). Solid line indicates complete agreement.

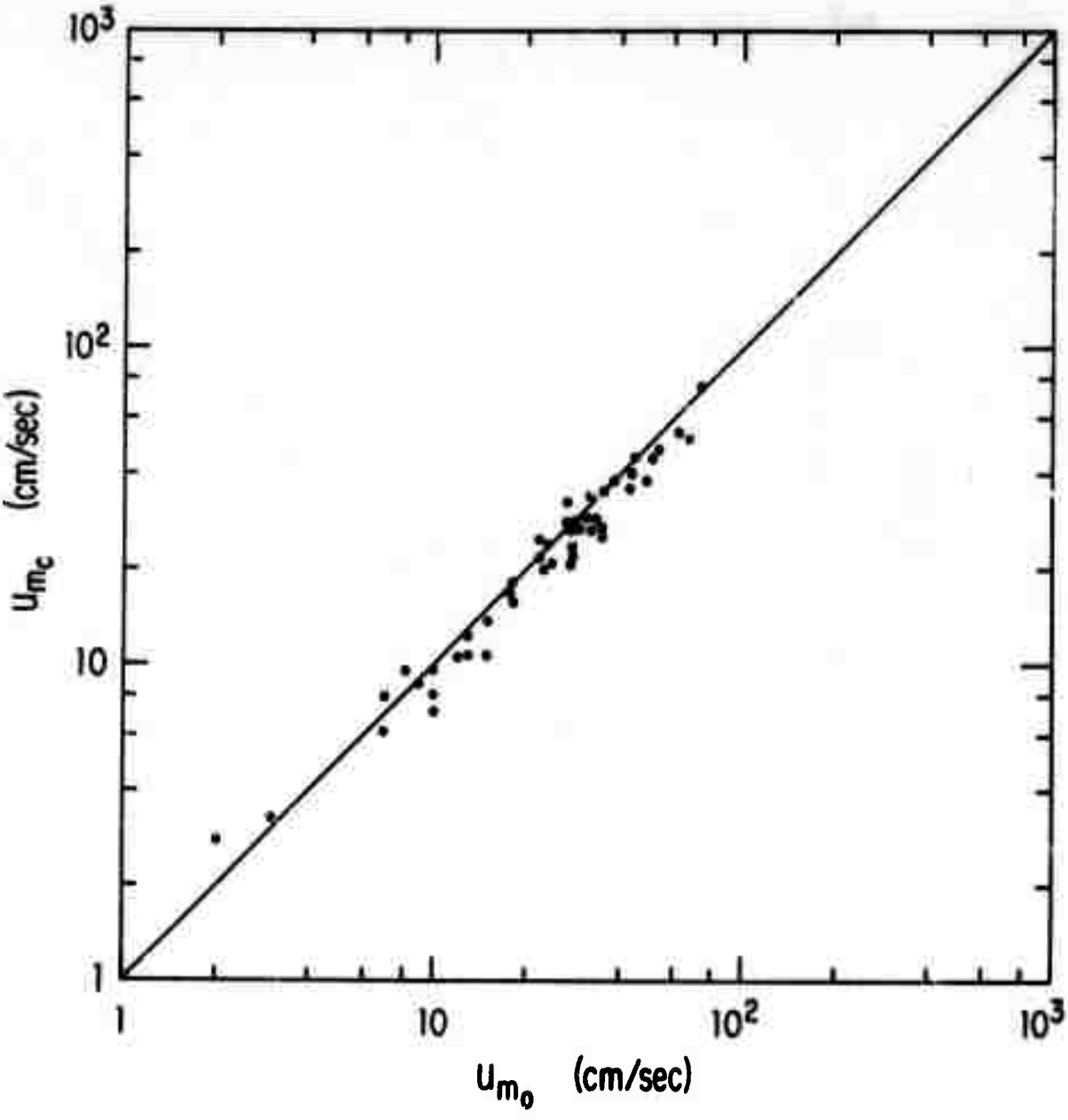

Figure 19. Comparison of maximum horizontal velocity as calculated from Airy theory (u_{m_c}) with values observed in films (u_{m_o})$_o$. Solid line indicates complete agreement

Part IV

ELECTROMAGNETIC ROUGHNESS OF THE OCEAN SURFACE

Co-Principal Investigators

Dr. William A. Nierenberg
Phone (714) 453-2000, Extension 1101

Dr. Walter H. Munk
Phone (714) 453-2000, Extension 1741

ADVANCED OCEAN ENGINEERING LABORATORY

Sponsored by

ADVANCED RESEARCH PROJECTS AGENCY
ADVANCED ENGINEERING DIVISION

ONR Contract N00014-69-A-0200-6012

Part IV

Electromagnetic Roughness of the Ocean Surface

Table of Contents

List of Figures

List of Appendices

I. SUMMARY

The electromagnetic roughness studies are being conducted jointly by two groups, one at Stanford University, and one at Scripps Institution of Oceanography. The work uses HF radio waves scattered from the ocean surface to measure the statistical properties of this surface, particularly the ocean-wave directional spectrum.

The major proportion of our work for the second six months of the contract has been concerned with conducting two experiments: 1). In the first experiment LORAN A radio signals were used in a bistatic geometry to measure the directional spectrum of ocean waves in a trade-winds region north of Hawaii. 2). In the second experiment 30 MHz radio waves were backscattered from the ocean in an attempt to measure the non-linear scatter of radio waves from the ocean.

The radar equipment used in this work was developed during the first six months of the contract by the Stanford group, and the antennas were constructed during the present reporting period. In addition, we have accepted delivery of 1) a pitch-and-roll, wave-measuring buoy with a low-power data recorder. This buoy is being evaluated and modified. 2). A surplus, multifrequency, pulse-Doppler radar (a Grainger Ionosounder). This radar is presently being repaired.

II. TECHNICAL REPORT

A. Bistatic LORAN Equipment

a) General

During the first two weeks of September, LORAN A radio signals, scattered from the sea surface, were recorded at several locations on and near the Hawaiian Islands. The purpose of these measurements was to: 1) evaluate the bistatic-geometry method of measuring ocean-wave, directional spectra at sea, and 2) obtain measurements of the directional spectrum of a trade-wind generated sea (i.e. a sea generated by a homogeneous, stationary, wind field).

Data was recorded by a radar receiver located: 1) at sea on

the R/V HOLOKAI (operated by the Oceanic Institute at Makapuu Point, Oahu, Hawaii) on August 30 - September 3; 2) at Kailua on the north coast of Oahu on 6-8 September; 3) at Hana on the NE tip of Maui on 9-10 September. These points are shown on the map in figure 1, the receiver was located at points marked R, the LORAN transmitters were at T. Data from the land stations were recorded for comparison with data recorded at sea. The land stations were chosen so the terrain would partially exclude signals from some directions; and the ocean station was chosen so the two baselines (from receiver to transmitter) would be perpendicular and parallel to the wind direction.

b). Bistatic Geometry

When the radar receiver and transmitter are located at different positions (bistatic geometry) scattered signals with a constant time delay (range) are scattered by areas located along an ellipse; and signals with a constant Doppler frequency are scattered by areas along circular arcs. This geometry is shown in figure 2. If the radar data are plotted in range-Doppler space, only certain values of range and Doppler are possible, and signals from waves moving toward a constant direction, but at different ranges, fall along the curves drawn in figure 3. The direction of the scattering waves (and thus the ocean-wave, directional spectrum) can be calculated from this range-Doppler data, provided the fourfold ambiguities can be eliminated. If the receiver moves (e.g. is on a drifting ship), the received signals have an additional Doppler frequency due to the receiver motion, and the range-Doppler plot is distorted. In this case, waves coming from several different directions (in addition to the four ambiguities already noted) may have the same range-Doppler coordinate, (see figure 4), and the calculation of the ocean-wave, directional spectrum from the range-Doppler data is much more complicated.

Further information on the bistatic geometry is given in reference 1.

c). Equipment

In the Hawaiian experiment, the fourfold symmetry was

eliminated by using two different antenna arrays, one composed of two whip antennas separated by the length of the ship, the other composed of two loop antennas similarly arranged. The arrays were calibrated by slowly rotating the ship and measuring the strength of the direct LORAN pulse. The antenna responses are given in figure 5.

The ocean waves were measured by an Ocean Applied Research wave buoy consisting of a disc shaped float and pressure transducer hanging 150 feet below it. (reference 2) The frequency modulated signal from the buoy was telemetered to the ship and counted to determine its frequency. The number from the counter was recorded along with the radar data; least count was equivalent to 2.5 cm of wave height. The pitch-and-roll wave buoy was delivered by the contractor in August, but not in time to be used in this experiment. The buoy is now being evaluated and modified.

A block diagram of the LORAN receiver and pertinent specifications are given in Appendix 1. The LORAN data was recorded in 20 minute segments, to obtain a frequency resolution of 0.001 Hz, with the antenna array oriented in various directions.

d). Data

During the week that data was recorded the wind blew steadily from the ENE with a velocity of 9-12 knots (4-6 m/s). The velocity varied from day to day, but usually was constant during one day, so the waves were expected to be in equilibrium with the wind. A typical ocean-wave spectrum is shown in figure 6. This spectrum is similar to previously-recorded, trade-wind spectra: its high frequency part falls off as f^{-4}, and there is little indication of swell. The peak is at 7.1s waves, very close to the backscatter frequency limit for the radio frequency used.

By using topographic shielding, and the directional resolution of the antennas, the ambiguous scattering areas can be resolved for the land-based radar data. The wave-number directional spectrum obtained from part of this data is shown in figure 7.

More data is being analysed to help fill in some parts of the spectrum not covered by the data in the figure. This spectrum shows that the wave energy is concentrated in a relatively narrow band of directions; furthermore, the range-Doppler plot of this data indicates that ocean currents do not add any significant Doppler component to the data.

The radar data from the ship is much more difficult to analyse because of the ship's motion. At the present time we are investigating the seriousness of this difficulty, and the best way to analyse the data.

B. 30 MHz Radar Experiment

The analysis of the data from the bistatic experiment assumes only first-order scattering is important; if higher order (non-linear) radio-wave scattering is also important, the assumed analysis is incorrect. The 30 MHz experiment was designed to determine experimentally the strength of the second-order scattering.

In the experiment a 30 MHz radar set was operated at the coast near San Francisco using an omnidirectional antenna. Data was collected for 15 minute intervals to obtain a Doppler resolution of 0.001 Hz using 50μs pulses to obtain a range resolution of 7.5 km. A block diagram of the radar is included in the appendix.

During the experiment the scattering ocean waves of 5 m wavelength (1.8s period) were superimposed on long-period swell. The swell was expected to modulate the primary scattering waves and produce second-order sidebands.

Because of low transmitted power of approximately one watt, scattered signals were observed only at short ranges (approximately 10 km). A Doppler spectrum obtained from our first attempt to measure second-order scatter is shown in figure 8. The peak at zero frequency is due to scatter from the land, and its narrow width confirms the stability of the radar. The peaks on either side are due to scatter from the ocean. No second-order scatter was observed. The width of the ocean scatter peak cannot be explained at this time, although we suspect it is caused by either non-homogeneous or non-stationary ocean currents.

A second experiment is being planned to improve upon the results observed in the first experiment. We are increasing the radar signal-to-noise ratio to see if the expected second-order scatter was buried in noise in the first experiment; furthermore, we will use a directional antenna to eliminate effects of non-homogeneous, ocean currents and at the same time improve the signal to noise ratio.

III REFERENCES

1. Teague, Calvin C. 1971 High-Frequency Resonant Scattering Techniques for the Observation of Directional Ocean-Wave Spectra. Stanford University, Radiosciences Laboratory Rept. SU-SEL-71-039.

2. Gaul, R. D. and N. L. Brown, 1969 A Comparison of Wave Measurements from a Free-Floating Wave Meter and the 'Monster-Buoy'. Marine Technology Society Jour.

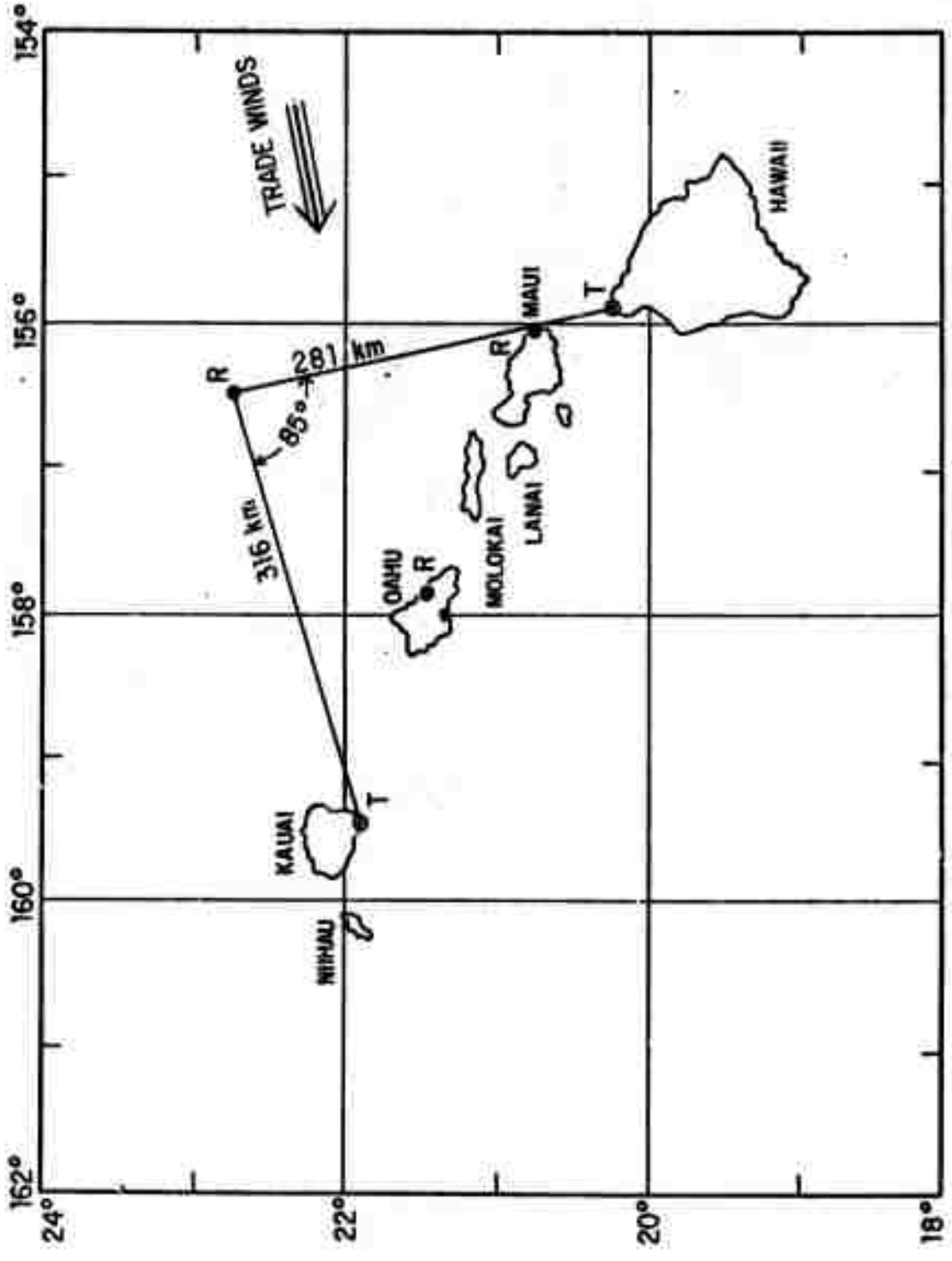

Figure 1. Location of receiver (R) and transmitters (T) in Hawaiian, bistatic experiments. Wind arrow is aligned with observed winds.

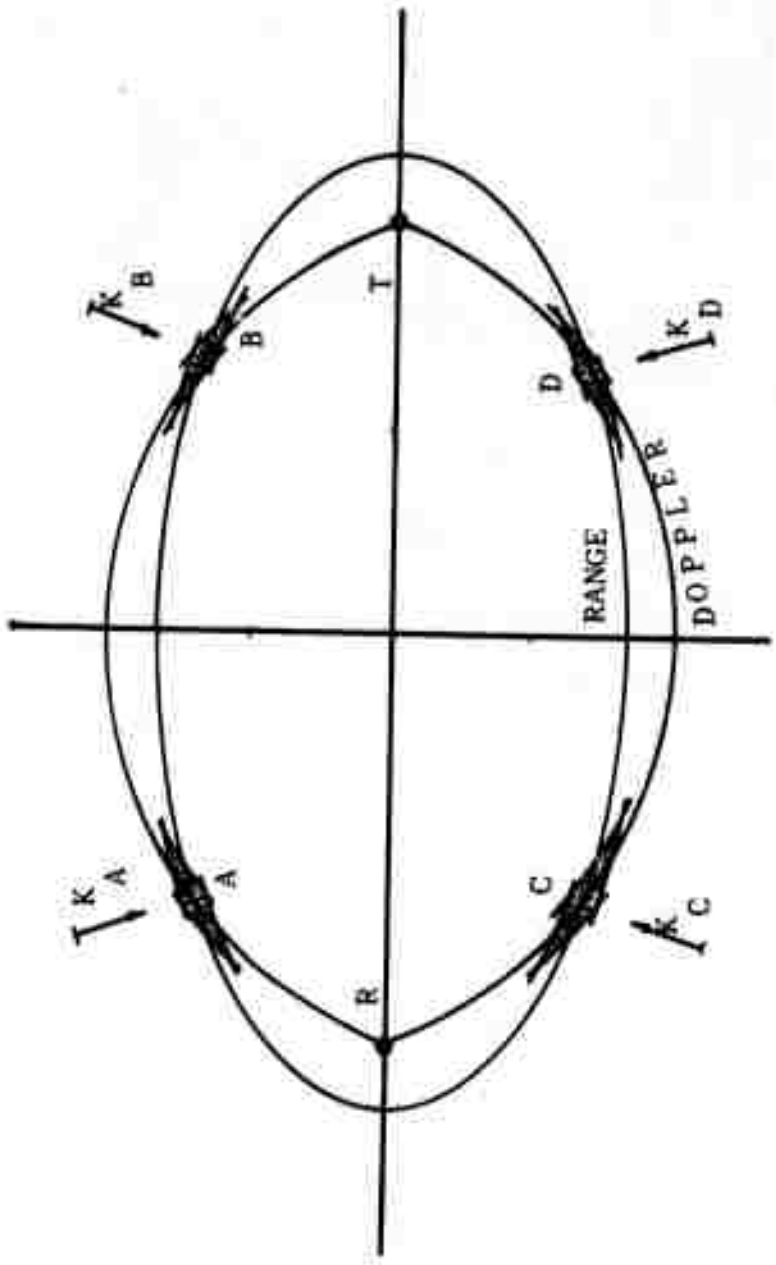

Figure 2. Plan view of bistatic geometry. The transmitter is at T, the receiver at R. The locus of constant range is an ellipse, the locus of constant Doppler frequency is two circular arcs. Four different ocean waves ($k_{A,D}$) scatter radio waves with the same range-Doppler coordinate toward the receiver.

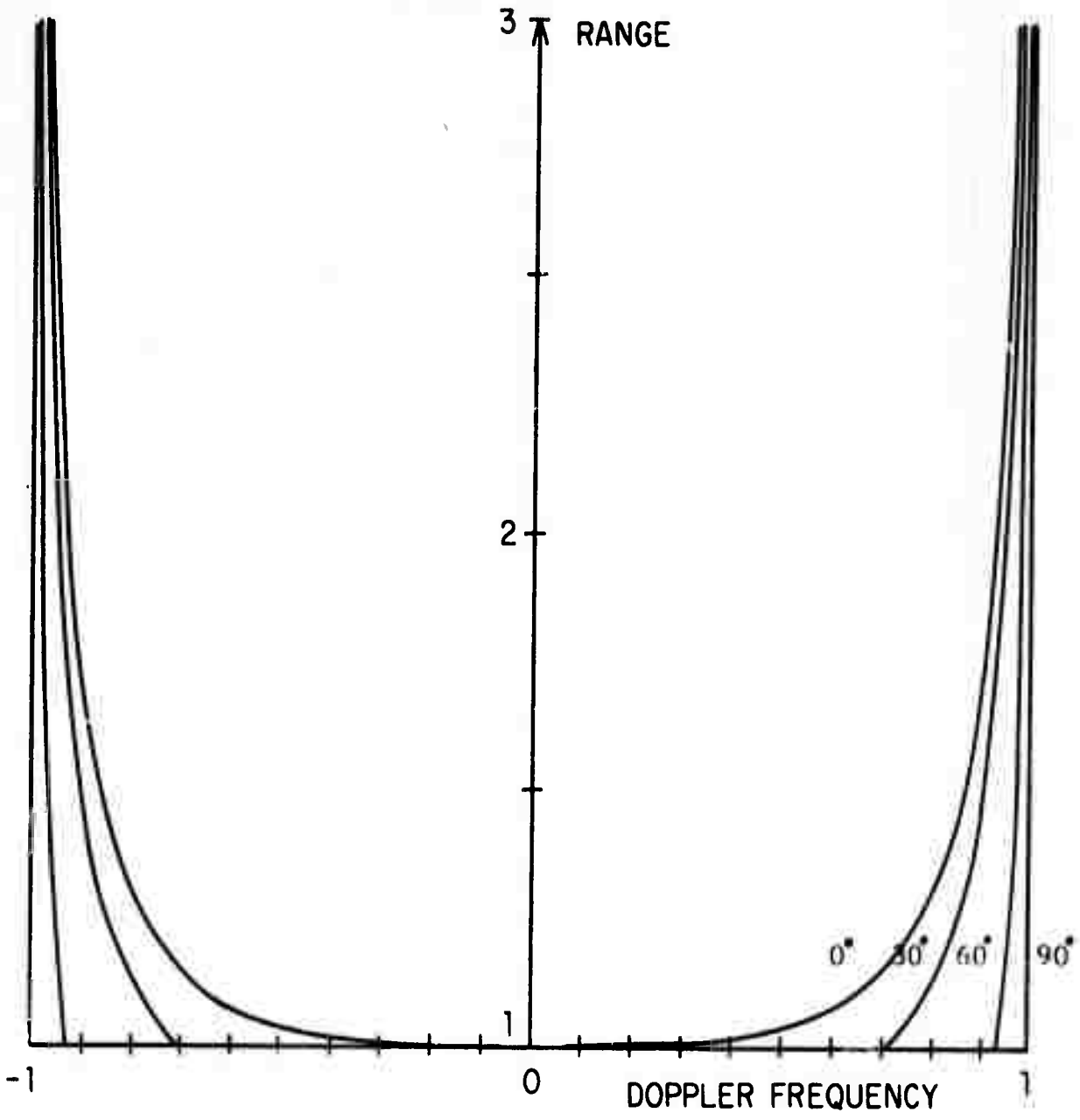

Figure 3. Range-Doppler locus for waves travelling in constant direction.

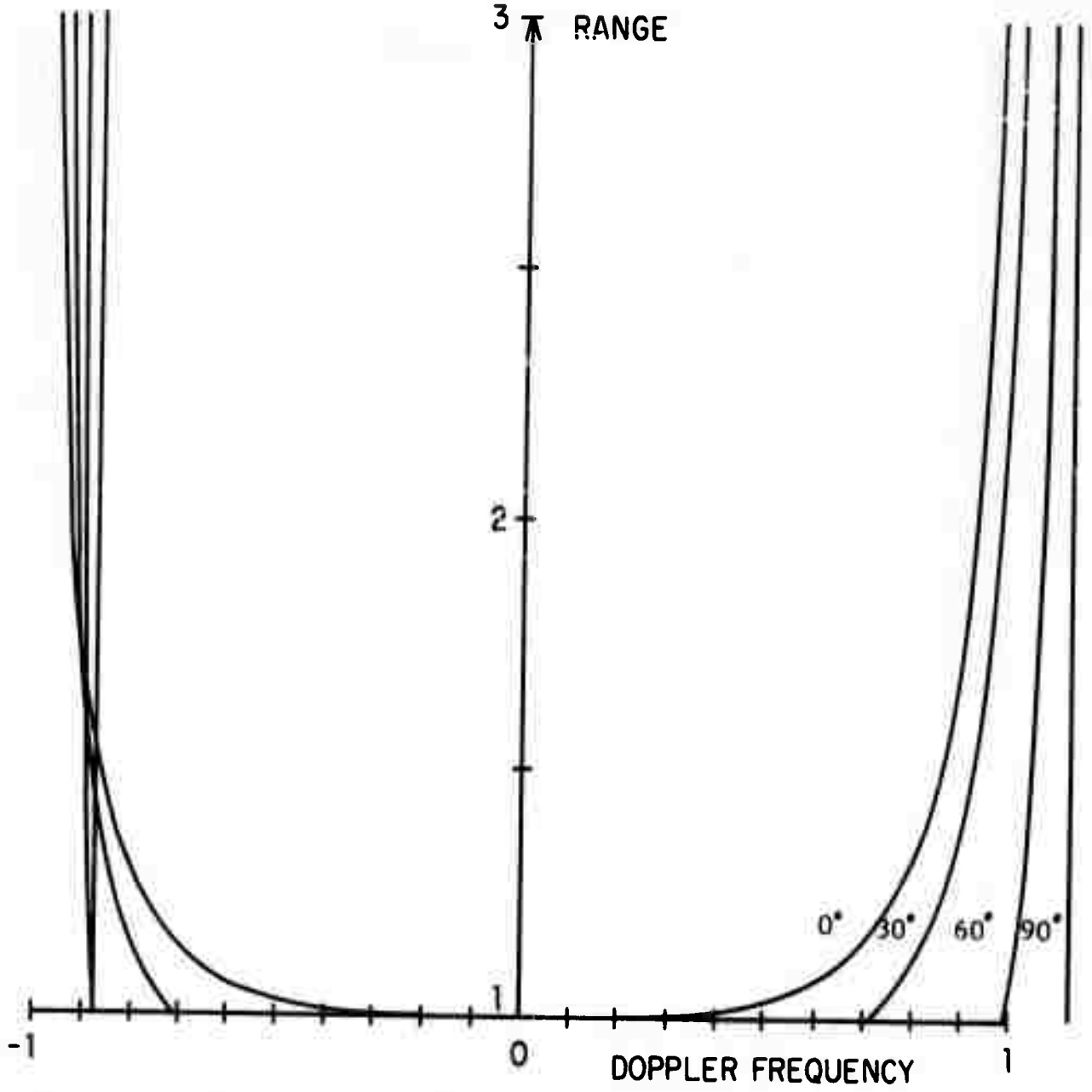

Figure 4. Range-Doppler locus for waves travelling in a constant direction, with an additional Doppler shift due to receiver motion. This plot is for radio waves coming from a single scattering quadrant in figure 2, for a receiver velocity of 2.16 m/sec (4 knots) perpendicular to the baseline.

a) Whip antenna array

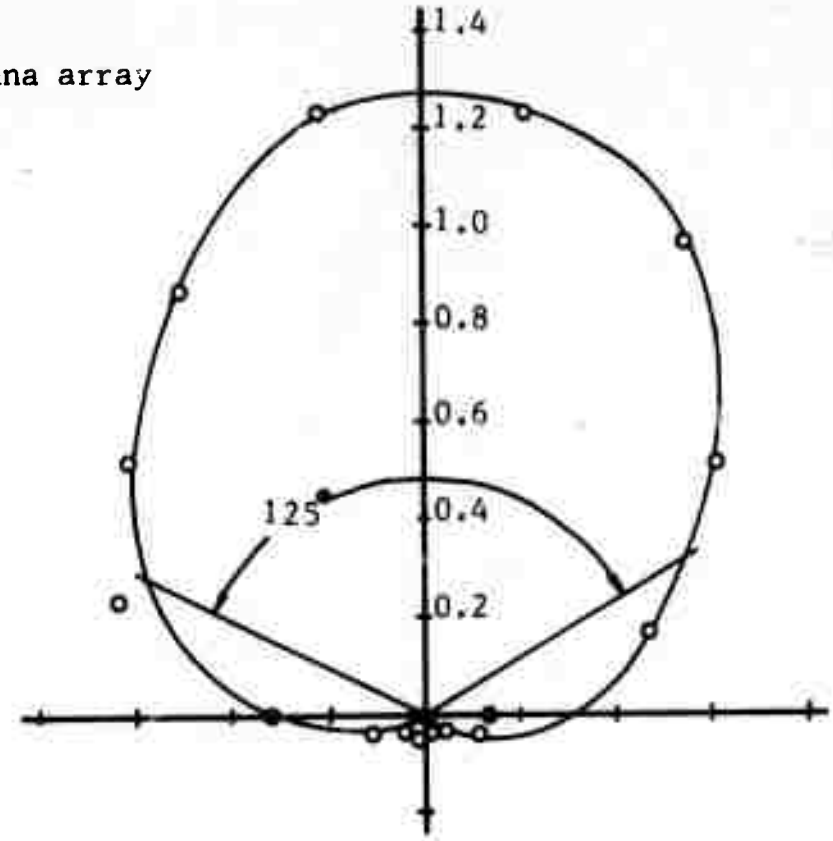

b) Loop antenna array

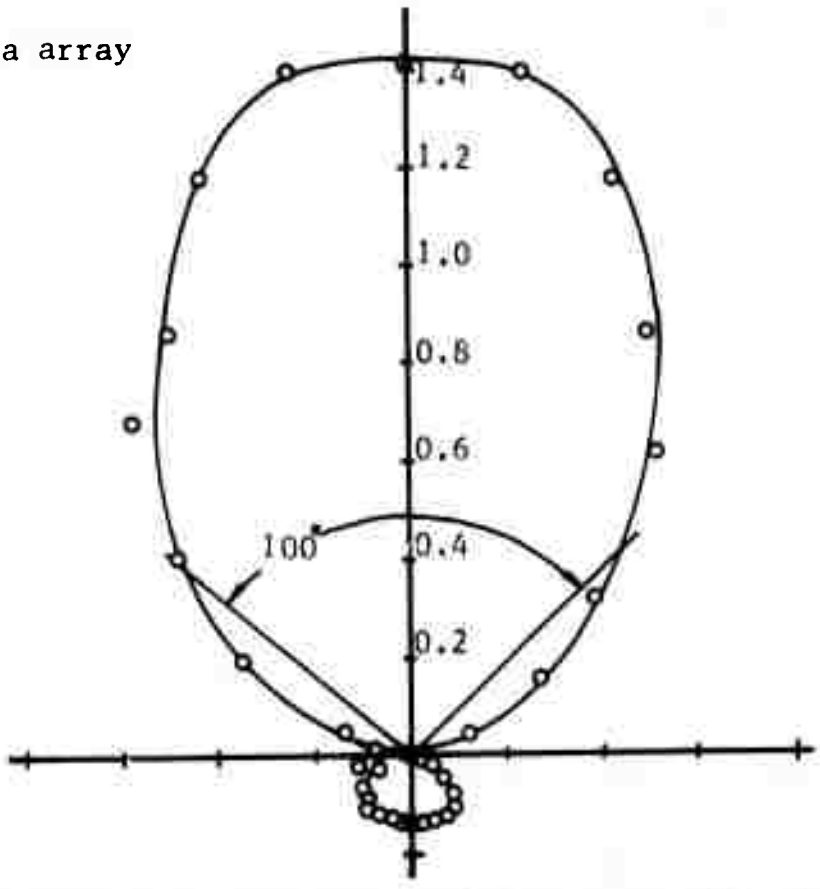

Figure 5. Directional response of arrays used in bistatic experiment.

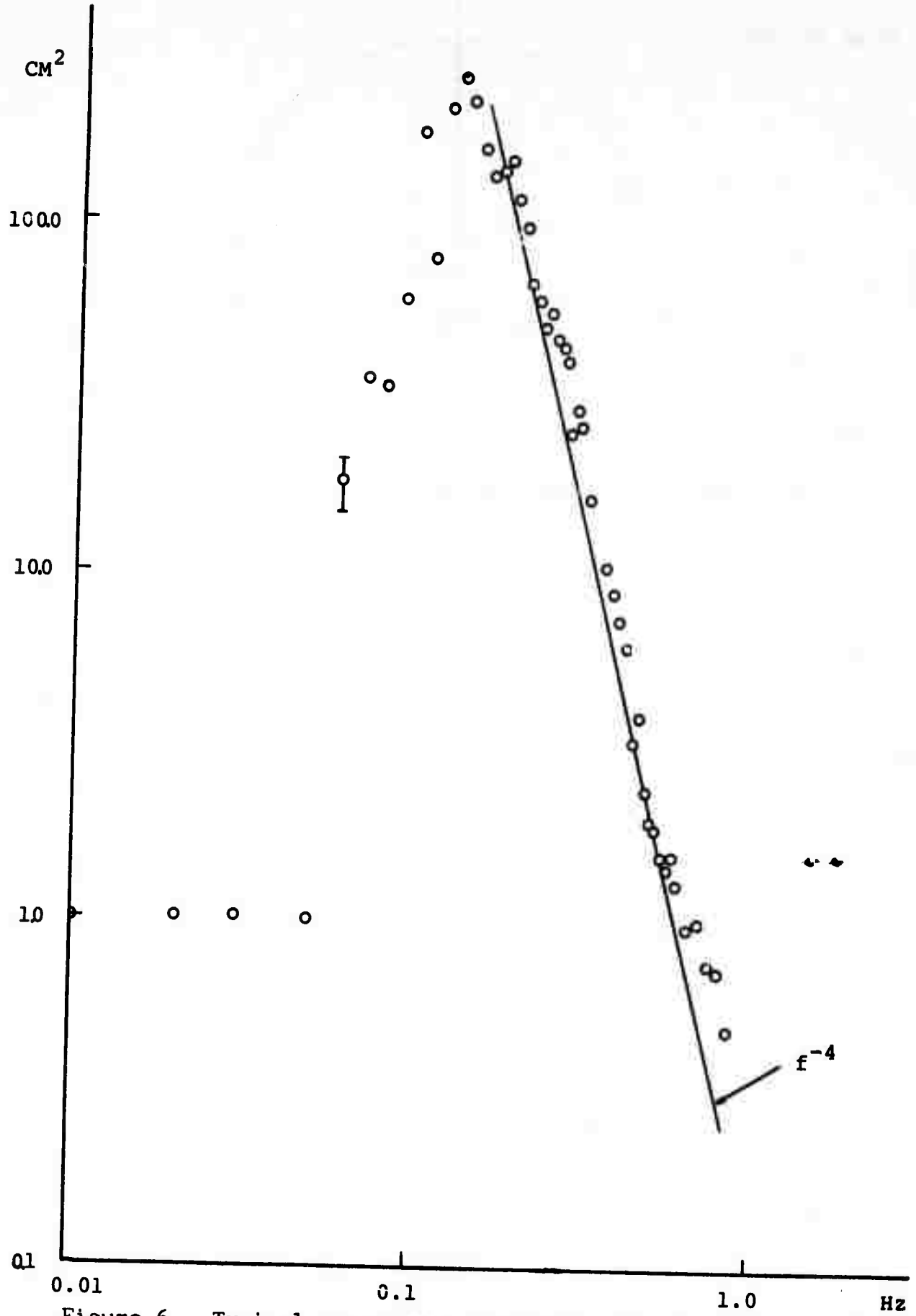

Figure 6. Typical ocean-wave frequency spectrum observed during bistatic experiment.

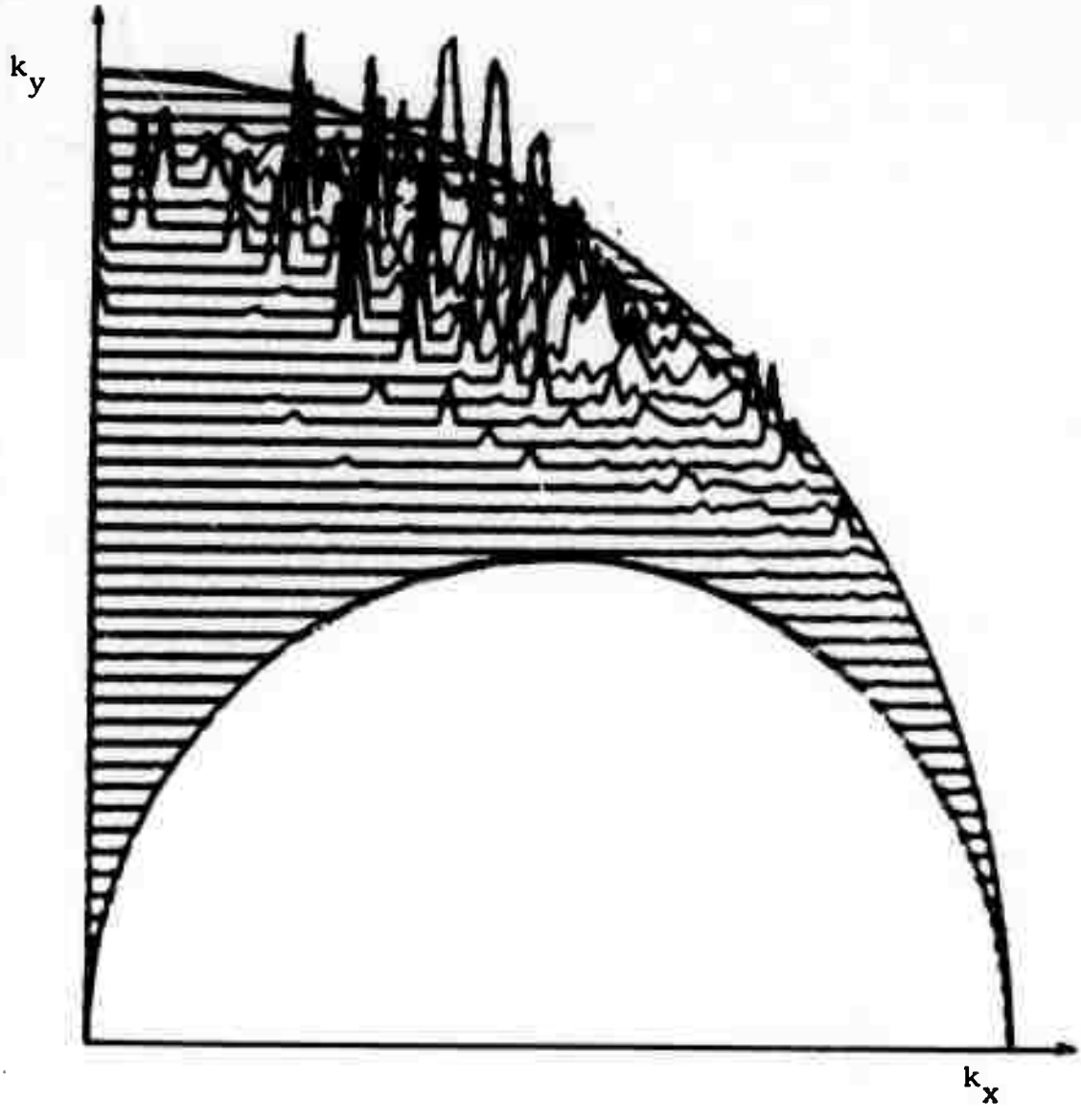

Figure 7. Ocean-wave, directional spectrum measured by land stations during bistatic experiment.

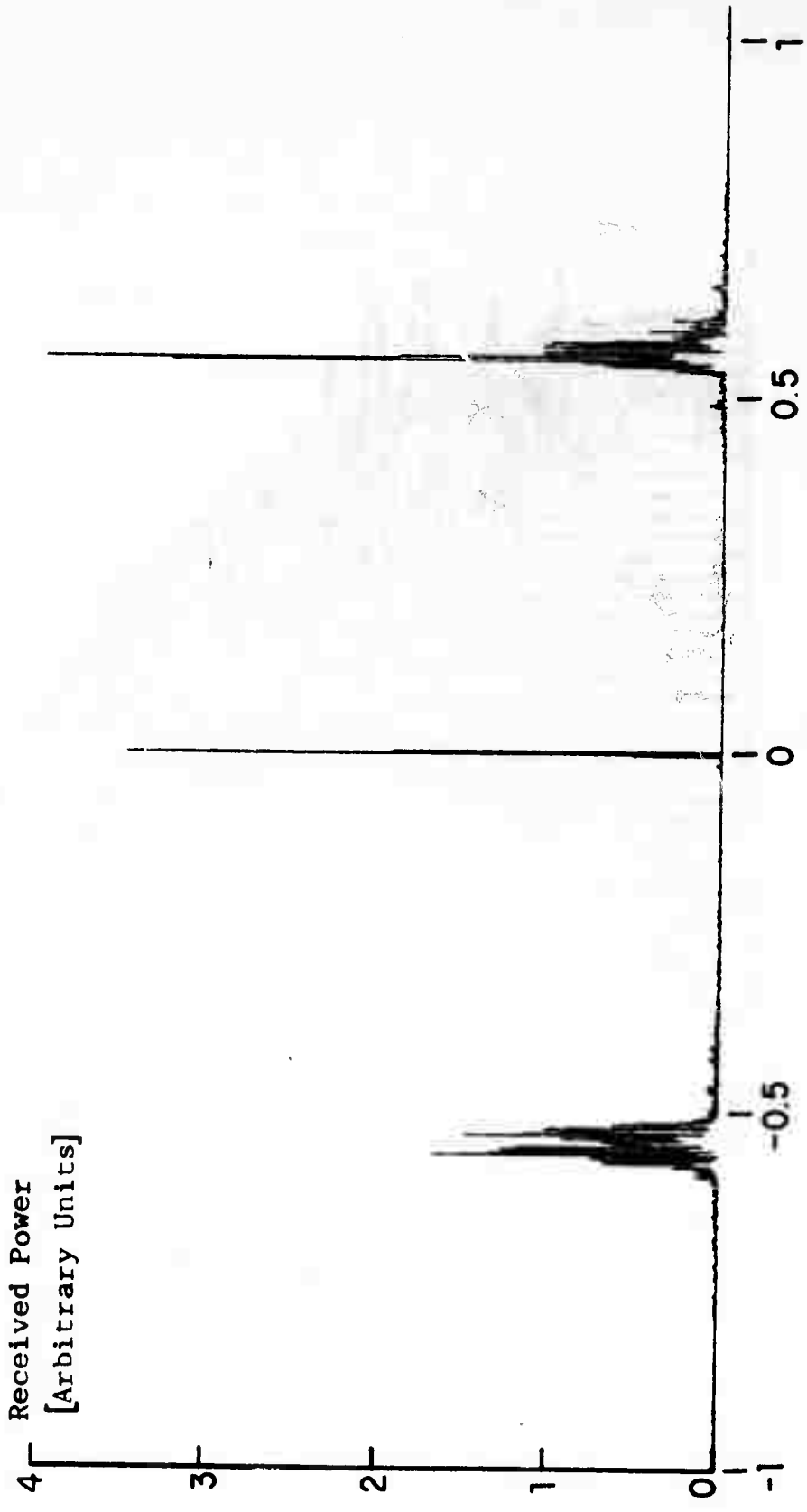

Figure 8. 30 MHz Doppler spectrum. Peaks at $\pm$ 0.55 Hz are due to scatter from short ocean waves; peak at 0 Hz is scatter from the land.

Stanford LORAN Receiver Specifications

Frequency:	1.85 or 1.95 MHz (internal adjustments)
LORAN Rates:	HO-H7, LO-L7
Bandwidth:	22 KHz (3 dB points; linear phase for optimum LORAN pulse response).
Sensitivity:	0.2μV for 0 dB SNR in Doppler channel.
LO Stability:	1×10^{-9}/day, $\pm 2 \times 10^{-10}/^{o}c$; 1 hour to reach $\pm 6 \times 10^{-8}$ max, $\pm 1 \times 10^{-8}$ typ., of turnoff frequency.
LO Offset:	Continuously adjustable up to about 2 Hz.
Doppler channel modes:	Ch.1, Ch.2, Ch.1 + Ch.2, alternate between Ch.1 and Ch.2. Separate gain controls for Ch.1 and Ch.2.
Envelope channel:	Separate input and gain control. Provides sync pulse to all Tracking Range Gates.
Sync modes:	Master only, Slave only, Both. Tracking Range Gate automatically locks on to and tracks correct rate. (Main and Aux. rates).
Blanking:	Main rate: Master, Slave, Both, Off; Aux. rate: Master, Slave, Both, Off. Blanking interval about 75μs (internally adjustable). Blanking inserts 0's in data stream.
Delay resolution:	5μs.
ADC resolution:	8 bits (2's complement code).
Sampling interval:	Every 25μs for 64 range bins, taking every n^{th} LORAN pulse, where $n_L \leq n \leq 15$. Lower limit n_L depends on LORAN rate and bit rates, with $4 \leq n_L \leq 9$. Triggered by Master, Slave, or Both.
Data format:	Serial PCM Manchester II code, 5 or 10 kbits/sec. 132 8-bit + parity words/frame, with some dead time between frames. First four words are preamble: sync word (8 bits), ID word (thumbwheel set-8 bits), frame counter (4 bits), receiver status (4 bits), external digital inputs (8 bits). Next 64 words are Master samples. Last 64 words are Slave samples.
Buffer storage:	1100 - bit MOS shift register.
Tape recorder:	Pioneer T-3300 audio cassette tape deck, 1-7/8 IPS. Use of chromium Dioxide tape allows data rates to 10 kbits/sec.
Power requirements:	115 VAC, 60 Hz. 100 Watts for receiver, 25 Watts for recorder.

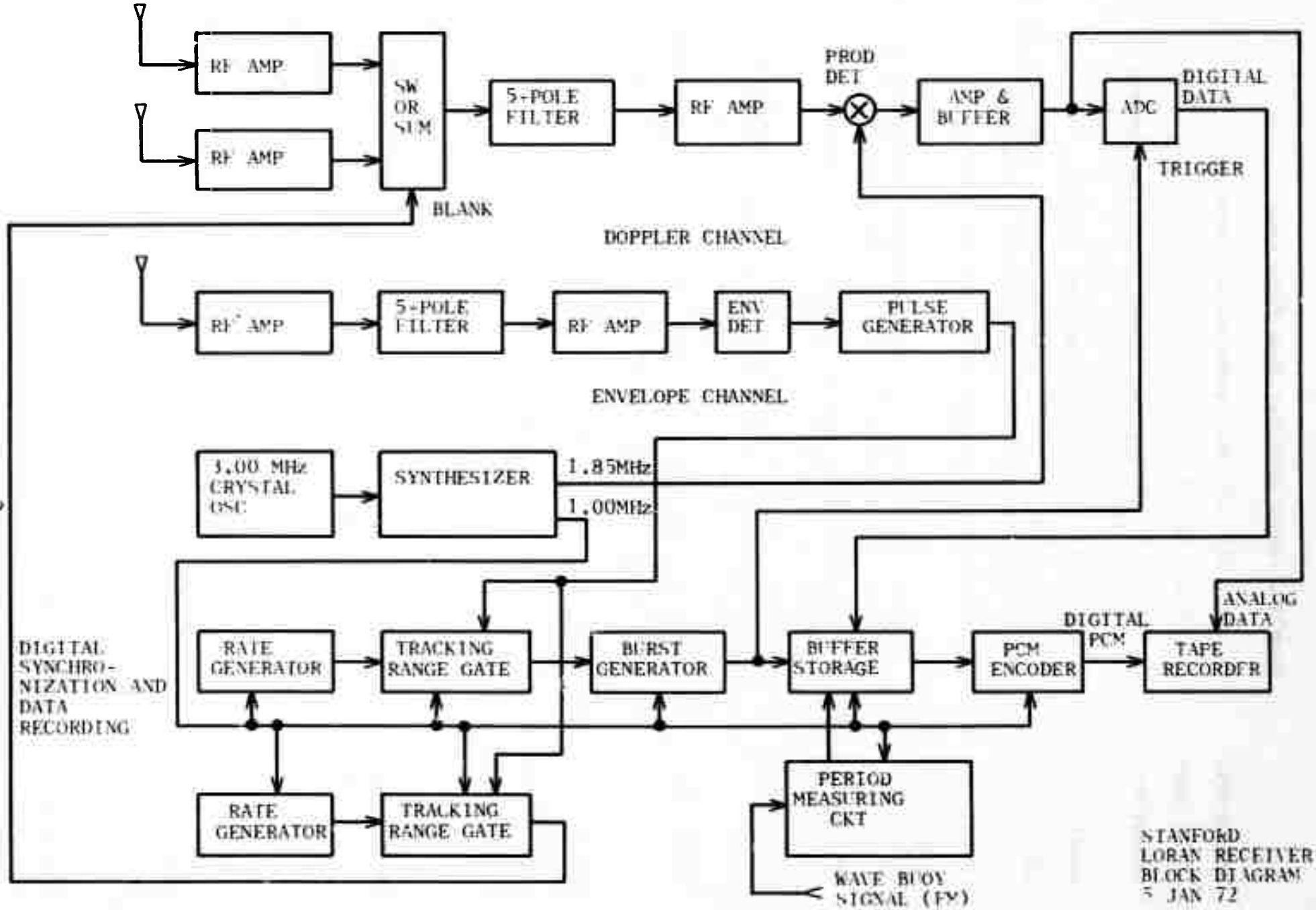
RF AMP
RF AMP
SW OR SUM
BLANK
5-POLE FILTER
RF AMP
PROD DET
AMP & BUFFER
ADC
DIGITAL DATA
TRIGGER
DOPPLER CHANNEL
RF AMP
5-POLE FILTER
RF AMP
ENV DET
PULSE GENERATOR
ENVELOPE CHANNEL
3.00 MHz CRYSTAL OSC
SYNTHESIZER
1.85MHz
1.00MHz
ANALOG DATA
DIGITAL PCM
DIGITAL SYNCHRO-NIZATION AND DATA RECORDING
RATE GENERATOR
TRACKING RANGE GATE
BURST GENERATOR
BUFFER STORAGE
PCM ENCODER
TAPE RECORDER
RATE GENERATOR
TRACKING RANGE GATE
PERIOD MEASURING CKT
WAVE BUOY SIGNAL (FM)
STANFORD LORAN RECEIVER BLOCK DIAGRAM 5 JAN 72

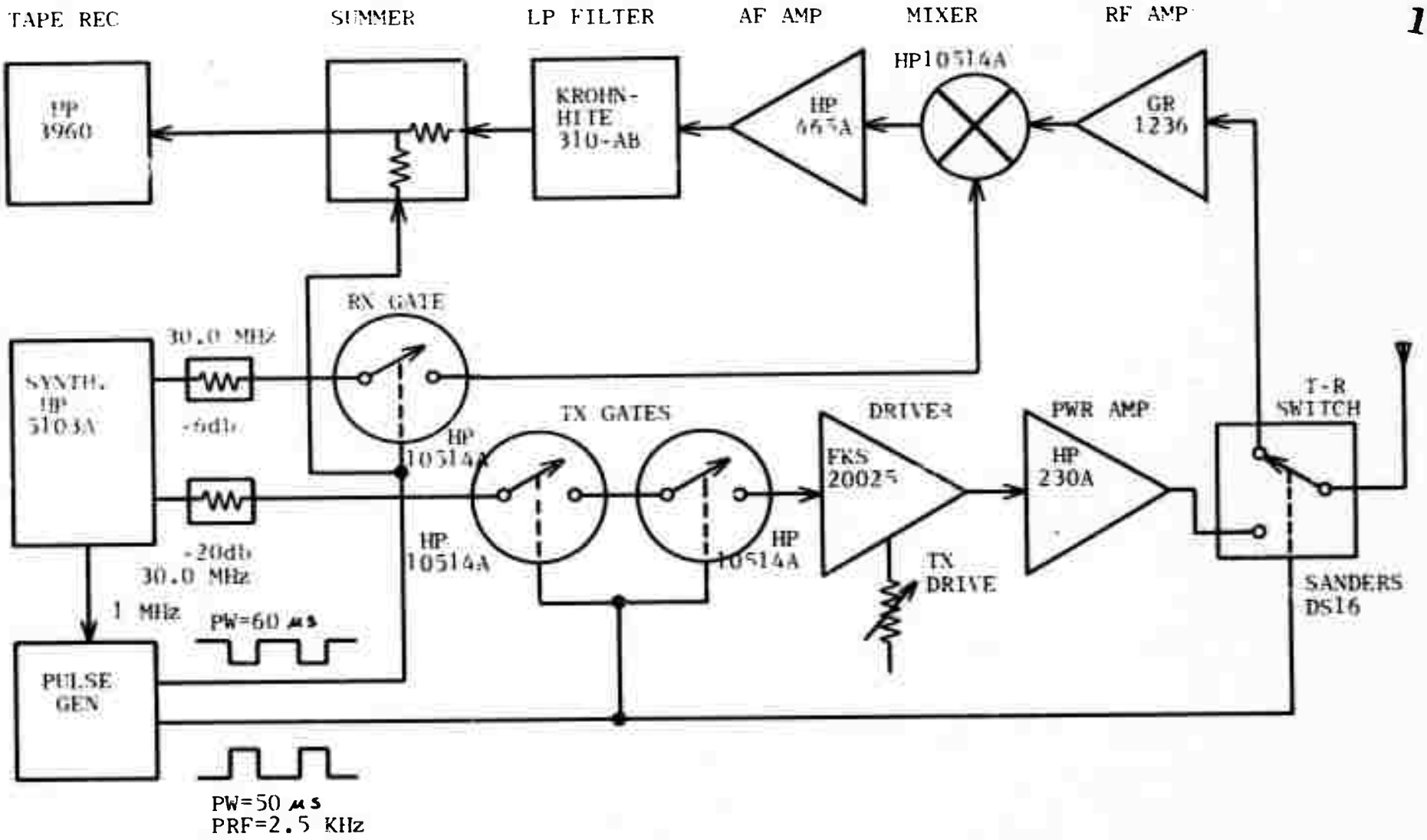

STANFORD
30 MHz OCEAN SCATTER RADAR
720107